Discrete Dynamics in Nature and Society

Performance Analysis and Synthetisation of Complex Systems with Event-triggered Communication Scheduling

Lead Guest Editor: Guoliang Wei
Guest Editors: Wangyan Li and Licheng Wang

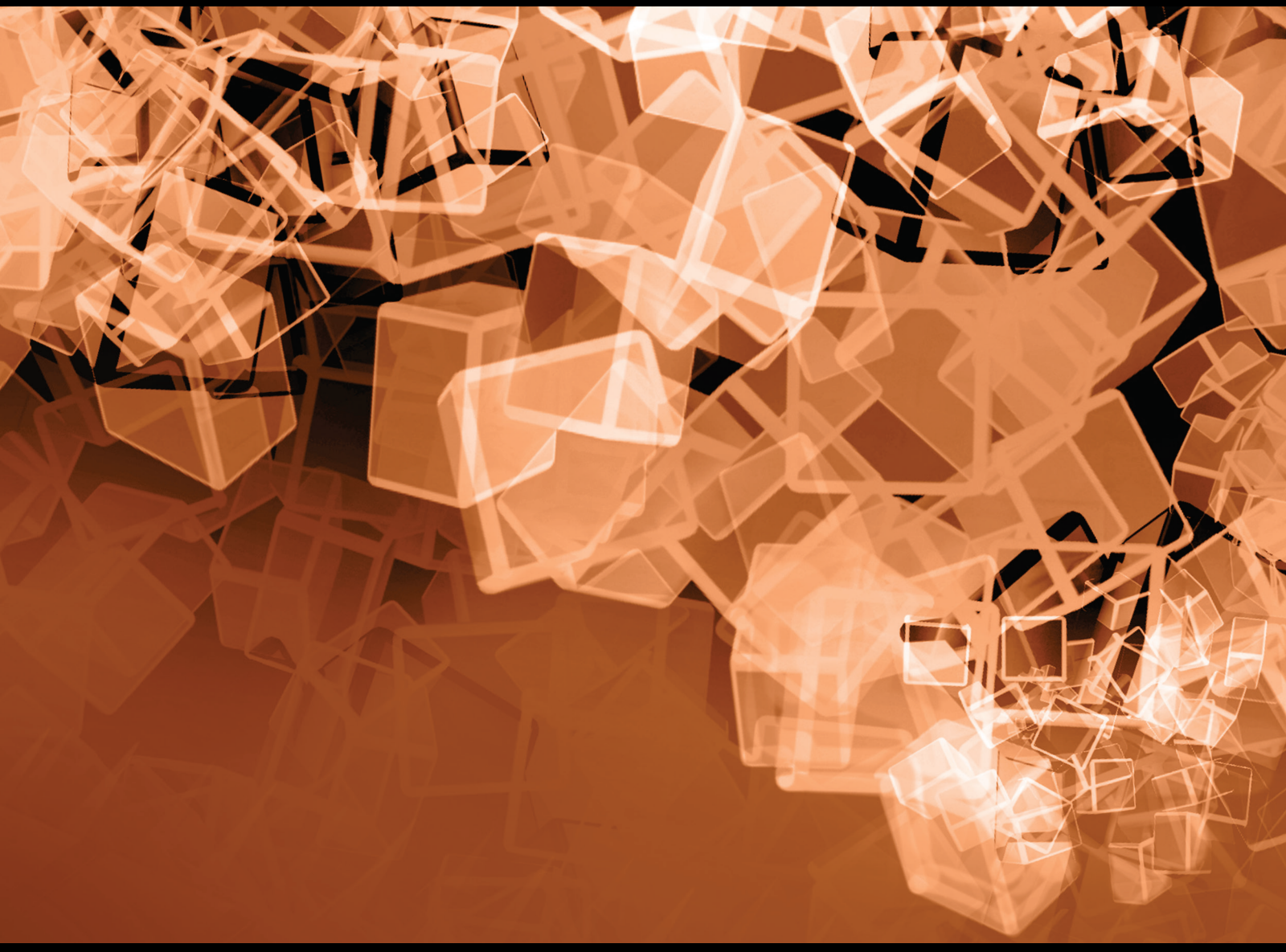

Performance Analysis and Synthetisation of Complex Systems with Event-triggered Communication Scheduling

Discrete Dynamics in Nature and Society

Performance Analysis and Synthetisation of Complex Systems with Event-triggered Communication Scheduling

Lead Guest Editor: Guoliang Wei
Guest Editors: Wangyan Li and Licheng Wang

Contents

Hindawi
Discrete Dynamics in Nature and Society
Volume 2021, Article ID 6698910, 10 pages
https://doi.org/10.1155/2021/6698910

Research Article

Graph Evaluation and Review Technique for Emergency Logistics Distribution in Complex Environment

Lin Lu,[1] **Liguo Yang**,[2] **and Xiaochun Luo**[1,3]

[1]*College of Economics and Management, Guangxi Normal University, Guilin, China*
[2]*School of Business, Guilin University of Electronic and Technology, Guilin, China*
[3]*College of Economics and Management, Nanjing University of Aeronautics and Astronautics, Nanjing, China*

Correspondence should be addressed to Xiaochun Luo; 57747278@qq.com

Received 21 November 2020; Revised 6 March 2021; Accepted 25 March 2021; Published 5 April 2021

Academic Editor: Wangyan Li

Emergency logistics is one of the important measures to solve the unconventional sudden disaster. The research on the distribution design of emergency logistics project has an important supporting role for the whole emergency rescue system. Therefore, it is necessary to analyze and plan the emergency logistics project scientifically in order to better serve the emergency rescue system. In view of the defect that the current emergency logistics model cannot completely describe the whole emergency logistics process, this paper proposes a new emergency logistics distribution model by using GERT random network. From the perspective of system, this model fully considers the possible situation in the process of emergency material transportation and puts forward the corresponding countermeasures, so as to improve the transportation efficiency of rescue materials in the actual disaster relief activities to speed up disaster relief. Based on the properties of moment generating function and the calculation method of Mason formula, this paper fully considers the success probability, risk probability, delivery time, and other factors of the distribution route and puts forward the transshipment scheme of each logistics site to the disaster sites. After that, the effectiveness of GERT stochastic network in the process of emergency distribution is verified by an example of a logistics distribution route, which provides decision-making basis for relevant departments. Compared with the literature, this paper uses GERT network model to intuitively and clearly express the overall process of emergency material distribution, breaks through the thinking mode of simply choosing the distribution path in the distribution process, combines with the dynamic changes of the distribution environment, and comprehensively considers the timeliness and traffic capacity of emergency material distribution in sudden disasters, so as to provide reference for emergency management in complex and random situations for decision-making reference.

1. Introduction

Emergency logistics and military logistics are closely linked at first. After World War II, with the deepening of the understanding of sudden disasters, emergency logistics as the premise of solving sudden disasters system has been gradually recognized by people. The United States, Japan, Australia, and some European countries are pioneers in disaster research, which has entered a mature stage of development. However, facing the needs of complex emergency relief activities, especially the challenge of medical material transportation under the impact of the COVID-19, the emergency logistics system needs to be more flexible and adaptive. It is important to study the problem of emergency logistics route planning to improve transportation efficiency in complex and changing transportation environment. Sudden disasters have the characteristics of insufficient precursors, prone to secondary and derivative disasters, serious losses and consequences, and difficulty in accurate prevention and effective control [1]. First proposed by Carter, emergency logistics is a special logistics activity that guarantees emergency supply of materials in response to public emergencies such as natural disasters, accidents, public health incidents, and social conflicts. Although it is the same as normal logistics in its essential attributes, there is a big difference. It is the material supply realized to meet the

sudden material demand in a special period; the demand has the characteristics of strong timeliness, high uncertainty, and high supply risk [2]. With the frequent occurrence of emergency events such as the Wenchuan earthquake, the Haiti earthquake, the Chile earthquake, and the Nepal earthquake, more and more researchers have begun to pay attention to the issue of emergency logistics. The suddenness, paroxysmal, and destructive nature of sudden disasters and the urgency of emergency rescue make emergency logistics require timely and fast response. From the actual feedback information of work, the emergency logistics system should solve the following problems: How to locate the emergency facility [3, 4]? How to optimize the transportation route of emergency supplies [5, 6]? The former mainly solves the location allocation problem of facilities, and the latter solves the transportation and distribution problems of the entire logistics system. Therefore, it is necessary to study the emergency logistics distribution problems in emergencies.

Scholars study emergency logistics from various angles. For example, from the perspective of traditional emergency logistics network optimization [7], in order to further reflect the dynamics of the network, especially considering the information network [8], due to the advantages of parallelism, genetic algorithm is introduced [9]. Most of these studies ignore the complexity and dependence of emergency systems and may lose their research value for practical applications to a certain extent. Some scholars consider the coordination of the emergency rescue system based on the uncertainty of the system [10, 11]. However, emergencies are uncertain, and the damage caused is also unpredictable; the emergency logistics distribution environment is complex and uncertain.

There are many theories and methods for studying logistics routing and scheduling problems, such as stochastic programming model [12–14], nonlinear programming model [15, 16], integer programming model [17], multi-objective model [18–20], and robust optimization method [21]. Most of the existing studies consider a certain emergency logistics dispatch model based on ideal conditions, and most of them assume that the emergency logistics network is always connected normally after a disaster and the vehicle travel time between any sites is not affected by the disaster. The various problems encountered in the actual disaster are not considered from the perspective of emergency logistics process, such as road congestion and construction caused by secondary disasters. These uncertainties will affect the time and volume of logistics distribution. Graph evaluation and review technique (GERT) is a network technology that can reflect the relationship between a variety of random factors and random variables. In the GERT model, many kinds of random components such as time, cost, quality, benefits, and the randomness problems of various activities in the system and their mutual influence can be dealt with; thus it provides an effective way for the research of many complicated problems with many random factors. Compared with the above literature, this paper uses GERT network model to intuitively and clearly express the overall process of emergency material distribution, which combines with the dynamic changes of the distribution environment and comprehensively considers the timeliness and traffic capacity of emergency material distribution in sudden disasters, so as to provide reference for emergency management in complex and random situations for decision-making reference.

2. Graph Evaluation and Review Technique

Graph evaluation and review technique (GERT) is a combination of network theory, probability theory, simulation technology, and signal flow graph. It uses directed network graph with probability to analyze, which is completely based on the real emergency logistics distribution process. It allows considering the feedback loop of logistics distribution lines, the selection and abandonment of each distribution path, and the learning effect brought about by repeating a certain process [22]. This method is not affected by the inherent limitations of the method itself.

In the $\mathbf{G} = (\mathbf{N}, \mathbf{A})$ network, the site types in a collection are classified as "exclusive" or "sites." Let the random variable T_{ij} be the active state of A in (ij). From the site logic, activity (ij) must be implemented on i. Therefore, to ensure the implementation of the activity (ij), it needs to know the probability of activity (ij) being executed under the condition of given site i implementation and the probability distribution of t_{ij} (discrete) or probability density function (continuous variable). The conditional moment generating function of the random variable is (ij), which is the conditional probability density function of $f(t_{ij})$:

$$M_{ij}(s) = \int_{-\infty}^{\infty} e^{st_{ij}} f\left(t_{ij}\right) \mathrm{d}t_{ij}. \tag{1}$$

When site i is implemented, the probability of activity *(ij)* being executed is P_{ij}.

Define $W_{ij}(s)$ as the transfer function of active (ij); $W_{ij}(s) = P_{ij} \cdot M_{ij}(s)$.

Each activity of G network has two parameters P_{ij} and t_{ij}, it can always find a network G' to replace G, and G' is the same as the original network structure, but there is only one parameter $W_{ij}(s)$ on each activity.

By using a principle flowchart equivalent to a function, $W_E(s)$ is $W_{ij}(s)$ function and the network function is solved according to the characteristics of the generating function of moments. Thus, two network equivalent parameters, P_E and T_E, are obtained. The moment generating function and principle in the process flowchart of GERT provide a tool to solve the random network.

3. Model Simulation

A serious disaster suddenly occurred in a place, and the national emergency logistics distribution center A delivers materials to the provincial emergency logistics distribution center B. At the same time, emergency logistics distribution centers A and B also deliver emergency relief materials to the material distribution sites scattered around the disaster area. In view of the actual complex situation, the GERT stochastic network model diagram of emergency logistics distribution

process is constructed according to the situation of disaster-stricken areas by using the idea of system theory and GERT stochastic network principle, as shown in Figure 1.

In Figure 1, sites 3, 9, 12, 13, and 15 are the main disaster sites, and the disaster situation is more serious. The other sites are the disaster sites affected by emergencies, and the disaster situation is lighter. Therefore, two emergency logistics distribution centers, A and B, mainly distribute disaster relief materials to disaster sites 3, 9, 12, 13, and 15 and distribute corresponding emergency materials along the way through the disaster sites less affected by emergencies. According to the operation of emergency logistics distribution, the meaning of each activity in the network diagram is listed in Table 1.

In GERT network, the parameters such as the time required for the operation process of each activity and the probability of realization are usually analyzed by experts according to the actual situation and combined with the previous data of emergency logistics distribution, and the approximate estimation and judgment are given. In order to simplify the calculation, this paper uses two kinds of state distribution to describe the complexity of emergency logistics activities, that is, normal distribution to describe the emergency logistics distribution activities with complex road conditions and constant distribution to describe the emergency logistics distribution activities with smooth road conditions. The GERT random network parameters are shown in Table 2. The length of time is determined by the road condition and distance. The better the road condition is, the shorter the distance is, and the shorter the time is.

3.1. Calculation of Expected Time. The transportation material data from the material distribution center A to disaster site 13 are calculated as follows:

$$\begin{aligned} W_{A\longrightarrow 13} &= \frac{1\times e^{s}\times 0.95\times e^{0.5s}\times 1}{1} = 0.95e^{1.5s}, \\ p_{A\longrightarrow 13} &= W_{A\longrightarrow 13}|_{s=0} = 0.95, \\ M_{A\longrightarrow 13} &= \frac{W}{p} = \frac{0.95\times e^{1.5s}}{0.95} = e^{1.5s}, \\ M'_{A\longrightarrow 13} &= 1.5e^{1.5s}, \\ E_{A\longrightarrow 13} &= M'_{A\longrightarrow 13}|_{s=0} = 1.5. \end{aligned} \tag{2}$$

Calculation of various data from the material distribution center A to disaster site 3 is as follows:

$$\begin{aligned} W_{A\longrightarrow 3} &= \frac{1\times e^{s}\times\left(0.6\times e^{2s+s^{2}}+0.4\times e^{s}\right)\times 0.8\times e^{2s+s^{2}}\times 0.4\times e^{s}\times 1}{1-0.4e^{s}} = \frac{0.4\times 0.8e^{4s+s^{2}}\times\left(0.6e^{2s+s^{2}}+0.4e^{s}\right)}{1-0.4e^{s}}, \\ p_{A\longrightarrow 3} &= W_{A-3}|_{s=0} = \frac{0.8\times 0.4}{0.6} = 0.533\approx 0.53, \\ M_{A\longrightarrow 3} &= \frac{W}{p} = \frac{0.32e^{4s+s^{2}}\times\left(0.6e^{2s+s^{2}}+0.4e^{s}\right)}{0.535\times\left(1-0.4e^{s}\right)}, \\ M'_{A\longrightarrow 3} &= 0.6\times\frac{\left[0.6\times(6+4s)\times e^{6s+2s^{2}}+0.4\times(5+2s)\times e^{5s+s^{2}}\right]\times\left(1-0.2e^{6s}\right)+1.2e^{6s}\left(0.6\times e^{6s+2s^{2}}+0.4e^{5s+s^{2}}\right)}{\left(1-0.4e^{s}\right)^{2}}, \\ E_{A\longrightarrow 3} &= M'|_{s=0} = 9.467\approx 9.47. \end{aligned} \tag{3}$$

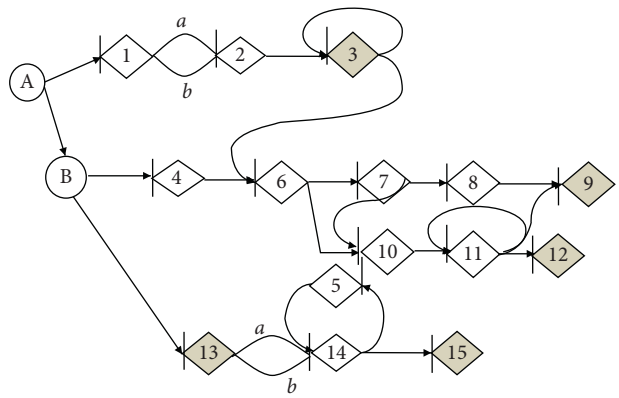

Figure 1: The route map of emergency logistics distribution center delivering materials to material distribution sites around the disaster site.

Table 1: The network diagram of the meaning of each site activity.

Activity	Activity description
(A, B)	The delivery route from the national emergency logistics distribution center A to the provincial logistics center B
(A, 1)	The delivery route from the national emergency logistics distribution center A to site 1
(1, 2)	There are two routes from site 1 to site 2. Route a is long journey but in good road condition. Route b is short distance but in bad road condition
(2, 3)	Transport supplies from site 2 to disaster site 3
(3, 3)	Disaster site 3 has a wide variety of materials, too many to load, to other sites
(3, 6)	Starting from disaster site 3, load the car back with full load and arrive at site 6
(B, 4)	Starting from the provincial logistics distribution center, load the goods to site 4
(4, 6)	From site 4 to site 6
(5, 14)	Inform the superior who has arrived at a major disaster area in advance that the road is being repaired and the convoy cannot move forward and supplement the supplies to the logistics site
(6, 7)	Some of the vehicles arriving at site 6 deliver materials to site 7
(6, 10)	Some of the vehicles arriving at site 6 deliver materials to site 10
(7, 10)	The road from site 7 to site 8 is heavily congested and difficult to pass, so vehicles can only drive up to site 10
(7, 8)	After the road is clear, the car arriving at site 7 drives to site 8
(8, 9)	Starting from site 8, go to disaster site 9
(10, 11)	Starting from site 10, go to site 11
(11, 11)	Load at site 11 and send to other areas
(11, 9)	Starting from site 11, go to disaster site 9
(11, 12)	Starting from site 11, go to disaster site 12
(B, 13)	From the provincial logistics and distribution center, a full load of supplies to disaster site 13
(13, 14)	There are two routes from disaster site 13 to site 14. Route a is long journey but in good road condition. Route b is short distance but in bad road condition
(14, 5)	The road from site 14 to site 5 was repaired successfully, and the motorcade supplied materials and transported them to the disaster area
(14, 15)	Starting from site 14, go to disaster site 15

Table 2: GERT random network parameters.

Activities	P_{ij}	Distribution type	Time (hours)	Moment function
(A, B)	1	Constant	$t = 1$	e^{s}
(A, 1)	1	Constant	$t = 1$	e^{s}
(1a, 2)	0.6	Normal distribution	$t = 2, \partial = 2$	e^{2s+s^2}
(1b, 2)	0.4	Constant	$t = 1$	e^{s}
(2, 3)	0.8	Normal distribution	$t = 2, \partial = 2$	e^{2s+s^2}
(3, 3)	0.4	Constant	$t = 1$	e^{s}
(3, 6)	0.6	Constant	$t = 3$	e^{3s}
(B, 4)	0.6	Constant	$t = 1$	e^{1s}
(4, 6)	0.9	Constant	$t = 3$	e^{3s}
(5, 14)	1	Constant	$t = 3$	e^{3s}
(6, 7)	0.4	Constant	$t = 3$	e^{3s}

Table 2: Continued.

Activities	P_{ij}	Distribution type	Time (hours)	Moment function
(6, 10)	0.6	Normal distribution	$t = 2, \partial = 2$	e^{2s+s^2}
(7, 10)	0.3	Normal distribution	$t = 1, \delta = 2$	e^{1s+1s^2}
(7, 8)	0.7	Constant	$t = 2$	e^{2s}
(8, 9)	0.8	Constant	$t = 2$	e^{2s}
(10, 11)	0.9	Constant	$t = 0.5$	$e^{0.5s}$
(11, 11)	0.3	Constant	$t = 1$	e^{s}
(11, 9)	0.5	Constant	$t = 4$	e^{4s}
(11, 12)	0.2	Constant	$t = 2$	e^{2s}
(B, 13)	0.95	Constant	$t = 0.5$	$e^{0.5s}$
(13a, 14)	0.6	Normal distribution	$t = 2, \partial = 2$	e^{2s+s^2}
(13b, 14)	0.4	Constant	$t = 1$	e^{s}
(14, 5)	0.2	Constant	$t = 3$	e^{3s}
(14, 15)	0.5	Constant	$t = 3$	e^{3s}

The transportation material data from the material distribution center A to disaster site 15 are calculated as follows:

$$\begin{aligned}
W_{A\longrightarrow 15} &= \frac{e^s \times 0.95 \times e^{0.5s}\left(0.6 \times e^{2s+s^2} + 0.4e^s\right) \times 0.5e^{3s} \times 0.2e^{3s} \times e^{3s}}{1 - 0.2e^{3s} \times e^{3s}} = \frac{0.095e^{10.5s} \times \left(0.6e^{2s+s^2} + 0.4e^s\right)}{1 - 0.2e^{6s}},\\
p_{A\longrightarrow 15} &= W_{A-15}|_{s=0} = \frac{0.095}{0.8} = 0.11875 \approx 0.12,\\
M_{A\longrightarrow 15} &= \frac{W}{p} = \frac{0.095e^{10.55} \times \left(0.6e^{2s+s^2} + 0.4e^s\right)}{0.11875\left(1 - 0.2e^{6s}\right)},\\
M'_{A\longrightarrow 15} &= 0.8 \times \frac{\left[0.6(12.5 + 2s)e^{12.5s+s^2} + 0.4 \times 11.5e^{11.5s}\right] \times \left(1 - 0.2e^{6s}\right) + 1.2e^{6s} \times \left[0.6e^{12.5+s^2} + 0.4e^{11.5s}\right]}{\left(1 - 0.2e^{6s}\right)^2},\\
E_{A\longrightarrow 15} &= M'|_{s=0} = 0.8 \times \frac{0.8 \times (7.5 + 4.6) + 1.2}{0.8^2} = 13.6.
\end{aligned} \tag{4}$$

From the material distribution center A to disaster site 9, it can be decomposed into the following.

By the route of $A \longrightarrow 1 \longrightarrow 2 \longrightarrow 3 \longrightarrow 6 \longrightarrow 7 \longrightarrow 10 \longrightarrow 11 \longrightarrow 9$,

$$\begin{aligned}
&e^s \times \left(0.6e^{2s+s^2} + 0.4e^s\right) \times 0.8e^{2s+s^2} \times 0.6e^{3s} \times 0.4e^{3s}\\
&\quad \times 0.3e^{s+s^2} \times 0.9e^{0.5s} \times 0.5e^{4s}(1 - 0) \times 0.4e^s \times 0.3e^s\\
&\quad = 0.00311e^{16.5s+2s^2}\left(0.6e^{2s+s^2} + 0.4e^s\right).
\end{aligned} \tag{5}$$

By the route of $A \longrightarrow 1 \longrightarrow 2 \longrightarrow 3 \longrightarrow 6 \longrightarrow 7 \longrightarrow 8 \longrightarrow 9$,

$$\begin{aligned}
&e^s\left(0.6^{2s+s^2} + 0.4e^s\right) \times 0.8e^{2s+s^2} \times 0.6e^{3s} \times 0.4e^{3s}\\
&\quad \times 0.7e^{2s} \times 0.8e^{2s} \times 0.4e^s\left(1 - 0.3e^s\right)\\
&\quad = 0.043e^{14s+s^2}\left(0.6e^{2s+s^2} + 0.4e^s\right) \times \left(1 - 0.3e^s\right).
\end{aligned} \tag{6}$$

By the route of $A \longrightarrow 1 \longrightarrow 2 \longrightarrow 3 \longrightarrow 6 \longrightarrow 10 \longrightarrow 11 \longrightarrow 9$,

$$\begin{aligned}
&e^s\left(0.6^{2s+s^2} + 0.4e^s\right) \times 0.8e^{2s+s^2} \times 0.6e^{3s} \times 0.6e^{2s+s^2}\\
&\quad \times 0.9e^{0.5s} \times 0.5e^{2s} \times 0.4e^s \times 0.3e^s(1 - 0)\\
&\quad = 0.015552e^{12.5s+2s^2}\left(0.6e^{2s+s^2} + 0.4e^s\right).
\end{aligned} \tag{7}$$

By the route of $A \longrightarrow B \longrightarrow 4 \longrightarrow 6 \longrightarrow 7 \longrightarrow 8 \longrightarrow 9$,

$$\begin{aligned} & e^s 0.6e^s \times 0.9e^{3s} \times 0.4e^{3s} \times 0.7e^{2s} \times 0.8e^{2s} \\ & \times \left(1 - 0.4e^s - 0.3e^s + 0.12e^{2s}\right) \\ & = 0.12e^{12s}\left(1 - 0.4e^s - 0.3e^s + 0.12e^{2s}\right). \end{aligned} \tag{8}$$

By the route of $A \longrightarrow B \longrightarrow 4 \longrightarrow 6 \longrightarrow 7 \longrightarrow 10 \longrightarrow 11 \longrightarrow 9$,

$$\begin{aligned} & e^s 0.6e^s \times 0.9e^{3s} \times 0.4e^{3s} \times 0.3e^{s+s^2} \times 0.9e^{0.5s} \\ & \times 0.5e^{4s} \times 0.3e^s \times \left(1 - 0.4e^s\right) \\ & = 0.008748e^{14.5s+s^2}\left(1 - 0.4e^s\right). \end{aligned} \tag{9}$$

By the route of $A \longrightarrow B \longrightarrow 4 \longrightarrow 6 \longrightarrow 10 \longrightarrow 11 \longrightarrow 9$,

$$\begin{aligned} & e^s 0.6e^s \times 0.9e^{3s} \times 0.6e^{2s+s^2} \times 0.9e^{0.5s} \times 0.5e^{4s} \times 0.3e^s \times \left(1 - 0.4e^s\right) \\ & = 0.04374e^{12.5s+s^2}\left(1 - 0.4e^s\right), \\ & W_{A\longrightarrow 9} = \frac{((1)+(2)+(3)+(4)+(5)+(6))}{\left(1 - 0.4e^s - 0.3e^s + 0.12e^{2s}\right)}, \\ & p_{A\longrightarrow 9} = W_{A\longrightarrow 9}|_{s=0} = \frac{0.0301 + 0.00311 + 0.015552 + 0.0504 + 0.00525 + 0.0262}{0.42} = \frac{0.130612}{0.42} = 0.3109 \approx 0.31, \\ & M_{A\longrightarrow 9} = \frac{W}{p} = \frac{W_{A\longrightarrow 9}}{0.3109}, \\ & E_{A\longrightarrow 9} = M'|_{s=0} = \frac{1}{0.3109} \times \frac{1.665 \times 0.42 - 0.1306 \times (-0.46)}{0.42^2} = \frac{1}{0.3109} \times \frac{0.759376}{0.42^2} = 13.846 \approx 13.85. \end{aligned} \tag{10}$$

The calculation of various parameters from the material distribution center A to disaster site 12 can be broken down as follows.

By the route of $A \longrightarrow 1 \longrightarrow 2 \longrightarrow 3 \longrightarrow 6 \longrightarrow 7 \longrightarrow 10 \longrightarrow 11 \longrightarrow 12$,

$$\begin{aligned} & e^s\left(0.6^{2s+s^2} + 0.4e^s\right) \times 0.8e^{2s+s^2} \times 0.6e^{3s} \times 0.4e^{3s} \\ & \times 0.3e^{s+s^2} \times 0.9e^{0.5s} \times 0.2e^{2s} \times 0.4e^s \times 0.3e^s (1 - 0) \\ & = 0.00124e^{14.5s+2s^2}\left(0.6e^{2s+s^2} + 0.4e^s\right). \end{aligned} \tag{11}$$

By the route of $A \longrightarrow 1 \longrightarrow 2 \longrightarrow 3 \longrightarrow 6 \longrightarrow 10 \longrightarrow 11 \longrightarrow 12$,

$$\begin{aligned} & e^s\left(0.6^{2s+s^2} + 0.4e^s\right) \times 0.8e^{2s+s^2} \times 0.6e^{3s} \times 0.6e^{2s+s^2} \\ & \times 0.9e^{0.5s} \times 0.2e^{2s} \times 0.4e^s \times 0.3e^s \times 1 \\ & = 0.00622e^{12.5s+2s^2}\left(0.6e^{2s+s^2} + 0.4e^s\right). \end{aligned} \tag{12}$$

By the route of $A \longrightarrow B \longrightarrow 4 \longrightarrow 6 \longrightarrow 7 \longrightarrow 10 \longrightarrow 11 \longrightarrow 12$,

$$\begin{aligned} & e^s \times 0.6e^s \times 0.9e^{3s} \times 0.4e^{3s} \times 0.3e^{s+s^2} \times 0.9e^{0.5s} \\ & \times 0.2e^{2s} \times 0.3e^s \times \left(1 - 0.4e^s\right) \\ & = 0.00349e^{12.5s+s^2}\left(1 - 0.4e^s\right). \end{aligned} \tag{13}$$

By the route of $A \longrightarrow B \longrightarrow 4 \longrightarrow 6 \longrightarrow 10 \longrightarrow 11 \longrightarrow 12$,

$$e^s \times 0.6e^s \times 0.9e^{3s} \times 0.6e^{2s+s^2} \times 0.9e^{0.5s} \times 0.2e^{2s} \times 0.3e^s \times \left(1 - 0.4e^s\right) = 0.0175e^{10.5s+s^2}\left(1 - 0.4e^s\right),$$

$$W_{A\longrightarrow 12} = \frac{(\mathrm{I} + \mathrm{II} + \mathrm{III} + \mathrm{IV})}{\left(1 - 0.4e^s - 0.3e^s + 0.12e^{2s}\right)},$$

$$p_{A\longrightarrow 12} = W_{A\longrightarrow 12}|_{s=0} = \frac{0.00124 + 0.00622 + 0.0021 + 0.0105}{0.42} = 0.0478 \approx 0.05, \tag{14}$$

$$M_{A\longrightarrow 12} = \frac{W}{p} = \frac{W_{A\longrightarrow 12}}{0.0478},$$

$$E_{A\longrightarrow 12} = M'|_{s=0} = \frac{1}{0.0478} \times \frac{0.2355 \times 0.42 - 0.02 \times (-0.46)}{0.42^2} = \frac{1}{0.0478} \times \frac{0.10811}{0.42^2} = 12.82.$$

The GERT network parameters calculated from the above emergency supplies dispatching center to multiple emergency supplies distribution networks are all active calculated values, as shown in Table 3.

According to the random network model of emergency distribution GERT and the calculated values of the parameters of emergency distribution activities of each emergency logistics distribution center in the network, the following conclusions can be drawn:

(1) The probability of successful delivery of emergency supplies to disaster site 3 is 0.53, the risk to be borne is 47%, and the arrival time is 9.47 hours. This conclusion shows that the success probability of distribution to disaster site 3 is close to the risk probability. It should increase the quantity of materials to make up for the material loss and delay after transportation failure. When the materials in disaster site 3 are sufficient, they can be converted into material storage transfer station to supply resources for other disaster areas.

(2) The probability of successful distribution of emergency materials to disaster site 9 is 0.31, which needs to bear 69% of the risk, and it is estimated that it will take 13.85 hours. The probability of successful distribution of emergency materials to the disaster site 9 is low and the risk is high. This is because there is congestion from site 7 to site 8 during transportation. In addition, some materials are transferred to the disaster area after meeting the needs of disaster site 3. It is necessary to dispatch enough emergency materials from provincial emergency logistics distribution center B to the disaster area, dredge the traffic, and open up a green channel. At the same time, the vanguard team bypasses the congested area and transports materials from site 11 to disaster sites 9 and 12 at the same time.

(3) The probability of successful distribution of emergency supplies to disaster site 12 is 0.05, which needs to bear 95% of the risk. It is estimated that it will take 12.82 hours. From the model, it can be seen that there are four distribution routes leading to disaster site 12, which should increase the possibility of successful distribution to a certain extent. However, after calculation, we find that there are still some problems, such as low success rate of distribution, high risk, and long transportation time, which lead to the possibility of this phenomenon. The factors are as follows: ① like the materials transported to disaster site 9, some of the relief materials must meet the needs of the disaster site in front before they can be delivered, and ② the road condition from site 7 to site 8 is very poor, which brings about risks to the distribution process.

(4) The probability of successful distribution of emergency materials to disaster site 13 is 0.95, which needs to bear 5% of the risk and is expected to take 1.5 hours. The probability of success is the largest among all disaster areas. This is because the road conditions leading to disaster site 13 are good, and they are directly distributed by the provincial emergency logistics distribution center, which reduces the risk of transshipment from other places.

(5) The probability of successful delivery of emergency supplies to disaster site 15 is 0.12, which needs to bear 88% of the risk. It is estimated that it will take 13.6 hours. This is because site 14 to disaster site 15 may encounter road damage halfway and need to transit at site 5, which increases the time and risk.

From the model, it can be seen that if the emergency logistics distribution center is established in advance between site 9 and site 12, the risk of transferring materials from other disaster sites can be reduced, and the distribution process can be completed in the shortest time, which can improve the success probability to a certain extent. When the transportation link of rescue materials breaks in the process of emergency relief, the successful distribution will be caused. When the road patency probability is too low, we should immediately take a detour plan and remove obstacles to establish a green channel. In addition, through the establishment of emergency logistics distribution, we can

Table 3: Active calculated values of the GERT network parameter

Activity	Realize probability P_{ij}	Risk probability $P_V = 1 - P_E$	Expected time (hours)
$W_{1\longrightarrow 3}$: emergency supplies to disaster site 3	0.53	0.47	9.47
$W_{1\longrightarrow 9}$: emergency supplies to disaster site 9	0.31	0.69	13.85
$W_{1\longrightarrow 12}$: emergency supplies to disaster site 12	0.05	0.95	12.82
$W_{1\longrightarrow 13}$: emergency supplies to disaster site 13	0.95	0.05	1.5
$W_{1\longrightarrow 15}$: emergency supplies to disaster site 15	0.12	0.88	13.6

reduce transportation links and effectively reduce transportation risks.

3.2. The Number of Times Expected in a Complex Environment. Suppose that the situation suddenly changes, and a new disaster site 21 appears behind the disaster area. Disaster site 21 has a long way to go, and the required materials can only be transferred from site 11. The terrain of the road from site 11 to disaster site 21 is complex and easy to be blocked. In this environment, the emergency logistics strategy is as follows: as long as there is a jam in the front, the transport vehicles return to the upper site to wait until the road is clear and then start the distribution. Let the road patency probability $p = 0.7$ and probability of blockage $q = 0.3$. Mark each traffic with z; then the coefficient u of z^u is the number of attempts to transport from site 11 to disaster site 21. According to the known data, the probability of transportation success, risk probability, and expected times are calculated.

There are six first-order loops in Figure 2, which are (1) self-loop of site 11, (2) self-loop of site 16, (3) self-loop of site 19, (4) self-loop of site 18, (5) loop $16 \longrightarrow 17 \longrightarrow 16$, and (6) loop $18 \longrightarrow 19 \longrightarrow 20 \longrightarrow 18$. Their values are, respectively, qz, qz, qz, qz, $pz \times qz$, and $pz \times qz \times pz \times pz \times qz$.

There are twelve second-order loops in Figure 2, which are (1) self-loop of site 11 and self-loop of site 16, (2) self-loop of site 11 and loop of $16 \longrightarrow 17 \longrightarrow 16$, (3) self-loop of site 11 and self-loop of site 19, (4) self-loop of site 11 and self-loop of site 18, (5) self-loop of site 11 and loop of $18 \longrightarrow 19 \longrightarrow 20 \longrightarrow 18$, (6) self-loop of site 16 and loop of $18 \longrightarrow 19 \longrightarrow 20 \longrightarrow 18$, (7) self-loop of site 16 and self-loop of site 19, (8) self-loop of site 16 and self-loop of site 18, (9) loop of $16 \longrightarrow 17 \longrightarrow 16$ and self-loop of site 19, (10) loop of $16 \longrightarrow 17 \longrightarrow 16$ and self-loop of site 18, (11) loop of $16 \longrightarrow 17 \longrightarrow 16$ and loop of $18 \longrightarrow 19 \longrightarrow 20 \longrightarrow 18$, and (12) self-loop of site 18 and self-loop of site 19. Their values are, respectively, $qz \times qz$, $qz \times qz \times pz$, $qz \times qz$, $qz \times qz$, $qz \times pz \times pz \times qz$, $qz \times pz \times pz \times qz$, $qz \times qz$, $qz \times qz$, $pz \times qz \times qz$, $pz \times qz \times qz$, $pz \times qz \times pz \times qz \times qz$, and $qz \times qz$.

There are nine third-order loops in Figure 2, which are (1) self-loop of site 11 and self-loop of site 16 and self-loop of site 19, (2) self-loop of site 11 and self-loop of 16 and loop of $18 \longrightarrow 19 \longrightarrow 20 \longrightarrow 18$, (3) self-loop of site 11 and self-loop of site 16 and self-loop of site 18, (4) self-loop of site 11 and self-loop of site 18 and loop of $16 \longrightarrow 17 \longrightarrow 16$, (5) self-loop of site 11 and self-loop of site 18 and self-loop of site 19, (6) self-loop of site 11 and self-loop of site 19 and loop of $16 \longrightarrow 17 \longrightarrow 16$, (7) self-loop of site 11 and loop of $16 \longrightarrow 17 \longrightarrow 16$ and loop of $18 \longrightarrow 19 \longrightarrow 20 \longrightarrow 18$, (8) self-loop of site 16 and self-loop of site 18 and self-loop of site 19, and (9) self-loop of site 18 and self-loop of site 19 and loop of $16 \longrightarrow 17 \longrightarrow 16$. Their values are, respectively, $qz \times qz \times qz$, $qz \times qz \times pz \times pz \times qz$, $qz \times qz \times qz$, $qz \times qz \times pz \times qz$, $qz \times qz \times qz$, $qz \times qz \times pz \times qz$, $qz \times pz \times qz \times pz \times pz \times qz$, $qz \times qz \times qz$, and $qz \times qz \times pz \times qz$.

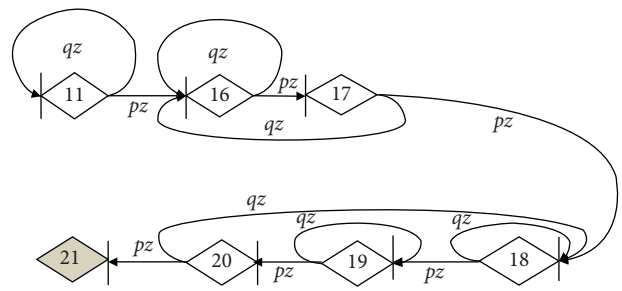

Figure 2: Random network diagram for distribution.

There are two fourth-order loops in Figure 2, which are (1) self-loop of site 11 and self-loop of site 16 and self-loop of site 18 and self-loop of site 19 and (2) self-loop of site 11 and loop of $16 \longrightarrow 17 \longrightarrow 16$and self-loop of site 18 and self-loop of site 19. Their values are, respectively, $qz \times qz \times qz \times qz$ and $qz \times pz \times qz \times qz \times qz$.

$$\begin{aligned}\Delta = 1 &- \left(4qz + pqz^2 + p^2qz^3\right) \\ &+ \left(6q^2z^2 + 3pq^2z^3 + 2p^2q^2z^4 + p^2q^3z^5\right) \\ &- \left(4q^3z^3 + p^2q^3z^5 + p^3q^2z^5 + 3pq^3z^4\right) \\ &+ \left(q^4z^4 + pq^4z^5\right).\end{aligned} \tag{15}$$

There is only one path from site 11 to disaster site 21, whose value is p^6z^6; and there are no loops in contact with the path, so $\Delta_1 = 1$.

$$W = \frac{p^6z^6 \times 1}{\Delta} = \frac{p^6z^6}{1 - 4qz + \left(6q^2 - pq\right)z^2 + \left(3pq^2 - p^2q - 4q^3\right)z^3 + \left(2p^2q^2 - 3pq^3 + q^4\right)z^4 + \left(pq^4 - p^3q^2\right)z^5}. \tag{16}$$

When $p = 0.7$ and $q = 0.3$ are substituted into equation, we can get

$$W = \frac{0.117649z^6}{1 - 1.2z + 0.33z^2 - 0.066z^3 + 0.0396z^4 - 0.0252z^5}. \tag{17}$$

Take the derivative of z with respect to W and set $z = 1$ to get the expected value of the number of attempts; namely,

$$W'|_{z=1} = \frac{0.705894 \times 0.0784 + 0.083013134}{0.0784^2} = 22.5094 \approx 23. \tag{18}$$

It takes 23 attempts to reach disaster site 21 at one time, which may be due to poor road conditions. Almost every road in front of the transportation site needs to be sorted out before passing. In order to reduce the risk of transportation failure, we can establish an emergency logistics reserve center in the nearby area in advance to transport and reserve disaster relief materials in advance. It can directly transport the materials from the reserve center to the disaster site, which improves the response speed of emergency rescue and the arrival rate of transportation.

4. Conclusions

Timely and reasonable resource distribution is one of the preconditions to ensure the normal development of emergency rescue activities, which is of great significance to improve the emergency rescue system. How to complete the task of emergency logistics distribution efficiently and with low risk is a challenge for the emergency logistics project. In this paper, GERT network is used to build a simulation model of emergency logistics distribution for emergency distribution of material reserve base to multiple disaster sites, analyze the transportation problems that may exist in the actual rescue, and calculate the realization probability and risk of logistics distribution in the transportation scheme of each logistics site to the disaster site and between the disaster sites, aiming at different realization probability and actual situation. This paper puts forward some effective countermeasures, such as increasing the transportation volume of materials, establishing temporary transfer centers, and opening up green channels, and draws conclusion that the reasonable layout of emergency logistics distribution centers can effectively reduce the risk of logistics distribution and improve the success probability. The conclusion provides a strategic reference for ensuring the efficient and safe transportation of rescue materials to the disaster-stricken areas. Compared with other traditional research methods of emergency logistics, GERT network considers the feedback self-loop problem, so it is more advanced, and the results are more accurate and closer to the actual situation.

However, the distribution type assumption of GERT network model activity parameters is simple in this paper; in addition, there are many areas not involved in the research. In complex environment, how to scientifically measure GERT random network activity parameters in order to more truly describe the actual situation of emergency logistics distribution and how to reasonably arrange the distribution plan (including material distribution and vehicle type selection, path planning, etc.) will be further studied.

Data Availability

The data used to support the findings of this study are available from the corresponding author upon request.

Conflicts of Interest

The authors declare that they have no conflicts of interest.

Acknowledgments

This study was supported by the Special Project of Guangxi Humanities and Social Sciences Development Research Center "Scientific Research Engineering Research on High-Quality Economic Development Theory of Later-Developed Areas" (GZL2019010).

References

[1] Q. H. Zhao, "Construction of fractal emergency logistics management system and its guarantee mechanism for major emergencies," *Jianghuai Forum*, vol. 4, pp. 13–20, 2020.

[2] W. N. Carter, "Natural disasters," *The Macedon Digest*, vol. 9, no. 4, pp. 32-33, 1994.

[3] C.-F. Zhu, Z.-K. Zhang, Q.-R. Wang, and F. Mauriello, "Path choice of emergency logistics based on cumulative prospect theory," *Journal of Advanced Transportation*, vol. 2019, pp. 1–11, 2019.

[4] J. R. Feng, W. M. Gai, J. Y. Li, and M. Xu, "Location selection of emergency supplies repositories for emergency logistics management: a variable weighted algorithm," *Journal of Loss Prevention in the Process Industries*, vol. 63, pp. 1–5, 2020.

[5] L. Lu and X. Luo, "Emergency transportation problem based on single-valued neutrosophic set," *Discrete Dynamics in Nature and Society*, vol. 2020, pp. 1–8, 2020.

[6] B. J. Qiu, J. H. Zhang, Y. T. Qi, and Y. Liu, "Grey-theory-based optimization model of emergency logistics considering time uncertainty," *PLoS One*, vol. 10, no. 9, pp. 1–13, 2015.

[7] A. Haghani and S.-C. Oh, "Formulation and solution of a multi-commodity, multi-modal network flow model for disaster relief operations," *Transportation Research Part A: Policy and Practice*, vol. 30, no. 3, pp. 231–250, 1996.

[8] C. F. Zhu, Z. K. Zhang, and C. X. Ma, "Research on emergency logistics dynamic network based on super network," *Latin American Applied Research*, vol. 47, no. 1, pp. 11–16, 2016.

[9] F. S. Chang, J. S. Wu, C. N. Lee, and H. C. Shen, "Greedy-search-based multi-objective genetic algorithm for emergency logistics scheduling," *Expert Systems with Applications*, vol. 41, no. 6, pp. 2974–2956, 2014.

[10] C. F. Zhu and H. J. Li, "Coordinated operation mechanism and coupled analysis of the virtual emergency logistics system," *Statistics & Decisions*, vol. 38, no. 8, pp. 54–56, 2014.

[11] B. Zheng, Z. Ma, and S. L. Li, "Integrated optimization of emergency logistics systems for postearthquake initial stage based on bi-level programming," *Journal of Systems Engineering*, vol. 29, no. 1, pp. 113–125, 2014.

[12] G. Barbarosoğlu and Y. Arda, "A two-stage stochastic programming framework for transportation planning in disaster

response," *Journal of the Operational Research Society*, vol. 55, pp. 43–53, 2017.

[13] A. M. Caunhye, Y. Zhang, M. Li, and X. Nie, "A location-routing model for prepositioning and distributing emergency supplies," *Transportation Research Part E: Logistics and Transportation Review*, vol. 90, pp. 161–176, 2016.

[14] B. Zhang, H. Li, S. Li, and J. Peng, "Sustainable multi-depot emergency facilities location-routing problem with uncertain information," *Applied Mathematics and Computation*, vol. 333, pp. 506–520, 2018.

[15] M. Ahmadi, A. Seifi, and B. Tootooni, "A humanitarian logistics model for disaster relief operation considering network failure and standard relief time: a case study on San Francisco district," *Transportation Research Part E: Logistics and Transportation Review*, vol. 75, pp. 145–163, 2015.

[16] K. Chang, H. Zhou, G. Chen, and H. Chen, "Multiobjective location routing problem considering uncertain data after disasters," *Discrete Dynamics in Nature and Society*, vol. 2017, pp. 1–7, 2017.

[17] S.-L. Hu, C.-F. Han, and L.-P. Meng, "A scenario planning approach for propositioning rescue centers for urban waterlog disasters," *Computers & Industrial Engineering*, vol. 87, pp. 425–435, 2015.

[18] S. Khalipourazari and A. A. Khamseh, "Bi-objective emergency blood supply chain network design in earthquake considering earthquake magnitude: a comprehensive study with real world application," *Annals of Operations Research*, vol. 283, pp. 355–393, 2019.

[19] Y. Deng, W. Zhu, and F. Wang, "Research on multi-objective robust vehicle routing problem in emergency logistics," *Computer Engineering and Applications*, vol. 55, no. 1, pp. 248–255, 2019.

[20] Y. Zhou, J. Liu, Y. Zhang, and X. Gan, "A multi-objective evolutionary algorithm for multi-period dynamic emergency resource scheduling problems," *Transportation Research Part E: Logistics and Transportation Review*, vol. 99, pp. 77–95, 2017.

[21] A. Bozorgi-Amiri, M. S. Jabalameli, and S. M. J. Mirzapour Al-e-Hashem, "A multi-objective robust stochastic programming model for disaster relief logistics under uncertainty," *OR Spectrum*, vol. 35, no. 4, pp. 905–933, 2013.

[22] Y. C. Feng, *Random Network and its Application*, Beijing Institute of Aeronautics Press, Beijing, China, 1987.

Hindawi
Discrete Dynamics in Nature and Society
Volume 2021, Article ID 6695353, 12 pages
https://doi.org/10.1155/2021/6695353

Research Article

Nonfragile Estimator Design for Fractional-Order Neural Networks under Event-Triggered Mechanism

Xiaoguang Shao, Ming Lyu, and Jie Zhang

School of Automation, Nanjing University of Science and Technology, Nanjing 210094, China

Correspondence should be addressed to Ming Lyu; lumtz@163.com

Received 25 December 2020; Revised 30 January 2021; Accepted 5 March 2021; Published 29 March 2021

Academic Editor: Wangyan Li

This paper is concerned with the nonfragile state estimation for a kind of delayed fractional-order neural network under the event-triggered mechanism (ETM). To reduce the bandwidth occupation of the communication network, the ETM is employed in the sensor-to-estimator channel. Moreover, in order to reflect the reality, the transmission delay is taken into account in the model establishment. Sufficient criteria are supplied to make sure that the augmented system is asymptotically stable by using the fractional-order Lyapunov indirect approach and the linear matrix inequality method. In the end, the theoretical result is shown by means of two numerical examples.

1. Introduction

The past several decades have witnessed that artificial neural network (ANN) has attracted particular research attention. Because of the outstanding performance, ANN has been extensively applied in image recognition, signal processing [1], fault diagnosis [2], and so on. With the rapid developments of artificial intelligence, the ANN has received considerable attention again by the scholars, which relates to synchronization, dissipativity, attractivity, stability, and state estimation (SE) for various kinds of ANNs [3–7].

As we all know, ANNs are composed of plenty of artificial neurons and the SE problem of the neurons plays a vital role in practical applications. As such, quite a lot of results have been reported on the SE issue (see [8–11] and the reference therein). For the practical systems, the parameter uncertainties are often considered. So far, a lot of research studies regarding uncertain systems have been conducted [12–14]. It is worth noting that the existing results assumed that parameter of the estimator is accurate, which, however, is unrealistic. To solve this problem, we aim to design a nonfragile estimator so as to alleviate the effects induced by the uncertainty of the estimator parameter on the system performance. Till now, some initial results have been published on the nonfragile controller design problems [14–17].

In the networked systems, the network bandwidth is always limited which therefore may result in network congestion when a large amount of data is transmitted. Up to now, the network-induced phenomena including transmission delay, packet loss, and quantification have been discussed adequately. In recent years, much attention has been focused on the ETM and many communication protocols, which aims to avoid the occurrence of the network-induced phenomena. Based on the ETM, plenty of literature has been available on stability analysis, event-triggered condition design, controller/filter design, and so on [18]. Noting that compared with time-triggered mechanism, the ETM exhibits better performance because the necessary sampling depends on the "event" rather than the "time" [19, 20].

In addition, by applying the fractional calculus to the ANNs, the researchers have found that the performance of the fractional-order models is better than integer-order ones, especially in the aspect of memory and hereditary. Till now, some novel fractional-order theories and methods concerning the ANNs have been proposed. For example, a nonfragile nonlinear fractional-order observer is designed in

[21] and an adaptive event-triggered scheme has been developed in [22]. But these existing fractional-order systems employed ETM are introduced with single delay or without only. Especially, it is a challenge in a fractional system. However, the problem of multiple time delays in real systems is often encountered. Nevertheless, there are few related studies on the nonfragile SE for fractional-order neural network based on ETM with multiple time delays, which motivates us to shorten this gap.

Inspired by the aforementioned lines, a nonfragile state estimator is designed for a class of fractional-order neural networks (FNNs) based on ETM. The advantages in this paper are as follows: (1) compared with the existing estimators, a fractional-order nonfragile estimator is first constructed; (2) to save bandwidth resources, an ETM is applied in the SE problem of the fractional-order neural network; (3) the LMI method and the fractional Lyapunov indirect method are adopted to design the state estimator.

The remaining content is outlined as follows. In Section 2, some preliminary knowledge is recalled. In Section 3, state estimation criteria are voiced. In Section 4, two numerical examples are given with some simulation figures to support the theorems.

Notation. Throughout this paper, Z^T and the symbol $*$ in matrix Z represent matrix transposition and the symmetric term, respectively. $\mathbb{R}$ is the set of integers, and $\mathbb{R}^n$ denotes the n-dimensional Euclidean space. I_n means n-dimensional identity matrix. $\mathscr{P} > 0$ ($\mathscr{P} < 0$) is defined as a positive-definite (negative-definite) matrix. $\|z\|$ is the Euclidean norm of a vector z in R_n. $\lambda_{\max}(R)$ ($\lambda_{\min}(R)$) represents the maximum (minimum) eigenvalue of R and $\mathrm{sym}(Y)$ means $Y + Y^T$.

2. Preliminaries and Problem Formulation

Some fractional definitions and model descriptions are presented firstly. In addition, some important lemmas that will be used in Section 3 are also presented.

Definition 1 (see [23, 24]). For $h(t)$, the fractional integral form is defined as

$$I^{\alpha}h(q) = \frac{1}{\Gamma(\alpha)}\int_{q_0}^{q}(q-\theta)^{\alpha-1}f(\theta)\mathrm{d}\theta, \quad \alpha \in \mathbb{R}^{+}, \tag{1}$$

where $q \geq q_0$ and $\Gamma(\cdot)$ is a gamma function.

Definition 2 (see [23, 24]). Caputo's derivative of $h(q)$ is denoted by

$$ {}_{q_0}^{C}D_q^{\alpha}h(q) = \frac{1}{\Gamma(z-\alpha)}\int_{q_0}^{q}(q-\theta)^{z-\alpha-1}h^{(z)}(\theta)\mathrm{d}\theta, \quad \alpha \in (z-1, z), h(t) \in \iota^{z}([t_0, \infty), \mathbb{R}), \tag{2}$$

where $q \geq q_0$ and z is a positive integer.

In what follows, D^{α} stands for ${}_{q_0}^{C}D_q^{\alpha}$ for the convenience of presentation. In this paper, let us consider the following FNN model:

$$\begin{cases} D^{\alpha}v(t) = -\mathscr{C}v(t) + \mathscr{A}\hbar(v(t)) + \mathscr{V}, \\ y(t) = Dv(t), \end{cases} \tag{3}$$

where $\alpha \in (0, 1)$ is the predetermined fractional order, $\mathscr{C} = \mathrm{diag}\{c_1, c_2, \ldots, c_n\}$ with $c_i > 0\,(i = 1, 2, \ldots, n)$, $\mathscr{A} = (a_{ij})_{n\times n}$ is the connection matrix, the vector $v(t) = (v_1(t), v_2(t), \ldots, v_n(t))^T \in \mathbb{R}^n$ stands for the neuron state, $\hbar(v(t)) = (\hbar_1(v_1), \hbar_2(v_2), \ldots, \hbar_n(v_n))^T$ denotes the activation function of the neurons, $y(t)$ is the measurement output, $\mathscr{V}$ is the system input, and D is a known constant matrix.

In what follows, ETM is introduced in order to reduce the communication burden. The event-triggered condition is predesigned as follows:

$$e_y^T(t)e_y(t) \leq \sigma y^T(t_kh + jh)y^T(t_kh + jh), \tag{4}$$

where $e_y(t) = y(t_kh + jh) - y(t_kh)$, σ is a given constant, jh and t_kh are the sampling instant and the release instant, respectively, $y(t_kh + jh)$ stands for the latest sampled signal, and $n_ih = t_{k+1}h - t_kh$ denotes the release period.

Remark 1. The sensor is time-driven at discrete instants, which can avoid the Zeno behavior. Moreover, when $\sigma = 0$, ETM becomes a time-triggered one.

In this paper, the transmission delay $d_k \in [0, \overline{d})$ between sensor and estimator is considered, where $\overline{d}$ is a positive scalar. Therefore, $t_kh + d_k$ is the arrival time of the transmitted data from sensor to estimator.

In view of [25], the holding interval can be rewritten as $[t_kh + d_k, t_{k+1}h + d_{k+1}) \cup_{j=0}^{j=d_M} I_j$, where $I_j = [t_kh + jh + \overline{d}, t_kh + jh + h + \overline{d})$. For the convenience of analysis, denote $d(t) = t - t_kh - jh$, and then we have $0 \leq d(t) \leq h + \overline{d} \triangleq d_M$. Then, the measurement outputs arrived at the estimator can be rewritten as

$$\overline{y}(t) = e_y(t) + y(t - d(t)) = De_k(t) + y(t - d(t)), \tag{5}$$

where $e_k(t)$ is the error vector.

Design a nonfragile state estimator for system (3) as follows:

$$D^{\alpha}\widehat{v}(t) = -\mathscr{C}\widehat{v}(t) + \mathscr{A}\widetilde{\hbar}(\widehat{v}(t)) + \mathscr{V} + (K + \Delta K)[\overline{y}(t) - D\widehat{v})], \tag{6}$$

where $\widehat{v}(t) \in \mathbb{R}^n$ stands for the estimate of $v(t)$, $K \in \mathbb{R}^{n\times q}$ is the gain matrix to be determined, and ΔK represents the gain variation that satisfies $\Delta K = M\mathscr{F}(t)N$, in which M and

N are known real matrices and $\mathscr{F}(t)$ is an unknown satisfying $\mathscr{F}^T(t)\mathscr{F}(t) \le I$.

Defining $e(t) = v(t) - \hat{v}(t)$, the estimation error dynamics can be obtained from (3) and (5) as follows:

$$\begin{aligned} D^\alpha e(t) = &-[\mathscr{C} - (K+\Delta K)D]e(t) + \mathscr{A}\hbar(e(t)) \\ &- (K+\Delta K)De_k(t) \\ &- (K+\Delta K)Dv(t-d(t)) + (K+\Delta K)Dv(t), \end{aligned} \tag{7}$$

where $\hbar(e(t)) \triangleq \tilde{\hbar}(v(t)) - \tilde{\hbar}(\hat{v}(t))$.

For notation simplicity, we define $\eta(t) \triangleq [v^T(t)\, e^T(t)]^T$. An augmented system model from (3) and (8) is given in the following form:

$$D^\alpha \eta(t) = \tilde{C}\eta(t) + \overline{A}\varphi(\eta(t)) + \tilde{E}e_k(t) + \tilde{K}\eta(t-d(t)), \tag{8}$$

where

$$\begin{aligned} &\overline{C} = \begin{bmatrix} -C & 0 \\ (K+\Delta K)D & -C-(k+\Delta K)D \end{bmatrix}, \overline{A} = \begin{bmatrix} \mathscr{A} & 0 \\ 0 & \mathscr{A} \end{bmatrix}, \tilde{K} = \begin{bmatrix} 0 & 0 \\ -(K+\Delta K)D & 0 \end{bmatrix}, \\ &\tilde{E} = \begin{bmatrix} 0 \\ -(K+\Delta K)D \end{bmatrix}, \varphi(\eta(t)) \triangleq \begin{bmatrix} \hbar^T(v(t)) & \tilde{\hbar}^T(e(t)) \end{bmatrix}^T. \end{aligned} \tag{9}$$

Lemma 1 (see [26]). *For ξ_1 and $\xi_2 \in \mathbb{R}^n$ and any positive scale $\epsilon > 0$, one has*

$$\psi_1^T\psi_2 + \psi_2^T\psi_1 \le \epsilon\psi_1^T\psi_1 + \epsilon^{-1}\psi_2^T\psi_2. \tag{10}$$

Lemma 2 (see [27]). *For $\forall\alpha \in (0,1)$ and $t \ge 0$, if $v(t) \in \mathbb{R}^n$ is continuous and differential, then*

$$D^\alpha v^T(t)Qv(t) \le 2v^T(t)QD^\alpha v(t). \tag{11}$$

Lemma 3 (see [28]). *For matrices $\varpi, \mathscr{E}, \mathscr{H}$, where ϖ is symmetric, the inequality*

$$\varpi + \mathscr{E}\mathscr{F}\mathscr{H} + (\mathscr{E}\mathscr{F}\mathscr{H})^T < 0 \tag{12}$$

holds if and only if

$$\varpi + \xi\mathscr{E}\mathscr{E}^T + \xi^{-1}\mathscr{H}^T\mathscr{H} < 0, \tag{13}$$

in which $\xi > 0$ refers to a scalar and $\mathscr{F}^T\mathscr{F} < I$.

Lemma 4 (see [29]). *Consider a class of fractional-order nonlinear systems:*

$$D^\alpha \eta(t) = h(t, \eta(t-d(t))), \tag{14}$$

and the initial condition is $\eta(t_0) = \phi \in C([t_0-\tau, t_0], \mathbb{R}^n)$. Suppose that $\omega_i(s)\,(i=1,2)$: $\mathbb{R} \longrightarrow \mathbb{R}$ are positive functions, and $\omega_1(0) = \omega_2(0) = 0, \omega_2(s_1) < \omega_2(s_2)\,(\forall 0 < s_1 < s_2)$. If there exist two constants $0 < \mu < \epsilon$ and a continuous differential function V: $\mathbb{R} \times \mathbb{R}^n$ such taht $\omega_1 \le V(t,x) \le \omega_2$ satisfying

$$\begin{aligned} D\alpha V(t,\eta(t)) \le &-\varepsilon V(t,\eta(t)) \\ &+ \mu \sup_{-d_M \le -d(t) \le 0} V(t+d(t), x(t+\eta(t-d(t)))), \end{aligned} \tag{15}$$

then the fractional-order system is globally uniformly asymptotically stable.

Lemma 5 (see [30]). *The matrix*

$$\phi = \begin{bmatrix} \phi_{11} & \phi_{12} \\ \phi_{12}^T & \phi_{22} \end{bmatrix} < 0, \tag{16}$$

holds if and only if (a) $\phi_{22} < 0, \phi_{11} - \phi_{12}\phi_{22}^{-1}\phi_{12}^T < 0$, or (b) $\phi_{11} < 0, \phi_{22} - \phi_{12}^T\phi_{11}^{-1}\phi_{12} < 0$.

Lemma 6 (see [31]). *V is continuous on $[t_0, +\infty)$ and bounded on $[t_0-\rho, t_0]$. If there exist p, q such that*

$$D_t^\alpha V(t) \le -pV(t) + \sum_{k=1}^m q_h \sup_{-\rho_h \le \omega \le 0} V(t+\omega), \quad t \ge t_0, \tag{17}$$

where $0 < \alpha < 1, q_k > 0, p > \sum_{k=1}^m q_k$, and $\rho = max\{\rho_1, \rho_2, \ldots, \rho_m\}$, then $lim_{t\longrightarrow\infty} V(t) = 0$.

3. Main Results

Theorem 1. *For the given positive scalars $\varepsilon > \mu > 0$, system (8) is globally asymptotically stable if there exist a symmetric matrix $\mathscr{P} = diag\{\mathscr{P}_1, \mathscr{P}_2\} > 0$ and four scalars $\beta_i\,(i=1,2,3) > 0, \gamma > 0$ satisfying the following LMI:*

$$\Phi = \begin{bmatrix} \Phi_{11} & \Phi_{12} & \Phi_{13} & \Phi_{14} \\ * & \Phi_{22} & 0 & 0 \\ * & * & \Phi_{33} & 0 \\ * & * & * & \Phi_{44} \end{bmatrix} < 0, \tag{18}$$

$$\beta_2\sigma\tilde{I}^T\tilde{I} + \beta_3\overline{I}_1^T\overline{I}_1 - \mu\mathscr{P} < 0, \tag{19}$$

where

$$\begin{aligned}
&\Phi_{11}=\begin{bmatrix}\Lambda_{11} & D^TX^T-\gamma D^TN^TND\\ * & \Lambda_2\end{bmatrix},\Phi_{12}=\begin{bmatrix}\mathscr{P}_1\mathscr{A} & 0\\ 0 & \mathscr{P}_2\mathscr{A}\end{bmatrix},\Phi_{14}=\begin{bmatrix}0 & 0\\ 0 & \mathscr{P}_2\overline{M}\end{bmatrix},\\
&\Phi_{13}=\begin{bmatrix}-\gamma D^TN^TND & -\gamma D^TN^TND\\ -XD-\gamma D^TN^TND & -XD-\gamma D^TN^TND\end{bmatrix},\Phi_{22}=\begin{bmatrix}-\beta_1\overline{I}_1 & 0\\ 0 & -\beta_1\overline{I}_1\end{bmatrix},\\
&\Phi_{33}=\begin{bmatrix}-\beta_2\overline{I}_1+\gamma D^TN^TND & \gamma D^TN^TND\\ * & -\beta_3\overline{I}_1+\gamma D^TN^TND\end{bmatrix},\Phi_{44}=\begin{bmatrix}-\beta_3\overline{I}_1 & 0\\ 0 & -\gamma\overline{I}_1\end{bmatrix},\\
&\Lambda_{11}=-\mathscr{P}_1C-C_1^T\mathscr{P}+\beta_1M_{11}^TM_{11}+\epsilon\mathscr{P}_1+\gamma D^TN^TND,\overline{I}_1=\mathrm{diag}\{I,I\},\\
&\Lambda_{22}=\mathrm{sym}\{-\mathscr{P}_2C-XD\}+\beta_1M_{12}^TM_{12}+\epsilon\mathscr{P}_2+\gamma D^TN^TND.
\end{aligned}\tag{20}$$

Furthermore, the nonfragile estimator gain K of (8) is designed as $K=\mathscr{P}_2^{-1}X$.

Proof. First, we denote

$$\widetilde{C}=\begin{bmatrix}-C & 0\\ KD & -C-KD\end{bmatrix},\overline{E}=\begin{bmatrix}0\\ -KD\end{bmatrix},\mathscr{P}=\begin{bmatrix}\mathscr{P}_1 & 0\\ 0 & \mathscr{P}_2\end{bmatrix},\overline{K}=\begin{bmatrix}0 & 0\\ -KD & 0\end{bmatrix}.\tag{21}$$

Considering system (8), design the following Lyapunov function:

$$V(t)=\eta^T(t)\mathscr{P}\eta(t).\tag{22}$$

From Lemma 2, one obtains

$$\begin{aligned}D^\alpha V(t)&\le 2\eta^T(t)\mathscr{P}D^\alpha\eta(t)\\ &=2\eta^T(t)\mathscr{P}\big[\widetilde{C}\eta(t)+\overline{A}\varphi(\eta(t))\\ &\quad+\widetilde{E}e_k(t)+\widetilde{K}\eta(t-d)\big].\end{aligned}\tag{23}$$

It follows from Lemma 3 that

$$\begin{aligned}2\eta^T(t)\mathscr{P}\overline{A}\varphi(\eta(t))&\le\beta_1^{-1}\eta^T(t)\mathscr{P}\overline{AA}^T\mathscr{P}\eta(t)\\ &\quad+\beta_1\eta^T(t)G^TG\eta(t),\end{aligned}\tag{24}$$

$$\begin{aligned}2\eta^T(t)\mathscr{P}\widetilde{E}e_k(t)&\le\beta_2^{-1}\eta^T(t)\mathscr{P}\overline{K}\widetilde{E}^T\mathscr{P}\eta(t)+\beta_2e_k^T(t)e_k(t)\\ &\le\beta_2^{-1}\eta^T(t)\mathscr{P}\widetilde{E}\widetilde{E}^T\mathscr{P}\eta(t)+\beta_2\sigma\eta^T(t-d(t))\widetilde{I}^T\widetilde{I}\eta(t-d(t)),\end{aligned}\tag{25}$$

$$\begin{aligned}2\eta^T(t)\mathscr{P}\overline{K}\eta(t-d(t))&\le\beta_3^{-1}\eta^T(t)\mathscr{P}\overline{KK}^T\mathscr{P}\eta(t)\\ &\quad+\beta_3\eta^T(t-d(t))\eta(t-d(t)),\end{aligned}\tag{26}$$

where $\overline{I}=[-I,I]$ and $\widetilde{I}=[I,0]$.

Combining (24)–(36), we can get

$$\begin{aligned}D^\alpha V(t)&\le\eta^T(t)\Big[\mathscr{P}\widetilde{C}+\mathscr{P}\widetilde{E}_1+\widetilde{C}^T\mathscr{P}+\widetilde{E}_1^T\mathscr{P}+\beta_1^{-1}\mathscr{P}\overline{AA}^T\mathscr{P}\\ &\quad+\beta_1G^TG+\beta_2^{-1}\mathscr{P}\widetilde{E}\widetilde{E}^T\mathscr{P}+\beta_3^{-1}\mathscr{P}\widetilde{K}\widetilde{K}^T\mathscr{P}\Big]\eta(t)\\ &\quad+\eta^T(t-d(t))\Big[\beta_2\sigma\widetilde{I}^T\widetilde{I}+\beta_3\overline{I}_1^T\overline{I}_1\Big]\eta(t-d(t)).\end{aligned}\tag{27}$$

By employing Lemma 5, $\Phi<0$ is equivalent to

$$\overline{\Phi}+\gamma\overline{N}^T\overline{N}+\gamma^{-1}\overline{MM}^T<0,\tag{28}$$

where

$$\begin{aligned}&\overline{\Phi}=\begin{bmatrix}\mathscr{P}\overline{C}+\overline{C}^T\mathscr{P}+\beta_1M_1^TM_1+\varepsilon\mathscr{P}_1 & \mathscr{P}\overline{A} & \mathscr{P}\overline{E} & \mathscr{P}\overline{E}\widetilde{I}\\ * & -\beta_1\overline{I}_1 & 0 & 0\\ * & * & -\beta_2\overline{I}_1 & 0\\ * & * & * & -\beta_3\overline{I}_1\end{bmatrix},\\
&\overline{M}^T=\big[0,M^T\mathscr{P}_2,0_{n\times5n}]^T\big],\overline{N}=[ND,-ND,0,0,-ND,-ND,0].\end{aligned}\tag{29}$$

Defining an equation as follows:

$$\Delta\Phi=\overline{M}F(t)\overline{N}+\overline{N}^TF^T(t)\overline{M}^T,\tag{30}$$

we have

$$\Delta\Phi\le\gamma^{-1}\overline{MM}^T+\gamma\overline{N}^T\overline{N}.\tag{31}$$

Furthermore, from (28) and (31), we arrive at $\overline{\Phi}+\Delta\Phi<0$.

Based on Lemma 3, we can obtain

$$\begin{aligned}&\mathscr{P}\widetilde{C}+\mathscr{P}\widetilde{E}_1+\widetilde{C}^T\mathscr{P}+\widetilde{E}_1^T\mathscr{P}+\beta_1^{-1}\mathscr{P}\overline{AA}^T\mathscr{P}+\beta_1G^TG\\&\quad+\beta_2^{-1}\mathscr{P}\widetilde{E}\widetilde{E}^T\mathscr{P}+\beta_3^{-1}\mathscr{P}\widetilde{K}\widetilde{K}^T\mathscr{P}<-\varepsilon\mathscr{P}.\end{aligned}\tag{32}$$

Combining (27) and (32), we have

$$\begin{aligned}D^\alpha V(t)&\le-\epsilon\eta^T(t)\mathscr{P}\eta(t)\\&\quad+\mu\sup_{0\le d(t)\le d_M}\eta^T(t-d(t))\mathscr{P}\eta(t-d(t))\\&=-\varepsilon V(t)+\mu\sup_{0\le d(t)\le d_M}V(t-d(t)).\end{aligned}\tag{33}$$

It follows from Lemma 4 that (4) is an asymptotical estimator and system (3) is globally asymptotically stable. The proof is completed.

It is worth noting that the parameter uncertainties are often unavoidable resulting from the inaccuracy of modeling or the changing environment. In addition, the network output is composed of linear and nonlinear parts. Therefore, the following model of FNN is established:

$$\begin{cases}D^\alpha v(t)=-(C+\Delta C)v(t)+(A+\Delta A)f(v(t))+(B+\Delta B)f(v(t-\tau(t)))+J,\\ y(t)=Dv(t)+\widetilde{g}(v(t)),\end{cases}\tag{34}$$

where $\tau(t)$ is a time-varying delay satisfying $0\le\tau(t)\le\tau_M$. Here, τ_M is a constant. $\Delta A,\Delta B,\Delta C$ are parameter uncertainties which satisfy the following condition:

$$[\,\Delta A\ \ \Delta B\ \ \Delta C\,]=\overline{M}_2F_1(t)[\,N_1\ \ N_2\ \ N_3],\tag{35}$$

where $\overline{M}_2,N_1,N_2,N_3$ are known matrices and $F_1(t)$ is an unknown matrix function which satisfies $F_1(t)^TF_1(t)\le I$. □

Assumption 1. $\widetilde{g}$: $\mathbb{R}^n\longrightarrow\mathbb{R}^q$ stands for the nonlinear disturbance which satisfies the Lipschitz condition:

$$|\widetilde{g}(t,a)-\widetilde{g}(t,b)|\le|F(a-b)|,\tag{36}$$

where $\widetilde{g}(t,0)=0$ and F is a known constant matrix.

The estimator and estimation error dynamics are obtained as follows:

$$\begin{cases}D^\alpha\widehat{v}(t)&=-(C+\Delta C)\widehat{v}(t)+(A+\Delta A)f(\widehat{v}(t))+(B+\Delta B)f(\widehat{x}(t-\tau(t)))+J+(K+\Delta K)(\overline{y(t)}-D\widehat{v(t)}),\\ D^\alpha e(t)&=[-C-(K+\Delta K)D]e(t)+[-\Delta C+\Delta K)D]v(t)+A\widetilde{f}(e(t))+\Delta Af(v(t)+B\widetilde{f}(e(t-\tau(t)))\\&\quad+\Delta Bf(x(t-\tau(t)))-(K+\Delta K)e_y(t)-(K+\Delta K)Dx(t-d(t))-(K+\Delta K)g(x(t-d(t))).\end{cases}\tag{37}$$

The augmented system is derived as follows:

$$\begin{aligned}D^\alpha\eta(t)&=\widetilde{C}\eta(t)+\widetilde{A}\varphi(\eta(t))+\widetilde{B}\varphi(\eta(t-\tau(t)))\\&\quad+\widetilde{H}\eta(t-d(t))-\widetilde{G}g(\widetilde{I}\eta(t-d(t)))-\widetilde{L}e_y(t),\end{aligned}\tag{38}$$

where

$$\begin{aligned}&\widetilde{C}=\begin{bmatrix}-C-\Delta C&0\\-\Delta C+(K+\Delta K)D&-C-(K+\Delta K)D\end{bmatrix},\widetilde{A}=\begin{bmatrix}A+\Delta A&0\\\Delta A&A\end{bmatrix},\\&\widetilde{B}=\begin{bmatrix}B+\Delta B&0\\\Delta B&B\end{bmatrix},\widetilde{H}=\begin{bmatrix}0&0\\-(K+\Delta K)D&0\end{bmatrix},\widetilde{I}=\begin{bmatrix}0&0\\I&0\end{bmatrix},\\&\widetilde{G}=\begin{bmatrix}0&0\\K+\Delta K&0\end{bmatrix},\widetilde{L}=\begin{bmatrix}0\\K+\Delta K\end{bmatrix}.\end{aligned}\tag{39}$$

The following theorem is given to ensure the above system is asymptotically stable.

Theorem 2. *For given positive scalars $\phi,\vartheta_1,\vartheta_2$ satisfying $\phi>\vartheta_1+\vartheta_2$, the augmented system (48) is asymptotically stable if there exist a symmetric matrix $\mathscr{P}=diag\{\mathscr{P}_1,\mathscr{P}_2\}>0$ and seven scalars $\gamma_i(i=1,2,3)>0$, $\beta_i(i=1,2,\ldots,4)>0$ satisfying the following LMI:*

$$\Pi=\begin{bmatrix}\Pi_{11}&\Pi_{12}&\Pi_{13}&\Pi_{14}&\Pi_{15}&\Pi_{16}\\*&\Pi_{22}&0&\Pi_{24}&\Pi_{25}&0\\*&*&\Pi_{33}&0&0&0\\*&*&*&\Pi_{44}&\Pi_{45}&0\\*&*&*&*&\Pi_{55}&0\\*&*&*&*&*&\Pi_{66}\end{bmatrix}<0,\tag{40}$$

$$\Theta=\begin{bmatrix}\Lambda2&0\\*&\beta_1I-\vartheta_1\mathscr{P}_2\end{bmatrix}<0,\tag{41}$$

$$\Phi = \begin{bmatrix} \beta_2 M_{11}^T M_{11} - \vartheta_2 \mathscr{P}_1 & 0 \\ * & \beta_2 M12^T M_{12} - \vartheta_2 \mathscr{P}_2 \end{bmatrix} < 0, \tag{42}$$

where

$$\begin{aligned}
\Pi_{11} &= \begin{bmatrix} \Lambda 1 & D^T X^T - \gamma_3 D^T N_4^T N_4 D \\ * & \overline{Q}_2 2 + \gamma_3 D^T N_4^T N_4 D \end{bmatrix}, \Pi_{12} = \begin{bmatrix} -\gamma_3 D^T N_4^T N_4 D & \gamma_2 M_{41}^T N_2^T N_3 \\ -X D + \gamma_3 D^T N_4^T N_4 D & 0 \end{bmatrix}, \\
\Pi_{13} &= \begin{bmatrix} \mathscr{P}_1 B & 0 \\ 0 & \mathscr{P}_2 B \end{bmatrix}, \Pi_{14} = \begin{bmatrix} \gamma_3 D^T N_4^T N_4 & 0 \\ X - \gamma_3 D^T N_4^T N_4 D & 0 \end{bmatrix}, \Pi_{66} = \begin{bmatrix} -\gamma_2 I & 0 \\ * & -\gamma_3 I \end{bmatrix}, \\
\Pi_{15} &= \begin{bmatrix} -\gamma_3 D^T N_4^T N_4 & -\mathscr{P}_1 \overline{M}_2 \\ X - \gamma_3 D^T N_4^T N_4 D & -\mathscr{P}_2 \overline{M}_2 \end{bmatrix}, \Pi_{22} = \begin{bmatrix} -\beta_1 I + \gamma_3 D^T N_4^T N_4 D & 0 \\ * & -\beta_1 I \end{bmatrix}, \\
\Pi_{16} &= \begin{bmatrix} \mathscr{P}_1 \overline{M}_2 & 0 \\ \mathscr{P}_2 \overline{M}_2 & \mathscr{P}_2 \overline{M}_3 \end{bmatrix}, \Pi_{24} = \begin{bmatrix} -\gamma_3 D^T N_4^T N_4 & 0 \\ 0 & 0 \end{bmatrix}, \\
\Pi_{45} &= \begin{bmatrix} \gamma_3 N_4^T N_4 & 0 \\ 0 & 0 \end{bmatrix}, \Pi_{33} = \begin{bmatrix} -\beta_2 I + \gamma_2 N_3^T N_3 & 0 \\ * & -\beta_2 I \end{bmatrix}, \\
\Pi_{44} &= \begin{bmatrix} -\beta_3 I + \gamma_3 N_4^T N_4 & 0 \\ * & -\beta_3 I \end{bmatrix}, \Pi_{25} = \begin{bmatrix} -\gamma_3 D^T N_4^T N_4 & 0 \\ 0 & 0 \end{bmatrix}, \Pi_{55} = \begin{bmatrix} -\beta_4 I + \gamma_3 N_4^T N_4 & 0 \\ * & -\gamma_1 I \end{bmatrix}, \\
\Lambda 1 &= \overline{Q}_{11} + \gamma_2 M_{41}^T N_2^T N_2 M_{41} + \gamma_3 D^T N_4^T N_4 D, \\
\Lambda 2 &= \beta_1 I + \beta_3 M_{22}^T M_{22} + \beta_4 \sigma D^T D + \beta_4 \sigma \operatorname{sym}\left\{D^T M_3\right\} + \beta_4 \sigma M_3^T M_3 - \vartheta_2 \mathscr{P}_2.
\end{aligned} \tag{43}$$

Furthermore, the nonfragile estimator gain K is designed as $K = \mathscr{P}_2^{-1} X$.

Proof. Construct the following Lyapunov functional:

$$V(t) = \eta^T(t) \mathscr{P} \eta(t). \tag{44}$$

From Lemma 2, the following inequality is obtained:

$$\begin{aligned}
D^\alpha V(t) &\le 2\eta^T(t) \mathscr{P} D^\alpha \eta(t) \\
&= 2\eta^T(t) \mathscr{P} [\widetilde{C}\eta(t) + \widetilde{H}\eta(t - d(t)) + \widetilde{A}\varphi(\eta(t)) \\
&\quad + \widetilde{B}\varphi(\eta(t - \tau(t))) - \widetilde{G}_1 g(\overline{I}\eta(t - d(t))) - \widetilde{L} e_y(t)].
\end{aligned} \tag{45}$$

By using Lemma 1 and Lipschitz condition, one gets

$$\begin{aligned}
2\eta^T(t) \mathscr{P} \widetilde{H} \eta(t - d(t)) &\le \beta_1^{-1} \eta^T(t) \mathscr{P} \widetilde{H} \widetilde{H}^T \mathscr{P} \eta(t) \\
&\quad + \beta_1 \eta(t - d(t))^T \eta(t - d(t)),
\end{aligned} \tag{46}$$

$$\begin{aligned}
2\eta^T(t) \mathscr{P} \widetilde{B} \varphi(\eta(t - \tau(t))) &\le 2\eta(t)^T \mathscr{P} \widetilde{B} M_1 \eta(t - \tau(t)) \\
&\le \beta_2^{-1} \eta(t) \mathscr{P} \widetilde{B} \widetilde{B}^T \mathscr{P} \eta + \beta_2 \eta^T(t - \tau(t)) M_1^T M_1 \eta(t - \tau(t)),
\end{aligned} \tag{47}$$

$$\begin{aligned}
-2\eta^T(t) \mathscr{P} \widetilde{G} g(\overline{I}\eta(t - d(t))) &\le \beta_3^{-1} \eta^T(t) \mathscr{P} \widetilde{G} \widetilde{G}^T \mathscr{P} \eta(t) \\
&\quad + \beta_3 \eta^T(t - d(t)) \overline{I}^T M_2^T M_2 \overline{I} \eta(t - d(t)),
\end{aligned} \tag{48}$$

$$-2\eta^T(t) \mathscr{P} \widetilde{L} e_y(t) \le \beta_4^{-1} \eta^T(t) \mathscr{P} \widetilde{L} \widetilde{L}^T \mathscr{P} \eta(t) + \beta_4 e_y(t)^T e_y(t). \tag{49}$$

From event-triggered condition (5), we can obtain

$$\begin{aligned} e_y(t)^T e_y(t) &\le \sigma y^T(t_k h + jh) y(t_k h + jh) \\ &\le \sigma y^T(t - d(t)) y(t - d(t)) \\ &\le \sigma \eta^T(t - d(t)) \overline{D}^T \overline{D} \eta(t - d(t)) \\ &\quad + \sigma \eta^T(t - d(t)) \left[\overline{D}^T M_3 \widetilde{I} + \sigma \widetilde{I}^T M_3^T \overline{D} \right] \eta(t - d(t)) \\ &\quad + \sigma \eta^T(t - d(t)) \widetilde{I}^T M_3^T M_3 \widetilde{I} \eta(t - d(t)). \end{aligned} \tag{50}$$

Combining (45)–(50), one can get

$$\begin{aligned} D^\alpha V(t) &\le 2\eta^T(t) \mathscr{P} D^\alpha \eta(t) \\ &\le \eta^T(t) \Big[\mathscr{P} \widetilde{C} \eta(t) + \widetilde{C}^T \mathscr{P} + \mathscr{P} \widetilde{A} M_4 + M_4^T \widetilde{A}^T \mathscr{P} \\ &\quad + \beta_1^{-1} \mathscr{P} \widetilde{H} \widetilde{H}^T \mathscr{P} + \beta_2^{-1} \mathscr{P} \widetilde{B} \widetilde{B}^T \mathscr{P} + \beta_3^{-1} \mathscr{P} \widetilde{G} \widetilde{G}^T \mathscr{P} \\ &\quad + \beta_4^{-1} \mathscr{P} \widetilde{L} \widetilde{L}^T \mathscr{P} \Big] \eta(t) \\ &\quad + \eta^T(t - d(t)) \Big[\beta_1 \check{I} + \beta_3 \overline{I}^T M_2^T M_2 \overline{I} + \beta_4 \sigma \overline{D}^T M_3 \widetilde{I} \\ &\quad + \beta_4 \sigma \widetilde{I}^T M_3^T \overline{D} + \widetilde{I}^T M_3^T M_3 \widetilde{I} \Big] \eta(t - d(t)) \\ &\quad + \eta^T(t - \tau(t))) \left[\beta_2 M_1^T M_1 \right] \eta^T(t - \tau(t))), \end{aligned} \tag{51}$$

and therefore

$$\begin{aligned} &D^\alpha V(t) + \phi V(t) - \vartheta_1 \sup_{-\tau_M \le \omega \le 0} V(t + \omega, x(t + \omega)) - \vartheta_2 \sup_{-d_M \le \omega \le 0} V(t + \omega, x(t + \omega)) \\ &\quad \le \eta^T(t) \Big[\mathscr{P} \widetilde{C} \eta(t) + \widetilde{C}^T \mathscr{P} + \mathscr{P} \widetilde{A} M_4 + M_4^T \widetilde{A}^T \mathscr{P} + \beta_1^{-1} \mathscr{P} \widetilde{H} \widetilde{H}^T \mathscr{P} + \beta_2^{-1} \mathscr{P} \widetilde{B} \widetilde{B}^T \mathscr{P} + \beta_3^{-1} \mathscr{P} \widetilde{G} \widetilde{G}^T \mathscr{P} + \beta_4^{-1} \mathscr{P} \widetilde{L} \widetilde{L}^T \mathscr{P} \Big] \\ &\quad \cdot \eta(t) + \eta^T(t - d(t)) \\ &\Big[\beta_1 \check{I} + \beta_3 \overline{I}^T M_2^T M_2 \overline{I} + \beta_4 \sigma \overline{D}^T M_3 \widetilde{I} + \beta_4 \sigma \widetilde{I}^T M_3^T \overline{D} + \widetilde{I}^T M_3^T M_3 \widetilde{I} \Big] \eta(t - d(t)) \\ &\quad + \eta^T(t - \tau(t)) \Big) \left[\beta_2 M_1^T M_1 \right] \eta^T(t - \tau(t)) \Big) + \phi V(t) - \vartheta_1 \eta^T(t - \tau(t)) \mathscr{P} \eta(t - \tau(t)) - \vartheta_2 \eta^T(t - d(t)) \mathscr{P} \eta(t - d(t)). \end{aligned} \tag{52}$$

Based on the above inequations, we have

$$\begin{aligned} &D^\alpha V(t) + \phi V(t) - \vartheta_1 \sup_{-\tau_M \le \omega \le 0} V(t + \omega, x(t + \omega)) - \vartheta_2 \sup_{-d_M \le \omega \le 0} V(t + \omega, x(t + \omega)) \\ &\quad \le \eta^T(t) Q_1 \eta^T(t) + \eta^T(t - d(t)) Q_2 \eta^T(t - d(t)) + \eta^T(t - \tau(t)) Q_3 \eta^T(t - \tau(t)), \end{aligned} \tag{53}$$

where

$$\begin{aligned}
Q_1 &= \operatorname{sym}\left\{\mathscr{P}\tilde{C} + \mathscr{P}\tilde{A}M_4\right\} + \beta_1\mathscr{P}\tilde{H}\tilde{H}^T\mathscr{P} + \beta_2\mathscr{P}\tilde{B}\tilde{B}^T\mathscr{P} \\
&\quad + \beta_1\mathscr{P}\tilde{G}\tilde{G}^T\mathscr{P} + \beta_4\mathscr{P}\tilde{L}\tilde{L}^T\mathscr{P} + \phi\mathscr{P}, \\
Q_2 &= \beta_1\check{I} + \beta_3\bar{I}^T M_2^T M_2\bar{I} + \beta_4\sigma\bar{D}^T\bar{D} + \operatorname{sym}\left\{\beta_4\sigma\bar{D}^T M_3\tilde{I}\right\} \\
&\quad + \beta_4\sigma\tilde{I}^T M_3^T M_3\tilde{I} - \vartheta_1\mathscr{P}, \\
Q_3 &= \beta_2 M_1^T M_1 - \vartheta_2\mathscr{P}.
\end{aligned} \tag{54}$$

By Lemma 5, $\Pi < 0$ is equivalent to

$$\left(\bar{Q} + \gamma_1 S_1^T S_1 + \gamma_2 S_2^T S_2 + \gamma_3 S_3^T S_3\right) + \gamma_1^{-1} R_1 R_1^T + \gamma_2^{-1} R_2 R_2^T + \gamma_3^{-1} R_3 R_3^T < 0, \tag{55}$$

where

$$\begin{aligned}
\bar{Q} &= \begin{bmatrix} \operatorname{sym}\{\mathscr{P}C_1 + \mathscr{P}A_1M_4\} & \mathscr{P}H_1 & \mathscr{P}B_1 & \mathscr{P}G_1 & \mathscr{P}L_1 \\ * & -\beta_1\check{I} & 0 & 0 & 0 \\ * & * & -\beta_2\check{I} & 0 & 0 \\ * & * & * & -\beta_3\check{I} & 0 \\ * & * & * & * & -\beta_4\check{I} \end{bmatrix}, \\
R_1 &= \begin{bmatrix} -\mathscr{P}_1\overline{M_2} \\ -\mathscr{P}_2\overline{M_2} \\ 0_{7n\times n} \end{bmatrix}, R_2 = \begin{bmatrix} \mathscr{P}_1\overline{M_2} \\ \mathscr{P}_2\overline{M_2} \\ 0_{7n\times n} \end{bmatrix}, \\
R_3 &= \begin{bmatrix} 0 \\ \mathscr{P}_2\overline{M_2} \\ 0_{7n\times n} \end{bmatrix}, S_1 = \left[\, N_1, 0_{n\times 8n} \,\right], \\
S_2 &= \left[\, N_2M_{41}, 0_{n\times 3n, N_3, 0_{n\times 4n}} \,\right], S_3 = \left[\, N_4D, -N_4D, -N_4D, 0_{n\times 3n}, N_4, 0, N_4 \,\right].
\end{aligned} \tag{56}$$

Let

$$\begin{aligned}
\bar{Q}' &= R_1F_1(t)S_1 + R_2F_1(t)S_2 + R_3F_2(t)S_3 + S_1^T F_1^T(t)R_1^T \\
&\quad + S_2^T F_1^T(t)R_2^T + S_3^T F_2^T(t)R_3^T \\
&\le \gamma_1 S_1^T S_1 + \gamma_2 S_2^T S_2 + \gamma_3 S_3^T S_3 + \gamma_1^{-1} R_1 R_1^T \\
&\quad + \gamma_2^{-1} R_2 R_2^T + \gamma_3^{-1} R_3 R_3^T.
\end{aligned} \tag{57}$$

Then, one gets $\bar{Q} + \bar{Q}' < 0$. Based on Lemma 5, (55) and (57) imply that $Q_1 \le 0$. According to (40) and (42), we know that $Q_2 < 0$, and $Q_3 < 0$. Therefore, we can obtain

$$\begin{aligned}
&D^\alpha V(t) + \phi V(t) - \vartheta_1 \sup_{-\tau_M \le \omega \le 0} V(t+\omega, v(t+\omega)) \\
&\quad - \vartheta_2 \sup_{-d_M \le \omega \le 0} V(t+\omega, v(t+\omega)) \le 0.
\end{aligned} \tag{58}$$

Therefore, system (37) is an asymptotical estimator of (34) by using Lemma 6. This completes the proof. □

4. Numerical Example

To illustrate the theoretical results, two numerical examples are shown in this section.

Example 1.

$$\mathscr{A} = \begin{bmatrix} -1.2 & -0.5 & 1 \\ 1 & -0.2 & 1.6 \\ 0.2 & 0.8 & -1 \end{bmatrix}, \mathscr{C} = \begin{bmatrix} 0.3 & 0 & 0 \\ 0 & 0.4 & 0 \\ 0 & 0 & 0.3 \end{bmatrix}, D = \begin{bmatrix} 0.2 & 0 & 0 \\ 0 & 0.28 & 0 \\ 0 & 0 & 0.1 \end{bmatrix}, \tag{59}$$

where $\overline{M} = \operatorname{diag}\{0.4, 0.4, 0.4\}$, $N = \operatorname{diag}\{0.3, -0.3, 0.3\}$, and $M_{11} = M_{12} = \operatorname{diag}\{0.2, 0.2, 0.2\}$.

The other parameters are given as $\alpha = 0.98$, $\tau = 1$, $\mathscr{V} = [0.5, 0.2, -0.8]^T$. The activation function is given as follows:

$$\hbar(v_1, v_2, v_3) = \left\{\sin(0.4\pi v_1), \cos(0.2\pi v_2), \sin(0.6\pi v_3)\right\}. \tag{60}$$

By using Matlab to solve LMIs (26) and (27), the gain matrix K can be obtained as

$$K = \begin{bmatrix} 1.5663 & 0.1752 & -1.0655 \\ 0.1475 & 1.9113 & -0.8569 \\ -0.7003 & -0.7138 & 1.6980 \end{bmatrix}. \tag{61}$$

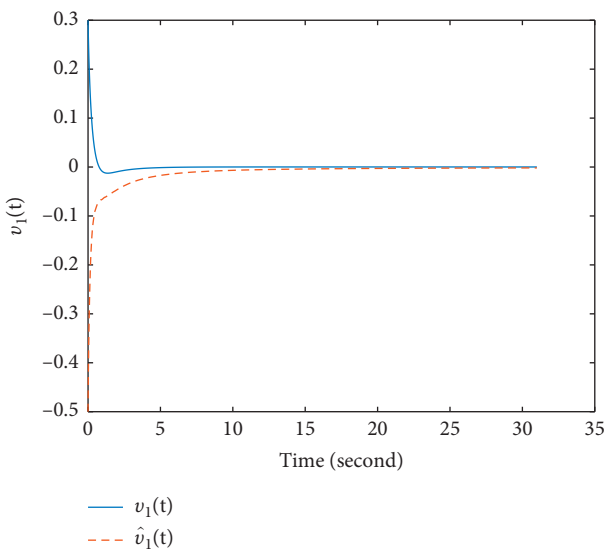

Figure 1: Trajectories of $v_1(t)$ and $\hat{v}_1(t)$.

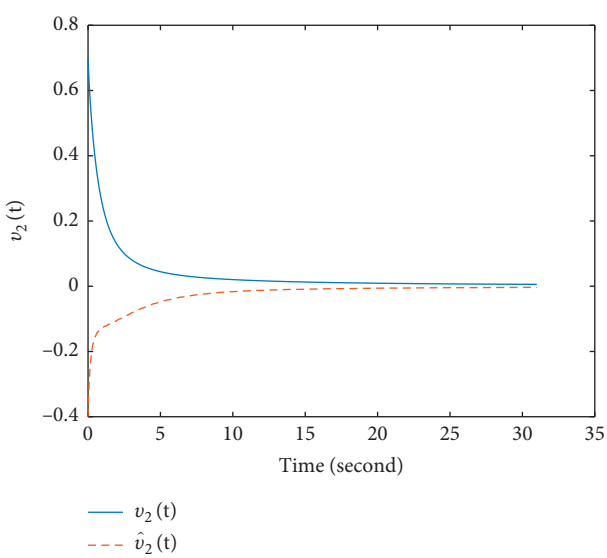

Figure 2: Trajectories of $v_2(t)$ and $\hat{v}_2(t)$.

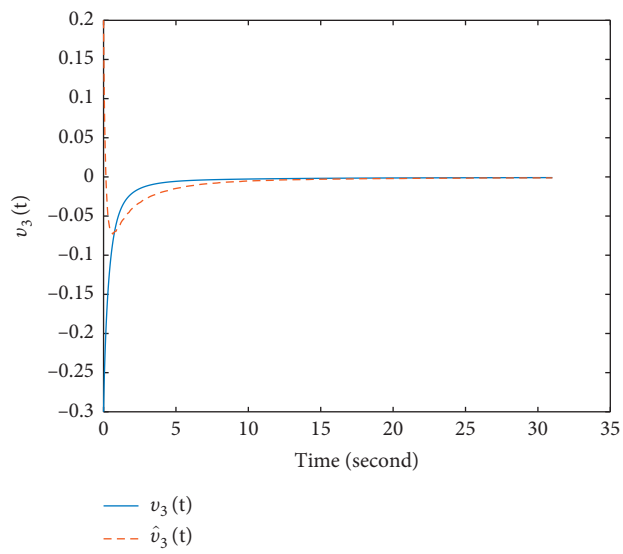

Figure 3: Trajectories of $v_3(t)$ and $\hat{v}_3(t)$.

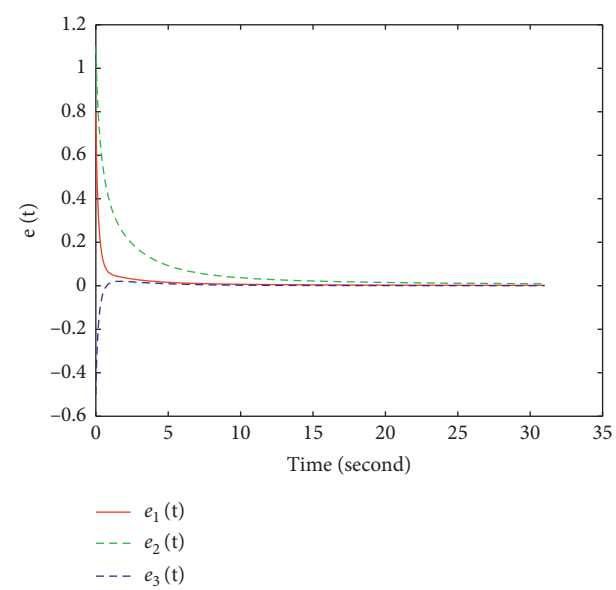

Figure 4: The estimation errors.

The simulation results are shown in Figures 1–3, where $v_1(t), v_2(t), v_3(t)$ represent the true states and their estimates $\hat{v}_1(t), \hat{v}_2(t), \hat{v}_3(t)$ and the initial conditions are ($\forall t \in [-1, 0]$): $v(t) = [0.3, 0.7, -0.3]^T, \hat{v}(t) = [-0.5, -0.4, 0.2]^T$.

Figure 4 shows the estimate error $e_i(t) \longrightarrow 0$ as $t \longrightarrow \infty$. According to the simulation results, we can see the effectiveness of the estimator design method. Figure 5 shows the release instants and intervals with the threshold parameter $\sigma = 0.06$.

Example 2. To verify that the estimator contains uncertain terms in (34), the following fractional-order model is shown, and the corresponding parameters are as follows:

$$A = \begin{bmatrix} -0.6 & -0.5 & 1 \\ 0.1 & -0.2 & 1 \\ 0.2. & 0.3 & -1 \end{bmatrix}, B = \begin{bmatrix} 0.2 & -0.2 & 0.1 \\ 0.3 & -0.2 & 0.1 \\ -0.4 & -0.1 & 0.3 \end{bmatrix}, C = \begin{bmatrix} 0.2 & 0 & 0 \\ 0 & 0.2 & 0 \\ 0 & 0 & 0.3 \end{bmatrix}, \tag{62}$$

where $\overline{M}_2 = \text{diag}\{0.4, 0.2, 0.4\}$, $\overline{M}_3 = \text{diag}\{0.1, 0.1, 0.1\}$, $M_{11} = M_{12} = M_{41} = M_{42} = \text{diag}\{0.2, 0.2, 0.2\}$, $N_1 = N_2 = \text{diag}\{0.1, 0.1, 0.1\}$, and $N_3 = N_4 = \{0.2, 0.2, 0.2\}$. Besides, $\alpha = 0.92$, and the time delays are set as $\tau_M = 1, d_M = 0.1, J = [0.01, 0.02, -0.01]^T$. The measurement output is $\tilde{g}(t, v) = [\tanh(0.4\pi v_1), \tanh(0.2\pi v_2), \tanh(0.6\pi v_3))]$. Let the activation function be $\hbar(v_1, v_2, v_3) = [\tanh(0.4\pi v_1), \tanh(0.3\pi v_2), \tanh(0.2\pi v_3))]$.

By using Matlab to solve the LMI (37), the gain matrix K can be obtained as

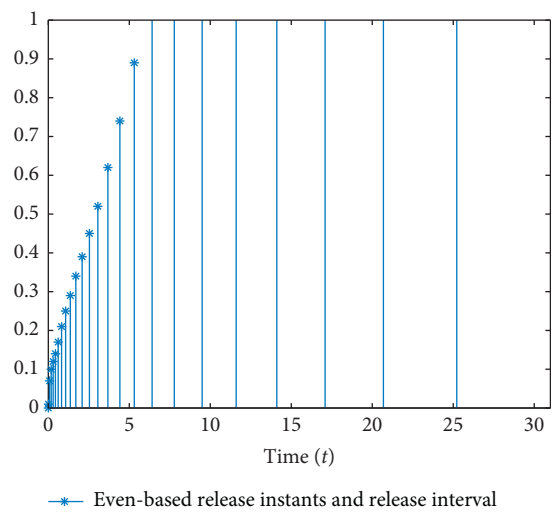

Figure 5: Event-triggered release instants and intervals of Theorem 1.

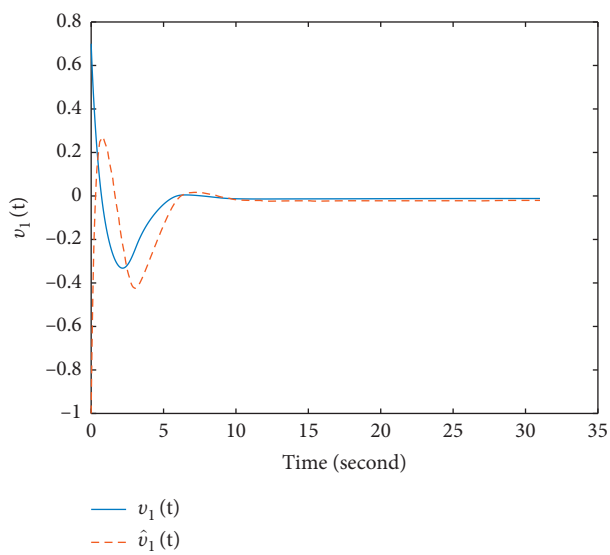

Figure 6: Trajectories of $v_1(t)$ and $\hat{v}_1(t)$.

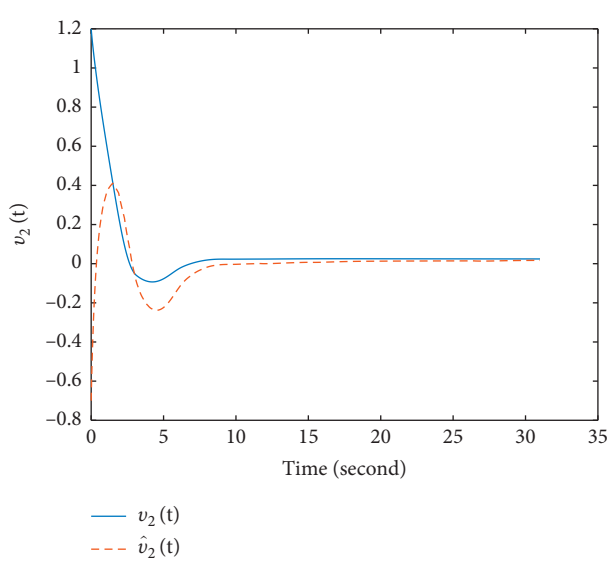

Figure 7: Trajectories of $v_2(t)$ and $\hat{v}_2(t)$.

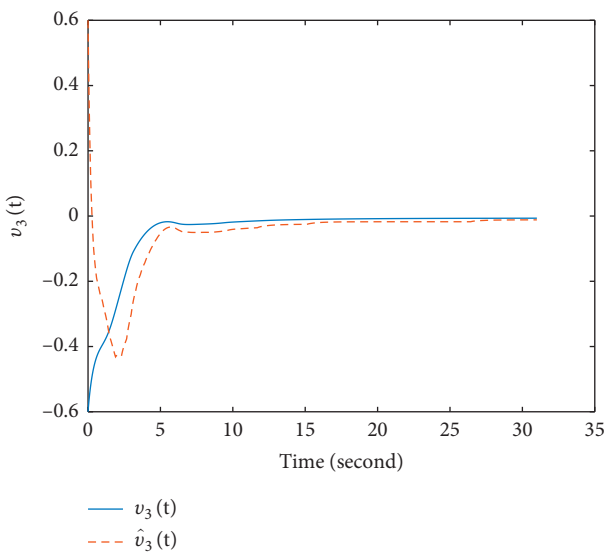

Figure 8: Trajectories of $v_3(t)$ and $\hat{v}_3(t)$.

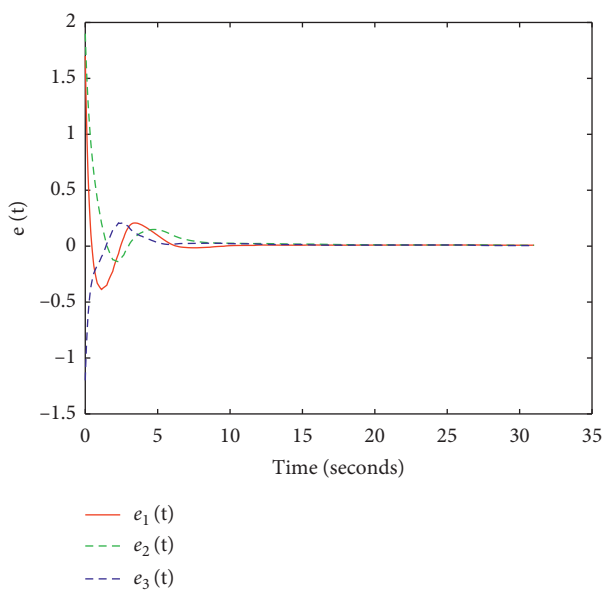

Figure 9: The estimation errors.

$$K = \begin{bmatrix} 1.4199 & 0.2566 & -1.4064 \\ 0.0808 & 1.2616 & -0.6868 \\ -0.3186 & -0.3723 & 2.8109 \end{bmatrix}. \quad (63)$$

The simulation results are shown in Figures 6–8, where $v_1(t), v_2(t), v_3(t)$ represent the true states and their estimates $\hat{v}_1(t), \hat{v}_2(t), \hat{v}_3(t)$ are depicted, respectively, with the initial condition ($\forall t \in [-1, 0]$.): $v(t) = [0.7; 1.2; \ -0.6]$, $\hat{v}(t) = [-1; -0.7; 0.6]$.

Figure 9 shows the estimate error $e_1(t), e_2(t), e_3(t)$, as $t \longrightarrow \infty$. In Figure 8, we can see clearly the error states $e_i(t) \longrightarrow 0$. Figure 10 shows the release instants and intervals with $\sigma = 0.06$. According to the figures, we can see that the simulation results voiced the effectiveness of the estimator design.

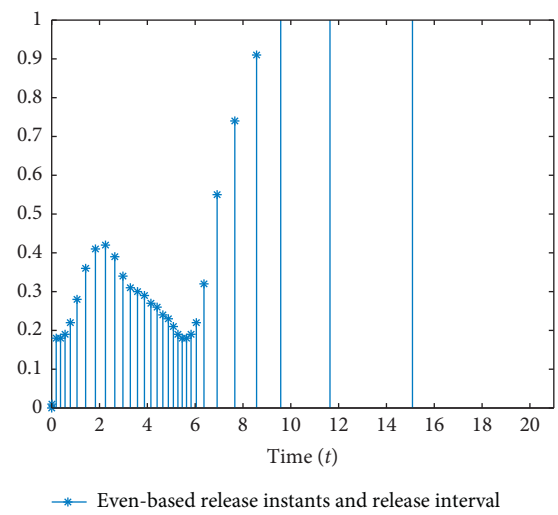

Figure 10: Event-triggered release instants and intervals of Theorem 2.

5. Conclusions

This paper has investigated the nonfragile SE issue under the ETM for the FNNs with time delays. Sufficient conditions have been obtained to ensure the asymptotic stability of the considered system by means of the fractional-order Lyapunov functions and the LMI method. The gain matrix of the nonfragile estimator has been characterized by a LMI. At last, two numerical results have confirmed the validity of the designed estimator. In addition, the results could be extended to the SE issue of discrete FNNs with fading measurements and so on.

Data Availability

In this paper, the initial conditions have been given. As a control system, the data in the Numerical Example is suffienct to support this study.

Conflicts of Interest

The authors declare that they have no conflicts of interest.

Acknowledgments

This study was supported by the Natural Science Funds of Jiangsu Province (no. BK20180467).

References

[1] Y. H. Hu, J. N. Hwang, and S. W. Perry, "Handbook of neural network signal processing," *IEEE Transactions on Neural Networks*, vol. 16, no. 3, p. 780, 2005.

[2] C. M. Bishop, "Neural networks for pattern recognition," *Journal of Scientific Research & Development Manuscript Pm*, vol. 12, no. 5, pp. 1235–1242, 1995.

[3] P. Selvaraj, R. Sakthivel, and O. M. Kwon, "Finite-time synchronization of stochastic coupled neural networks subject to Markovian switching and input saturation," *Neural Networks*, vol. 105, p. 154, 2018.

[4] Z. Feng and J. Lam, "Stability and dissipativity analysis of distributed delay cellular neural networks," *IEEE Transactions on Neural Networks*, vol. 22, no. 6, pp. 976–981, 2011.

[5] Z. Guo, J. Wang, Z. Yan et al., "Attractivity analysis of memristor-based cellular neural networks with time-varying delays," *IEEE Transactions on Neural Networks and Learning Systems*, vol. 25, no. 4, pp. 704–717, 2014.

[6] Y. Chen, Z. Wang, Y. Liu, and F. E. Alsaadi, "Stochastic stability for distributed delay neural networks via augmented Lyapunov-Krasovskii functionals noise filtering for diagnosing orthopedic implant failures, IEEE Trans," *Applied Mathematics and Computation*, vol. 338, no. 4, pp. 8691092–8811100, 2018.

[7] Z. Zhao, Z. Wang, L. Zou et al., "Finite-time state estimation for delayed neural networks with redundant delayed channels," *IEEE Transactions on Systems, Man, and Cybernetics*, vol. 52, pp. 1–11, 2019.

[8] H. Huang, G. Feng, J. Cao et al., "Robust state estimation for uncertain neural networks with time-varying delay," *IEEE Transactions on Neural Networks*, vol. 19, no. 8, pp. 1329–1339, 2008.

[9] X.-M. Zhang and Q.-L. Han, "State estimation for static neural networks with time-varying delays based on an improved reciprocally convex inequality," *IEEE Transactions on Neural Networks and Learning Systems*, vol. 29, no. 4, pp. 1376–1381, 2018.

[10] J. Liang, Z. Wang, X. Liu et al., "State estimation for coupled uncertain stochastic networks with missing measurements and time-varying delays: the discrete-time case," *IEEE Transactions on Neural Networks*, vol. 20, no. 5, pp. 781–793, 2009.

[11] D. Ding, Q.-L. Han, X. Ge, and J. Wang, "Secure state estimation and control of cyber-physical systems: a survey," *IEEE Transactions on Systems, Man, and Cybernetics: Systems*, vol. 51, no. 1, pp. 176–190, 2021.

[12] H. Dong, Z. Wang, S. X. Ding, and H. Gao, "Finite-horizon reliable control with randomly occurring uncertainties and nonlinearities subject to output quantization," *Automatica*, vol. 52, pp. 355–362, 2015.

[13] H. Gao and C. Wang, "A delay-dependent approach to RobustH_inftyFiltering for uncertain discrete-time state-delayed systems," *IEEE Transactions on Signal Processing*, vol. 52, no. 6, pp. 1631–1640, 2004.

[14] Y. Yu, H. Dong, Z. Wang, W. Ren, and F. E. Alsaadi, "Design of non-fragile state estimators for discrete time-delayed neural networks with parameter uncertainties," *Neurocomputing*, vol. 182, pp. 18–24, 2016.

[15] J. H. Park, "Robust non-fragile control for uncertain discrete-delay large-scale systems with a class of controller gain variations," *Applied Mathematics and Computation*, vol. 149, no. 1, pp. 147–164, 2004.

[16] F. Yang, H. Dong, Z. Wang, W. Ren, and F. E. Alsaadi, "A new approach to non-fragile state estimation for continuous neural networks with time-delays," *Neurocomputing*, vol. 197, no. 197, pp. 205–211, 2016.

[17] S. Rajavel, R. Samidurai, J. Cao, A. Alsaedi, and B. Ahmad, "Finite-time non-fragile passivity control for neural networks with time-varying delay," *Applied Mathematics and Computation*, vol. 297, pp. 145–158, 2017.

[18] D. Ding, Z. Wang, and Q.-L. Han, "A set-membership approach to event-triggered filtering for general nonlinear systems over sensor networks," *IEEE Transactions on Automatic Control*, vol. 65, no. 4, pp. 1792–1799, 2020.

[19] Z.-P. Jiang and T.-F. Liu, "A survey of recent results in quantized and event-based nonlinear control," *International Journal of Automation and Computing*, vol. 12, no. 5, pp. 455–466, 2015.

[20] L. Zou, Zi-D. Wang, and D.-H. Zhou, "Event-based control and filtering of networked systems: a survey," *International Journal of Automation and Computing*, vol. 14, no. 3, 2017.

[21] E. A. Boroujeni and H. R. Momeni, "Non-fragile nonlinear fractional order observer design for a class of nonlinear fractional order systems," *Signal Processing*, vol. 92, no. 10, pp. 2365–2370, 2012.

[22] M. Xiong, G. Ju, and Y. Tan, "Robust state estimation for fractional-order nonlinear uncertain systems via adaptive event-triggered communication scheme," *IEEE Access*, vol. 7, pp. 115002–115009, 2019.

[23] I. Podlubny, *Fractional Differential Equations: an Introduction to Fractional Derivatives, Fractional Differential Equations, to Methods of their Solution and Some of their applications*, Elsevier, Amsterdam, Netherlands, 1998.

[24] A. A. Kilbas, H. M. Srivastava, and J. J. Trujillo, *Theory and Applications of Fractional Differential equations*, Elsevier, Amsterdam, Netherlands, 2006.

[25] D. Yue, E. Tian, and Q. L. Han, "A delay system method for designing event-triggered controllers of networked control systems," *IEEE Transactions on Automatic Control*, vol. 58, no. 2, pp. 475–481, 2012.

[26] E. N. Sanchez and J. P. Perez, "Input-to-state stability (ISS) analysis for dynamic neural networks," *IEEE Transactions on Circuits and Systems I: Fundamental Theory and Applications*, vol. 46, no. 11, pp. 1395–1398, 1999.

[27] S. Zhang, Y. Yu, J. Yu et al., "LMI conditions for global stability of fractional-order neural networks," *IEEE Transactions on Neural Networks and Learning Systems*, vol. 28, no. 10, pp. 2423–2433, 2017.

[28] L. Xie, "Output feedback H∞ control of systems with parameter uncertainty," *International Journal of Control*, vol. 63, no. 4, pp. 741–750, 1996.

[29] Y. Li, Y. Chen, and I. Podlubny, "Stability of fractional-order nonlinear dynamic systems: Lyapunov direct method and generalized Mittag-Leffler stability," *Computers & Mathematics with Applications*, vol. 59, no. 5, pp. 1810–1821, 2010.

[30] S. Boyd, L. El Ghaoui, E. Feron et al., *Linear Matrix Inequalities in System and Control Theory*, Society for Industrial and Applied Mathematics, Philadelphia, PA, USA, 1994.

[31] P. Liu, M. Kong, and Z. Zeng, "Projective synchronization analysis of fractional-order neural networks with mixed time delays," *IEEE Transactions on Cybernetics*, 2020.

Hindawi
Discrete Dynamics in Nature and Society
Volume 2020, Article ID 6515142, 19 pages
https://doi.org/10.1155/2020/6515142

Research Article

A Fuzzy Programming Model for Positioning Customer Order Decoupling Point Based on QFD in Logistics Service with Mass Customization

Guanxiong Wang [1] **and Xiaojian Hu** [2,3]

[1] *School of Business, Anhui University, Hefei, China*
[2] *School of Management, Hefei University of Technology, Hefei, China*
[3] *Key Laboratory of Process Optimization and Intelligent Decision-Making, Ministry of Education, Hefei, China*

Correspondence should be addressed to Guanxiong Wang; 767747816@qq.com

Received 23 July 2020; Revised 20 October 2020; Accepted 21 October 2020; Published 6 November 2020

Academic Editor: Wangyan Li

Mass customization logistics service mode provides a new way to maintain the sustainable cooperative relationship between customers and integrators. One of the key factors to maintain the sustainable development of logistics service supply chain under MC mode is to locate a suitable customer order decoupling point (CODP) location. This paper investigates the problem of CODP in the logistics service supply chain based on the fuzzy set theory under the mass customization mode. With the help of a fuzzy QFD method and a new service quality function that we constructed, this paper quantifies the quality of a logistics service when the LSI selects a different CODP. Then, the fuzzy set of the high-quality logistics service and the fuzzy set of the satisfactory delivery time are built. Based on those two new fuzzy sets, this paper builds a new fuzzy programming model on CODP positioning. The solving methods of this model under different conditions are given. Finally, the influence of some important parameters on the optimal CODP position is studied by sensitivity analysis on a specific numerical case.

1. Introduction

Against the background of steadily growing transport volumes and increasingly fierce market competition, it is of paramount importance for the logistics service integrators (LSI) to provide customers with customized services to meet the diverse needs of the market and maintain sustainable partnership with customers. Based on this, more and more logistics enterprises are making use of the scale effect as much as possible to reduce the total logistics cost while providing customized services. In other words, those logistics enterprises try to implement mass customization (MC) in the logistics service supply chain [1, 2]. MC can be seen as a collaborative optimization process between a company and its customers with the goal of finding the best match between the company's capabilities and the customers' needs [3–5].

Compared with other types of service industries, there are some unique characteristics in the logistics service industry. At first, the degree of the customer's participation is not high in the process of providing logistics services. After the order is submitted, the customer only needs to wait for the order to complete, without the need for full participation in the logistics service process, which means that the fluctuation of the service requirement is low. Second, general service emphasizes the immediacy of service provision; however, customers have relaxed their requirements for time in the process of providing logistics service. Customers often set a time constraint and require logistics enterprises to fulfill orders within this time limit. For the abovementioned reasons, implementing mass customization in the logistics service supply chain is flexible.

An important issue of mass customization is locating the customer order decoupling point (CODP) [6–9]. In the

logistics service supply chain, CODP is the boundary between mass logistics services and customized logistics services [10]. Different CODP locations will not only affect the benefits of LSI but also affect the service quality of the whole logistics service supply chain. Therefore, evaluating the service quality level of logistics service supply chain with different CODP locations will help LSI to improve the logistics service process sustainably and provide customers with better service.

Regarding a mass customization logistics service, customer enterprises outsource their logistics tasks to LSIs. LSIs analyze the characteristics and the customized requirements of those logistics tasks after the orders arrived; then, they disassemble the logistics process into many specific service procedures according to the actual situation. Finally, by collaborating with functional logistics service providers (denoted as FLSPs), they provide mass service for that shared service part and customized logistics service for the subsequent processes that have special requirements. Thus, it is imperative to consider the effects of the position of the CODP both on the comprehensive performance of the LSI logistics service and the promotion of customer satisfaction [7, 9, 11].

For logistics service integrators, the goal is to maximize profits with a precondition of satisfying the customers' requirements [12, 13]. Different from providing standardized services, LSIs provide customized and variant service in the MC environment. Therefore, an LSI can charge different prices for logistics services according to the degree of customization, so as to maximize profits.

For customer enterprises, what they value most is logistics service quality (denoted as LSQ) [14–16]. Since there is no uniform standard to measure service quality, most of the current studies evaluate logistics service quality through qualitative research [17]. Many of those studies include lead time in the service evaluation system as an important quantitative index together with other qualitative indicators [18, 19]. Most studies considered that the sooner the LSI completes the logistics orders, the more satisfied the customer is. In reality, however, customer enterprises want lead time to be close to their preset time rather than the shortest delivery time, since the product recipient (for instance, terminal retailers) will increase inventory costs if the LSI delivers goods too early, and if the LSI delivers goods too late, it will affect the recipient's sale, inventory, and replenishment.

Based on a review of the literature and the analysis of practical problems related to logistics enterprises, we found that there are three problems that should be solved for the LSI in the mass customization circumstance. (1) How to measure logistics service quality: because there is no uniform standard to measure the logistics service quality, and the quality of service is difficult to quantify. Therefore, it is a complex problem to translate this type of indicators into specific constraint conditions in a programming model. (2) How to describe the uncertainty of the customers' service requirements: as mentioned above, the customers' requirements for service quality and lead time are indeterminate, how to reflect those uncertainties in mathematical model is another problem. In the previous research, customer requirements were regarded as deterministic and the variability and volatility of customer requirements were ignored. Therefore, most of the constraints on the optimized model for CODP positioning are deterministic [20–22]. (3) Pricing strategy of differentiated services: since the logistics services provided by the LSI are customized and differentiated, the costs and delivery time will be different due to the different degrees of customization. Therefore, an urgent problem for LSIs is how to price for differentiated services.

The problems mentioned above will be discussed in this paper and a fuzzy programming model for positioning CODP is developed. This paper combines quantitative analysis and qualitative analysis to measure customer satisfaction using qualitative indicators and quantitative indicators, and our contributions in this paper are as follows.

First, based on the fuzzy theory, this paper constructs two new fuzzy sets: the fuzzy set of high-quality logistics service and the fuzzy set of satisfactory delivery time. Then, based on those two fuzzy sets, a new fuzzy programming model on CODP positioning with fuzzy constraints is developed and introduced in this paper. Compared with deterministic constraints, fuzzy constraint sets can reflect the customer's demands more completely and more accurately. In this paper, the research on CODP position is extended from deterministic programming to fuzzy programming, which provides more ideas and methods for researchers or business decision makers.

Second, the fuzzy Quality Function Deployment method is used to characterize the logistics service quality under different CODP conditions as a specific score, and by using the logistics service quality function constructed in this paper, the score is expressed as a more intuitive result so that the decision maker can more clearly see the difference in service quality when choosing different CODPs. This method comprehensively considers the impact of various qualitative indicators on logistics service quality, so it can improve logistics service quality sustainably according to this method.

Third, through numerical case analysis, this paper discusses which parameters have a significant impact on the location of the CODP, to provide managers with effective management insights, improve logistics enterprise operation efficiency, and reduce logistics costs.

The rest of the paper is organized as follows. In Section 2, we review and summarize the research status of mass customization in service field and the research progress of CODP positioning. In Section 3, the conditional assumptions and the mathematical expression of this model are presented. In Section 4, the quantify methods of some important indicators are given in Section 4.1; then, we build a fuzzy programming model with two fuzzy constraints and provide methods to solve the model. In Section 5, the feasibility of the model is verified through a numerical example, and a sensitivity analysis is performed for the parameters of the model to evaluate the effect of those parameters on the results. In Section 6, we summarize the research process and the significance of this study and provide some important implications for management and a possible future research direction.

2. Literature Review

2.1. MC in the Service Industry. Mass customization mode originated from manufacturing industry [23]. Due to the heterogeneity and invisibility of services and the volatility of service demand, there are relatively few research studies on the implementation of mass customization mode in service industry. In the early stage, scholars and practitioners began to explore the possibility of implementing mass customization in service industry [3], for example, Moon et al. developed a method to design customized service families using game theory to simulate situations involving dynamic market environments [24]; Wang focused on service mass customization, analyzed the shortcomings of traditional SaaS and service composition methods, and proposed "service network" as a means to solve the contradiction between "large-scale standardization" and "personalization" [25].

At present, the research on mass customization mode of service industry can be roughly divided into two categories. The first one is about the concept, strategic thinking, and key elements of implementing mass customization mode in service industry, for instance, Peters et al. summarized the challenges of implementing mass customization in service environment and proposed the driving factors for enterprises to implement service mass customization mode [26]. The second kind of research mainly focuses on the specific operation problems of mass customization in the service supply chain, such as the joint optimization of supplier selection and order allocation [27] and optimal customization degree or CODP positioning under the mode of logistics service mass customization [21].

As can be seen from the literature review above, although mass customization has received increasing attention, the research and application of MC in the service industry is still relatively scarce; at present, only a small number of service industries have successfully implemented a mass customization service mode.

2.2. CODP Position. One of the key problems in mass customization production or service mode is to determine the optimal customer order decoupling point [11, 28]. Mass customization mode originated from the field of manufacturing, so the research on CODP is mostly focused on manufacturing industry [6], for instance, Jeong et al. proposed a dynamic model to simultaneously determine the optimal location of decoupling points and production inventory planning in the supply chain, so as to minimize the total cost of deviation from target productivity and target inventory level [29]. Schoenwitz proposed a systematic approach to determine the alignment of CODP configurations at product, category, and component levels, with customer preferences in terms of their customization requirements [30].

The research on CODP positioning can be divided into single CODP positioning research and multiple CODP positioning research. Research on single CODP, for instance, de Keizer et al. proposed a network design model for perishable products that integrates decision-making on hub locations with the positioning of the CODP and the determination of the level of postponement [31]; Liu et al. proposed the optimal decision model of customer of CODP for order insertion scheduling in the logistics service supply chain [13], research on multiple CODP, for instance. In order to adapt to the dynamic environment, Wang and Chen proposed a multi-CODP positioning and adjustment system [21]. Shidpour et al. studied the impact of single CODP and multiple CODPs on product diversity based on enterprise profit and customer perceived value under service time constraint [32]; Cannas et al. assessed the potential impact of a unique two-dimensional customer order decoupling point framework and evaluated the managerial approaches employed in different decoupling configurations [33].

With the development of the service supply chain, more and more scholars begin to pay attention to the positioning of CODP in the service supply chain. For example, Wang et al. proposed a joint optimization model considering both order allocation and CODP positioning under the mode of mass customization of logistics services [28]. Guo et al. proposed a Formulation-Exploration method to make decisions on CODP positioning and improve the supply chain to support mass customization [34]. Liu proposed a determination method of optimal customization degree of the logistics service supply chain with mass customization service [35].

From the above literature review, it is not difficult to find that there are few research studies on the positioning of CODP in the service industry, and the positioning methods of CODP are mostly quantitative or qualitative. However, the research on the combination of quantitative research and qualitative research to determine the optimal CODP location is still rare.

3. Model Description and Model Assumptions

After receiving orders from product demanders, customer enterprises outsource their logistics tasks (including transportation, labelling, assembly, and distribution) to the LSI. The first step for the LSI is to analyze the features of this logistics order and the customized requirements of the customer enterprises, break down complex tasks into N sequential subprocedures, and then assign those subprocedures to the appropriate FLSPs. In other words, the entire logistics task will be completed by the LSI and many FLSPs. The LSIs will price logistics service according to the degree of customization compared with standardized service. The customer enterprises not only propose customized requirements but also set high requirements for service flexibility and reliability, i.e., the higher the logistics service quality is, the more satisfied the customers are. In addition, customer enterprises desire a lead time close to the time interval that they preset instead of the shortest delivery time.

Our aim is to find an optimal CODP (the position of the CODP is denoted by $k = i$ or k_i), all of the subprocedures before the CODP will implement a mass service strategy, and the subprocedures after the CODP will implement a customized service strategy according to the customer's

requirements; thus, the LSI will maximize profits as well as meet customers' requirements under this mixed strategy. The logistics service supply chain structure under the mass customization environment is shown in Figure 1.

To develop a model that is tractable, we shall assume that as follows. The parameters for our model and their description are shown in Table 1.

Assumption 1. Considering the scale effect, we assume that the unit cost of every subprocedure could be denoted by $(1-\lambda \cdot tc_i n, q\lambda h \in {}_{[}0,1))$, and the scale effect coefficient is bigger than 0 but no more than 1 in the mass service mode, and the scale effect coefficient is equal to zero in the customized service mode.

Assumption 2. Considering the scale effect, we assume that the unit time of every subprocedure could be denoted by $(1-\lambda)^{-1} \cdot c_i, \lambda \in [0,1)$, where the scale effect coefficient is bigger than 0 but no more than 1 in the mass service mode, and the scale effect coefficient is equal to zero in the customized service mode.

Assumption 3. Assuming that the LSI provides two types of products, i.e., standardized service products and customized service products, the price of the former is constant, and the price of customized service will increase with greater the degree of customization.

Assumption 4. We assume that the degree of customization is described by the position of the CODP. The degree of customization will decrease with the movement of CODP from upstream of the supply chain to the downstream. We further assume that the degree of customization is equal to 1 when the CODP is located at the first subprocedure, and the degree of customization is equal to 0 when the CODP is located at the last subprocedure.

Assumption 1 means that, for the same subprocedures, the unit cost of a subprocedure in the mass service mode is lower than their unit cost in the customized mode. Assumption 2 means that, for the same subroutine, the unit time spent in the mass service model is more than the unit time spent in the customized service model. In other words, the service time is inversely associated with the service scales.

4. Model Building and Solving

In Section 4.1.1, we quantify the important indicators in the model: the operation cost indexes and operation time indexes; in Section 4.1.2, we determine the qualitative indicators of logistics service quality evaluation and then use the method of Fuzzy QFD to quantify these qualitative indicators, which lays the foundation for the constraints of the next step of the fuzzy programming model.

In Section 4.2, the objective function of the model is constructed, and two fuzzy constraint sets are built: the high-quality logistics service fuzzy set and the satisfactory delivery time fuzzy set; then, on the basis of the objective function and the fuzzy constrains, a fuzzy programming model for CODP location in the LSSC is built. In Section 4.3, we provide the solution method and the process for solving the model under different conditions. The overall proposed procedure for positioning CODP is illustrated in Figure 2.

4.1. Quantitative Index

4.1.1. Quantitative Cost Index and Time Index. As mentioned earlier, the subprocedures before k (including the k subprocedure) are implemented in the mass service mode, and the subsequent subprocedures are implemented in the customized mode, which means the total cost of the logistics service consists of two parts: the cost of mass service and the cost of customized service. According to Assumption 1, the total cost of mass service is $\sum_{i=1}^{k}(1-\lambda)\cdot c_i \cdot \mu$, the total cost of customized service is $\sum_{i=k+1}^{N} c_i \cdot \mu$. Therefore, the total cost can be expressed as follows:

$$C(k) = \sum_{i=1}^{k}(1-\lambda)\cdot c_i \cdot \mu + \sum_{i=k+1}^{N} c_i \cdot \mu. \tag{1}$$

Similarly, the total time of all logistics services also consist of two parts: the mass service time and the customized service time. According to Assumption 2, the total time of the mass service portion can be calculated as $\sum_{i=1}^{k}(1-\lambda)^{-1}\cdot t_i$. On the contrary, the scale effect has no impact on the time of the customized service, i.e., $\lambda = 0$. Therefore, the total time of the entire logistics service can be expressed as follows:

$$T(k) = \sum_{i=1}^{k}(1-\lambda)^{-1}\cdot t_i + \sum_{i=k+1}^{N} t_i. \tag{2}$$

Another important time index is the lead time, and we use an interval number $T = [T_s, T_l]$ to indicate the shortest and longest lead time of a service order that can be accepted by the customers. We use $T_E = 1/2(T_s + T_l)$ to refer to the customer's expected lead time, so the LSI lead time should be closest to T_E.

4.1.2. Quantitative Service Quality Index Using a Fuzzy Quality Function Deployment (Fuzzy QFD) Approach. Compared with the quantitative cost index and time index, it is more complex to quantify service quality. We utilize the Quality Function Deployment approach [11, 36–38] to analyze our problems. In this section, we use a mixed method and deliver qualitative insights based on semi-structured interviews and quantitative insights based on fuzzy QFD. The evaluation information is obtained by means of field visits and semistructured interviews with both logistics experts and customers, and then the information will be processed and filled into the house of quality (HOQ). According to the following algorithm, we first determine the ability factor and the quality factor and then calculate the influence degree of the capability factor on the quality factor. Then, combining the evaluation information about the logistics service ability when the LSI selects different CODPs, we calculate the scores of the logistics service quality. Finally,

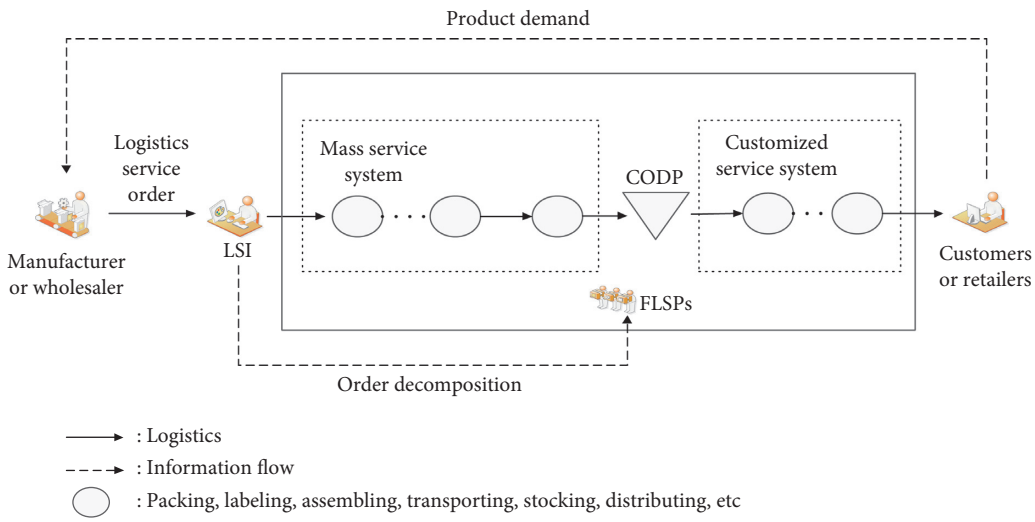

Figure 1: The logistics service supply chain structure under the mass customization environment.

Table 1: Parameters for the CODP position model.

Notations	Description
$G(k)$	Gross profit when the CODP is k
$P(k)$	Service price when the LSI sets the CODP at k
P_s	Price of standardized service products
$C(k)$	Total cost of order processing when the CODP is k
c_i	Unit cost of logistics service in the ith procedure
$T(k)$	Delivery time, i.e., total service time when the CODP is k
t_i	Operation time of logistics service in the ith procedure
$Q(k)$	Service quality when the CODP is k
T_s, T_l	The shortest and longest lead time of service orders that customers will accept, respectively
λ	Scale effect coefficient
μ	Amount of logistics service
i	Serial number of subprocedures
k_i	CODP locates at the ith subprocedure
k	The position of the CODP, $k = 1, \ldots, i, \ldots, N$, when, $i \leq k$, the ith subprocedure implements mass service; when $i > k$, ith subprocedure implements customized service
k^*	The optimal position of the CODP
N	Total number of procedures
α	Weight of logistics service quality
$1 - \alpha$	Weight of time index
β	Weight of objective function
$1 - \beta$	Weight of constraints

these scores are entered into the logistics service quality function constructed by this paper; thus, a more intuitive and more acceptable result is obtained.

Based on the intensive study of the related theory and previous work, we know that evaluating service quality is a continuous process, which can be summarized in the following steps:

(i) Identify the quality factors of the logistics service proposed by customers: "WHATs"

(ii) Assess and calculate the importance of every service quality factor

(iii) Identify logistics service ability factors that affect service quality: "HOWs"

(iv) Determine the relationship between the service quality factors and the service ability factors

(v) Determine the influencing degree of every ability factors on the overall service quality by matrix calculation

(vi) Evaluate the performance of the LSI service when the LSI selects different CODPs

(vii) Determine the service quality by means of HOQ, and then we can utilize our service quality function to obtain a more intuitive result to describe the quality of the logistics service

By referring to a large number of related studies [39, 40], we summarize the information on indexes into Table 2

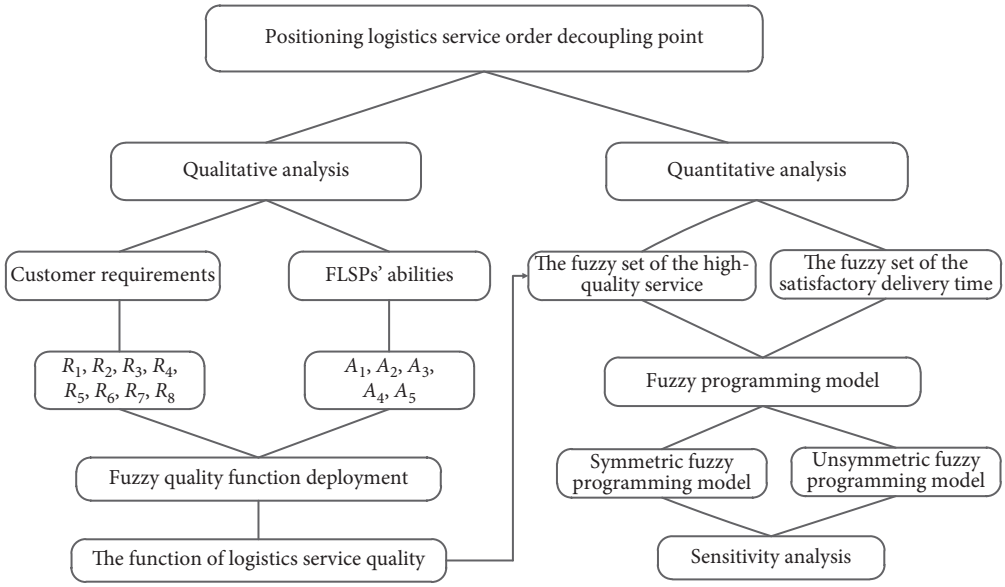

Figure 2: The proposed positioning CODP procedure.

Table 2: Customer service quality factors: WHATs.

Service quality requirements	Description
Accuracy (R_1)	Avoidance of mistakes and damages in order delivered
Organization accessibility (R_2)	Customer's opportunity to establish a contact with the LSI's staff
Flexibility (R_3)	Capability to modify orders in terms of due date and quantity when required by customers
Reliability (R_4)	Capability to deliver an order within the due date
Regularity (R_5)	The dispersion around the mean value of the delivered lead time
Complaints management (R_6)	Process following the recognition of some errors in the service provided, which allows service quality standards to be re-established
Frequency (R_7)	Number of deliveries accomplished in a given time period
Reasonable price (R_8)	The acceptable price that customers are willing to pay

(customer service quality requirements, i.e., service quality factors, "WHATs") and Table 3 (LSI service ability factors, "HOWs").

We obtained all of the above evaluating information by means of semistructured interviews [40], and then we use triangular fuzzy numbers to describe the information. For example, during the interview phase, there are H customers to answer the questions about the importance of quality factors, another L customers or experts to assess the degree of impact of the ability factor on the quality factor, and M experts to evaluate the performance of the LSI service ability that selects CODPs with different positions; all of the evaluation information should be described by a 7-point linguistic rating scale, ranging from VL (very low) to VH (very high). The fuzzy scale is shown in Table 4.The notations for Fuzzy QFD model are shown in Table 5.

According to the context, we build a house of quality, as shown in Figure 3. The next step is to develop the quantitative service quality index in terms of HOQ. The steps for this problem are as follows.

Step 1. Variable calculation.

First, we calculate the weight of the service quality factors according to the average method based on H customers' evaluation information. Similarly, we use the average method to calculate the degree of impact of every ability factor on every quality factor. The formula for the calculation is as follows:

$$\begin{aligned} \widetilde{\omega}_i &= \frac{1}{H} \otimes \sum_{h=1}^{H} \widetilde{\omega}_{ih}, i = 1, \ldots, I, \\ \widetilde{e}_{ij} &= \frac{1}{L} \otimes \sum_{l=1}^{L} \widetilde{e}_{ijl}, \quad i = 1, \ldots, I; j = 1, \ldots, J. \end{aligned} \tag{3}$$

Step 2. Create matrixes.

The matrixes for the LS quality factor weight and capacity factor are created, respectively, as follows, based on the results of Step 1:

Table 3: MC logistics service abilities: HOWs.

Service abilities	Description
Information technology (A_1)	Sharing information in a timely manner, tracking logistics information, timely communication with customers, etc
Process optimization capability (A_2)	The ability to integrate and optimize logistics business processes
Logistics network service ability (A_3)	The logistics network formed by different logistics nodes and logistics channels leading to different service abilities, which can be measured by the scale of the logistics network, coverage areas, etc
Facility integration capability (A_4)	The capability to integrate facilities in logistics nodes and the logistics network
Emergency service capacity (A_5)	Ability to adjust to changes in consumer demand, emergency events, and incidents

Table 4: Linguistic judgments and corresponding fuzzy numbers.

Judgement	Triangular fuzzy number
Very low	$(0, 0, 1.5)$
Low	$(0, 1.5, 3)$
Medium low	$(1.5, 3, 4.5)$
Medium	$(3, 4.5, 6)$
Medium high	$(4.5, 6, 7.5)$
High	$(7.5, 9, 10)$
Very high	$(9, 10, 10)$

Table 5: Notations for Fuzzy QFD model.

Notations	Description
Q_i	Logistics service quality index
$\tilde{\omega}_i$	Weight of Q_i
$\tilde{\omega}_{ih}$	The evaluation of the weight of the ith service quality index by the hth expert or customer
$\tilde{c}_j$	jth logistics services capability of the LSI
E	Correlation matrix
$\tilde{e}_{ij}$	The impact of the jth service capability on the ith service quality
i	Serial number of the logistics service quality index
I	Numbers of logistics service quality indexes
j	Serial number of the logistics service technology and capacity index
J	Numbers of the logistics service technology and capacity indexes
H	The number of customers involved in evaluating the quality factor weights
L	The number of experts involved in the evaluation of the impact factors on quality factors
M	The number of experts involved in the evaluation of logistics services capabilities when selecting different CODPs
$Y(k)$	Comprehensive evaluation of service quality based on logistics service abilities
$Q(Y)$	The function of logistics service quality

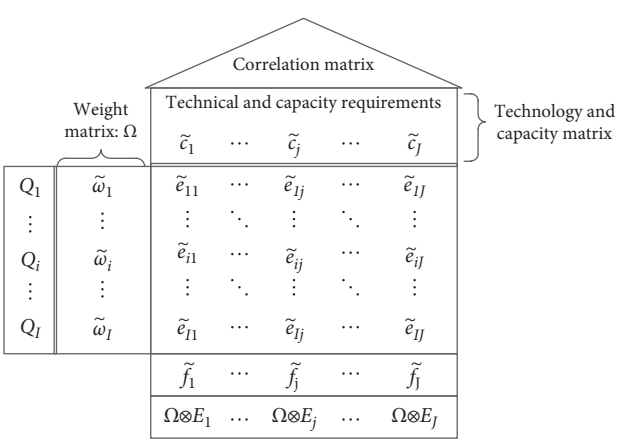

Figure 3: House of quality.

$$\Omega = \left(\tilde{\omega}_1, \ldots, \tilde{\omega}_i, \ldots \tilde{\omega}_I\right),$$
$$C = \left(\tilde{c}_1, \ldots, \tilde{c}_j, \ldots, \tilde{c}_J\right),$$
$$E = \left(E_1, \ldots, E_j, \ldots, E_J\right) = \begin{pmatrix} \tilde{e}_{11} & \ldots & \tilde{e}_{1j} & \ldots & \tilde{e}_{1J} \\ \vdots & \ddots & \vdots & \ddots & \vdots \\ \tilde{e}_{i1} & \cdots & \tilde{e}_{ij} & \cdots & \tilde{e}_{iJ} \\ \vdots & \ddots & \vdots & \ddots & \vdots \\ \tilde{e}_{I1} & \ldots & \tilde{e}_{Ij} & \ldots & \tilde{e}_{IJ} \end{pmatrix}, \quad (4)$$
$$E_j = \left(\tilde{e}_{1j}, \ldots, \tilde{e}_{ij}, \ldots, \tilde{e}_{Ij}\right)^{\mathrm{T}}.$$

Step 3. Matrix calculation.

In this step, we need to calculate the influence degree of every ability factors on the overall service quality: $\widetilde{f}_j$, all the $\widetilde{f}_j$ constitute a matrix vector F:

$$\widetilde{f}_j = \frac{1}{I} \otimes \Omega \otimes E_j = \frac{1}{I} \otimes (\widetilde{\omega}_1, \ldots, \widetilde{\omega}_i, \ldots \widetilde{\omega}_I) \otimes \left(\widetilde{e}_{1j}, \ldots, \widetilde{e}_{ij}, \ldots, \widetilde{e}_{Ij}\right)^{\mathrm{T}},$$

$$F = \frac{1}{I} \otimes \Omega \otimes E = \left(\widetilde{f}_1, \ldots, \widetilde{f}_j, \ldots, \widetilde{f}_J\right). \tag{5}$$

Step 4. Calculation of logistics service quality.

According to the above three steps, we know the influence degree of every ability factor on the overall service quality, so we can calculate the logistics service quality as long as we evaluate the LSI service ability under the condition that different CODPs are selected. Supposing there are M logistics experts, R_{jkm} is the evaluation for jth logistics service ability by the mth logistics expert when the CODP locates at k; then, we can calculate the overall evaluation for every logistics service ability when selecting different CODPs according to the average method based on M experts evaluating information, $\widetilde{R}_{jk}$. The formula for the calculation is as follows:

$$\widetilde{R}_{jk} = \frac{1}{M} \otimes \sum_{m=1}^{M} \widetilde{R}_{jkm}, \quad j = 1, \ldots, J; k = 1, \ldots, N. \tag{6}$$

Once R_{jk} has been computed, the overall service quality can finally be determined as formulation (7). Since both $\widetilde{R}_{jk}$ and $\widetilde{f}_j$ are triangular fuzzy numbers, the results of their multiplication operations are also fuzzy numbers, so we convert those fuzzy numbers into real numbers to make the results more intuitive. Let $\widetilde{A} = (a, b, c)$ be a triangular fuzzy number, using the formulation $A = (a + 2b + c)/4$ to convert $\widetilde{A} = (a, b, c)$ to an exact value:

$$Y(k) = \frac{1}{J} \otimes \sum_{j=1}^{J} \left(\widetilde{R}_{jk} \otimes \widetilde{f}_j\right), \quad k = 1, \ldots, N. \tag{7}$$

When we chose different scoring standards, such as the centesimal system or the 10-point system, the results of formulation (7) will be different. To make results much easier to read and understand, we conduct a logistics service quality evaluating function as formulation (8). Obviously, the larger the value of the function, the higher the service quality is. More specifically, as the value of the function is closer to 1 than 0, the service quality is increasingly improving. The logistics service quality evaluating function is shown as formulation (5):

$$Q(Y) = \left(1 + e^{-a \cdot (Y - b)}\right)^{-1}, \quad a > 0, b > 0. \tag{8}$$

In this function, the values of a and b depend on the value of Y, and the value of Y is closely related to the scoring criteria. More specifically, when all of the evaluations for the abilities are the worst, we obtain the minimum value of Y (denoted as $Y_{\min}$). Similarly, we obtain the maximum value of Y (denoted as $Y_{\max}$) when all of the evaluations for the abilities are the best. Then, evenly map the interval number $[Y_{\min}, Y_{\max}]$ to $[0, 1]$ through the service quality function. In formulation (8), we set $b = (Y_{\max} + Y_{\min})/2$, and the proper value of a is calculated by an undetermined coefficient method.

4.2. Model Building. The objective function is to maximize total profit of the LSI when they implement the MC service mode. In this model, we use the difference between service price and total costs to indicate the profit of the LSI.

According to Assumption 4, we set the function of the degree of customization as

$$D(k) = \frac{1}{1 - N} \cdot k + \frac{N}{N - 1}, \quad k = 1, \ldots, N. \tag{9}$$

Obviously, $1/1 - N < 0$, the degree of customization function is monotonically decreasing in$k$. $D(k) = 1$, when $k = 1$; $D(k) = 0$, when $k = N$; $0 < D(k) = N - k/N - 1 < 1$, when $1 < k < N$. Therefore, $D(k) \in [0, 1]$.

According to Assumption 3, we set the service price function as

$$P(k) = P_s \cdot \left[1 + \frac{1}{N(1 - \lambda)} D(k)\right], \quad k = 1, \ldots, N. \tag{10}$$

In formulation (10), $D(k)$ is the increased proportion of service price according to the degree of customization, $1/1 - \lambda$ is the price compensation caused by sacrificing the scale effect, $1/N$ is an adjustment coefficient designed to curb excessive price, and P_s is the price of standardized service and the value of P_s is decided by the LSI based on cost pricing. The formulation of P_s is as follows:

$$P_s = C(N) \cdot (1 + r) = \sum_{i=1}^{N} (1 - \lambda) c_i \cdot \mu \cdot (1 + r). \tag{11}$$

Formula (10) means the higher the degree of customization is, the higher the price of LSI service is. When the customization levels tend to be 0, the price of logistics service is close to P_s. In formula (11), $C(N) = \sum_{i=1}^{N} (1 - \lambda) c_i \cdot \mu$ refers to the total cost for the LSI when the CODP is located at the last subprocedure; in other words, $C(N)$ is the cost that the LSI implements for a complete large-scale logistics service. r is the target profit margin when the LSI provides mass service. Therefore, the objective function can be written as follows:

$$\begin{aligned} \max G(k) = & P(k) - C(k) = P_s \cdot \left[1 + \frac{1}{N(1 - \lambda)} D(k)\right] \\ & - \sum_{i=1}^{k} (1 - \lambda) c_i \mu - \sum_{i=k+1}^{N} c_i \mu, \quad k = 1, \ldots, N. \end{aligned} \tag{12}$$

To highlight the importance of lead time as well as reflect this new requirement for the time constraint, this paper separates lead time from other service evaluation indicators and sets it as an independent constraint condition. Therefore, there are two main constraints for this

programming: the service quality constraint and the lead time constraint.

On the one hand, customers pursue high-quality service, which means the higher the service quality, the higher the customer satisfaction and loyalty; however, different positions of CODPs will lead to differentiated logistics service quality. We use a fuzzy set $\widetilde{A}(Q)$ to denote "High-quality of service;" its membership function is as formula (13), and its corresponding function curve is Figure 4. $\widetilde{A}(Q)$ is the possibility that the logistics service provided by the LSI is "high-quality service" when the decoupling point is located at k; it can also be understood as customer satisfaction with service quality when the CODP is located at the k subprocedure:

$$A(Q) = \begin{cases} 0, & 0 \le Q \le 0.2, \\ \dfrac{(Q-0.6)^2}{0.32}, & 0.2 \le Q < 0.6, \\ 1 - \dfrac{(Q-0.9)^2}{0.18}, & 0.6 \le Q < 0.9, \\ 1, & 0.9 \le Q \le 1. \end{cases} \tag{13}$$

On the other hand, the LSI's delivery time should be close to the customer's expected lead time. We use fuzzy set $\widetilde{B}$ to indicate this constraint, and the membership function of $\widetilde{B}$ can be described as formula (14). The graph of its membership function (it can also be understood as the time satisfaction function) is shown in Figure 5. $B(T)$ is the possibility that the LSI's lead time is close to the customer's expected lead time when the decoupling point is located at k:

$$B(T) = \begin{cases} \left[1 + \dfrac{(T(k) - T_E)^2}{T_E}\right]^{-1}, & T_s \le T(k) \le T_l, \\ 0, & T(k) < T_s \text{ or } T(k) > T_l. \end{cases} \tag{14}$$

Except the constraints mentioned above, k should not be equal to 1 or N, since it means the LSI provides completely customized service, and when $k = 1$, $k = N$ means the LSI provides completely standardized service, all of which are inconsistent with the background of our model.

To summarize, the CODP position model for a single service order is constructed as follows:

$$\max G(k) = P(k) - C(k) = {}_{Ps} \cdot \left(1 + \frac{1}{N(1-\lambda)} D(k)\right) - \sum_{i=1}^{k} (1-\lambda)_{ci}\mu - \sum_{i=k+1}^{N} {}_{ci}\mu,$$
$$\text{s.t.} \quad \begin{cases} Q(k) \in \widetilde{A}, \\ T(k) \in \widetilde{B}, \\ 1 < k < N. \end{cases} \tag{15}$$

4.3. Model Solution. Before solving the model, the relative importance of the objective function and constraints need to be defined first. For LSIs, if they regard maximizing profits and customer requirements (including quality requirements and delivery time requirements) as equally important, namely, the objective function and constraints are equally important; then, this model is a symmetric fuzzy programming model. If the LSI places more weight on maximizing profits, or conversely, they attach more importance to customer requirements, namely, the objective function and constraints are not equally important; then, the model is a unsymmetric fuzzy programming model. In this section, the solution of these two cases is given by referring to [41].

4.3.1. Symmetric Fuzzy Programming Model. The model is a symmetric fuzzy programming model when the LSI considers the objective function and constraints as equally important. Since $G(k)$ is a discrete function and k is a finite integer, there must be a maximum $G(k)$ and a minimum $G(k)$. Therefore, we introduced a fuzzy set M_G to solve the above fuzzy programming model, and its membership function can be written as follows:

$$M_{G(k)} = \frac{G(k) - \min_{t \in N} G(t)}{\max_{t \in N} G(t) - \min_{t \in N} G(t)}, \quad k = 1, \ldots, N. \tag{16}$$

Obviously, if G reaches the maximum at k^1, $M_G(k^1) = 1$. If G obtains a minimum value at k^2, $M_G(k^2) = 0$. If G is neither maximum nor minimum at k, MGk∈(0,1). Therefore, $M_G(k)$ can be considered as the degree (or possibility) that $G(k)$ reaches the maximum at k, for $\forall k \in N^*$. In this view, the original model can be rewritten as

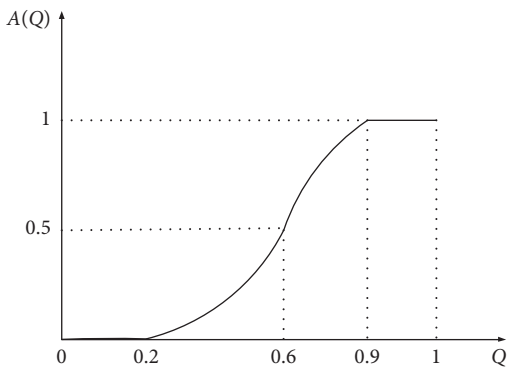

Figure 4: The membership function of fuzzy set $\widetilde{A}$.

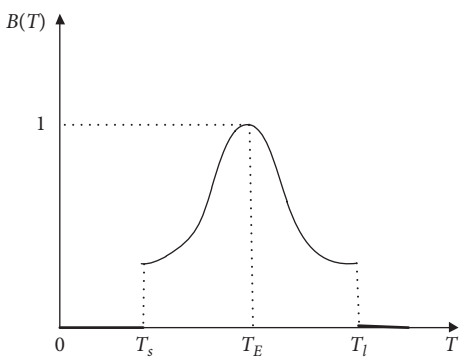

Figure 5: Fuzzy set B's membership function.

$$\max y = M_G(k),$$
$$\text{s.t.} \begin{cases} Q(k) \in \widetilde{A}, \\ T(k) \in \widetilde{B}, \\ 0 < k < N. \end{cases} \tag{17}$$

Let $\widetilde{A}_\alpha$, $\widetilde{B}_\beta$ be the α–cut set of $\widetilde{A}$ and the β– cut set of $\widetilde{B}$, respectively. Clearly, the process of finding the maximum of $G(k)$ on $\widetilde{A}_\alpha$ and $\widetilde{B}_\beta$ is equivalent to searching for the k^* that meets the following condition:

$$M_G(k^*) = \max_{k \in \widetilde{A}_\alpha, k \in \widetilde{B}_\beta} M_G(k). \tag{18}$$

Based on this, we transform model (17) into

$$\max y = M_G(k),$$
$$\text{s.t.} \begin{cases} Q(k) \in \widetilde{A}_\alpha, \\ T(k) \in \widetilde{B}_\beta, \\ 1 < k < N. \end{cases} \tag{19}$$

Model (19) transforms the fuzzy constraints A and B into the deterministic constraints, and those deterministic constraints depend on the value of α– and β–. In other words, the solution of the above model must depend on the value of α and β.

A synthetic constraint fuzzy set is introduced to indicate all constraints. The expression of this synthetic constraint will change according to the preferences of different customers. Without loss of generosity, let $\alpha = \beta$, and the solution of model is recorded as $k(\alpha)$, and $k(\alpha)$ is a special k that causes Gk to reach the maximum at the α-level, where $\alpha \epsilon 0{,}1$ can be explained as the possibility (or guaranteeing rate) that $G(k)$ reaches the maximum under the fuzzy constrains:

$$\widetilde{S}(k) = h(\widetilde{A}(k), \widetilde{B}(k)) = \omega_1 \otimes \widetilde{A}(k) + \omega_2 \otimes \widetilde{B}(k),$$
$$0 \le \omega_1, \omega_2 \le 1, \omega_1 + \omega_2 = 1. \tag{20}$$

To solve model (19), we first analyze the general property of $M_G(k)$ and give the definition of absolutely optimal level. Let $\alpha_1, \alpha_2 \in (0, 1]$ and $k(\alpha_1)$ and $k(\alpha_2)$ are the solutions of the model at the $\alpha 1$ and $\alpha 2$ level, respectively. Then,

$$\alpha_1 < \alpha_2 \Longrightarrow S_{\alpha_2} \subseteq S_{\alpha_1} \Longrightarrow M_G(k(\alpha_2)) \le M_G(k(\alpha_1)). \tag{21}$$

Formula (21) means $M_G(k(\alpha))$ is a nonincreasing function of α.

Definition 1. If there exist a $\alpha^* \in (0, 1)$, when$\alpha > \alpha^*$, $M_G(k(\alpha^*)) > M_G(k(\alpha))$, and when $0 < \alpha < \alpha^*$, $M_G(k(\alpha^*)) = M_G(k(\alpha))$; then, α^* is described as the absolutely optimal level under the fuzzy constraint condition $\widetilde{S}(k)$, and its geometric description is shown as Figure 6.

Since $M_G(k(\alpha))$ is a nonincreasing function of α, $M_G(k(\alpha)) > M_G(k(1))$ is always true for any $\alpha^* \in (0, 1]$, namely, $M_G(k(\alpha)) \in [M_G(k(1)), M_G(k(\alpha^*))], \forall \alpha \in (0, 1]$. That means the possibility that $M_G = M_G(k(1))$ is 1, but the value of $M_G(k(1))$ is relatively small. On the other hand, the possibility that $M_G = M_G(k(\alpha^*))$ is α^*, and it is impossible for MG to reach a value that is larger than $M_G(k(\alpha^*))$, but $\alpha^* \in (0, 1]$ is relatively small, which indicates that it is risky for the decision maker to get the maximal value (i.e., $M_G(k(\alpha^*))$. Therefore, it is of great importance for the decision maker to choose an appropriate $\alpha^* \in (0, 1]$, making M_G reach a relatively satisfactory large value in the case of low risk.

According to the above analysis, we give the definition of the optimized point of the model.

Definition 2. Let constraint condition $\widetilde{S}(k)$ and objective $\widetilde{M}_G$ be the fuzzy sets in N^*, if

$$M_G(k^*) \wedge S(k^*) = \max_{k \in N^*} (M_G(k) \wedge S(k)). \tag{22}$$

Then, we call k^* the optimized point and call $G(k^*)$ the optimal value under the fuzzy constraint condition $\widetilde{S}(k)$, where N^* is the universe of discourse.

4.3.2. Unsymmetric Fuzzy Programming Model. If the LSI pays different attention to the profit target and customer's request, it can express the different preference by setting different weight values to the objective function and the constraint condition, and the model is an unsymmetric fuzzy programming model.

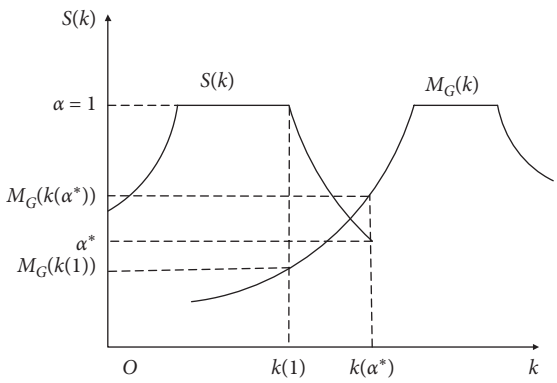

Figure 6: Absolutely optimal level.

Based on Section 4.3.1, introducing the fuzzy set $\widetilde{U} = \beta M_G + (1-\beta)\widetilde{S}$, $0 \le \beta \le 1$, $\forall k \in N$, where β is the weight of the objective function and$1-\beta$ is the weight of the constraint. The greater the β, the greater the LSI's attention to its short-term profit levels. Conversely, the LSI pays more attention to customer experience and customer satisfaction.

If $k^* \in N$, subjected to $\widetilde{U}(k^*) = \max_{k\in N}\widetilde{U}(k)$, then k^* is the optimal point among N and $G(k^*)$ is regarded as the best value.

5. Numerical Study

In this section, at first, the reliability of the model is proven through a numerical case; then, the effect on the outcome is observed when some parameters are changed by the sensitivity analysis. Finally, some important conclusions are obtained through the analysis of the results.

5.1. A Case Study. A LSI receives a logistics order from a customer enterprise, and the quantity of goods is $\mu = 100$. After the analysis, it is found that the order can be divided into 8 service subprocedures. The LSI matches these subprocedures to the appropriate FLSPs. The unit operating cost of each subroutine (c_i) and the operating time (t_i) are shown in Table 6. The target profit margin is equal to 0.2 when the LSI provides standardized service, and the scale effect coefficient (λ) is equal to 0.1. The customer expectation delivery time is not less than 132 hours and is not more than 156 hours; the most suitable delivery time is 144 hours.

To enhance customer satisfaction, the LSI invited 5 customers to score the 8 service quality indicators mentioned above to determine the importance of those indicators, and three experts were asked to score the impact of the LSI's 5 logistics capabilities on the 8 services quality indicators. In addition, three experts were asked to score the logistics capabilities of the LSI when the LSI selected different CODPs, see Appendix for the specific scoring. Now, we need to determine a suitable decoupling point location to maximize the profit of the LSI as much as possible to meet the customer's requirements.

According to Table 6 and formulations (1), (2), and (12), we could calculate the total cost, total time, and gross profit when the LSI selects different CODPs. The results are shown in Table 7.

Based on the fuzzy QFD model and Appendix , we could obtain the score of the overall level of the logistics service quality. In this numerical case, we set the logistics service quality function as $Q(Y) = [1 + e^{-0.02(Y-220)}]^{-1}$, and its function image is shown in Figure 7, and the results are shown in Table 8.

From Table 8, we can clearly see that there are obvious differences in the logistics service quality when the LSI selects different CODPs. Among them, when $k = 6$, the logistics service quality is the best. When $k = 1$ or $k = 2$, the logistics service quality is obviously poorer.

The membership function image of $\widetilde{A}$ and $\widetilde{B}$ are shown as Figures 8 and 9, respectively. According to Tables 7 and 8 and formulations (10) and (11), we could calculate the membership of $k^* \in \widetilde{A}, k^* \in \widetilde{B}$ when k^* is equal to different value, respectively. Let the fuzzy set $\widetilde{S}(k) = 0.5 \otimes \widetilde{A} + 0.5 \otimes \widetilde{B}$ express synthetic constraints and calculate the membership of $\widetilde{S}$. According to Table 7 and formulation (16), we could calculate the membership of $k^* \in \widetilde{M}_G$. All of the above calculation results are shown in Table 9.

Consider the first case, namely, finding the optimal CODP when the objective function and constraints are equally important. According to model (21), the results are shown in Table 10.

Based on Table 9 we know, when $M_G(k(\alpha^*)) = 1$, the absolutely optimal level α^* is equal to 0.2446 under the synthetic constraint; in this case, $k(\alpha^*) = 1$. In other words, when the profit reaches the maximum under the condition of the comprehensive fuzzy constraint, the position of the CODP is in the first subprocedure, but the guarantee rate is only 0.2446. Because $k \neq 1$ and $k \neq N$, we can only choose the second largest M_G ($M_G = 0.867526$); therefore, $\alpha^* = 0.2551, k(\alpha^*) = 2$.

Utilizing model (22),

$$M_G(k) \cap S = \frac{0.2246}{k_1} + \frac{0.2551}{k_2} + \frac{0.607}{k_3} + \frac{0.55}{k_4} + \frac{0.3749}{k_5} + \frac{0.2488}{k_6} + \frac{0.1}{k_7} + \frac{0}{k_8}. \tag{23}$$

According to the maximum principle of membership degree, to maximize the profits of LSI in the case of comprehensive constraints, then we should select the 3rd subprocedure as the position of CODP, namely, $\alpha^* = 0.607, k(\alpha^*) = 3$.

From the above results, it is not difficult to find that when $k = 3$, and the LSI can neither make the most profit nor maximize the customer satisfaction, but under the fuzzy programming model, the decision maker can make a tradeoff between the profit goal and customer satisfaction, namely, considering profit and customer satisfaction; we consider $k = 3$ as the optimal decoupling point.

Table 6: The unit cost and time of every service procedures.

i	1	2	3	4	5	6	7	8
Cost (c_i)	96	77	45	88	60	80	70	90
Time (t_i)	19	13	15	15	18	16	14	17

Table 7: Calculation results of total cost, total time, and gross profit.

	$k = 1$	$k = 2$	$k = 3$	$k = 4$	$k = 5$	$k = 6$	$k = 7$	$k = 8$
Total cost	59640	58870	58420	57540	56940	56140	55440	54540
Total time	129.1111	130.5556	132.2222	133.8889	135.8889	137.6667	139.2222	141.1111
Gross profit	14898	14369.43	13520.86	13102.29	12403.71	11905.14	11306.57	10908

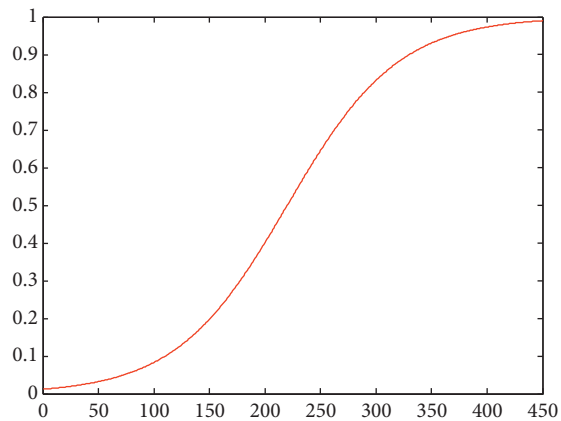

Figure 7: Logistics service quality function.

Table 8: Calculation results of logistics service quality.

CODP	Service quality described by fuzzy numbers	Service quality described by real numbers	The value of logistics quality function service
$k = 1$	(116.96, 235.64, 376.22)	241.12	0.5102
$k = 2$	(106.37, 232.43, 386.26)	239.37	0.4892
$k = 3$	(109, 240.87, 435.29)	256.51	0.7046
$k = 4$	(134.63, 268.47, 429.33)	275.22	0.8768
$k = 5$	(141.32, 267.72, 427.21)	279.7	0.9024
$k = 6$	(131.91, 275.45, 456.4)	284.80	0.9267
$k = 7$	(138.41, 266.72, 415.11)	271.74	0.8539
$k = 8$	(146.55, 261.62, 397.5)	266.82	0.8166

5.2. Sensitivity Analysis. In Section 5.1, we assume that the objective function and the constraint condition are equally important; in the following section, we discuss the change of the optimal decoupling point with the change of some parameters when the objective function and the constraints are unequally important. By observing the form of the objective function, we can see that when the position of the CODP moves downstream, both $P(k)$ and $C(k)$ are monotonically decreasing. If $P(k)$ decreased faster than $C(k)$ (denoted as the pricing strategy of 1), then the profit function $G(k)$ is monotonically decreasing, if $P(k)$ decreased slower than $C(k)$ (denoted as pricing strategy 2), then the profit function $G(k)$ is monotonically increasing. The impact of the scale effect coefficient and the objective function weight coefficient on the CODP position will be discussed in the following two cases.

5.2.1. Sensitivity Analysis of λ and B *under the Pricing Strategy of 1.* If we change the pricing function to $P(k) = P_s \cdot [1 + 1/1 - \lambda \cdot D(k)]$ to meet the requirements of pricing strategy 1, the profit function is monotonically decreasing. Consider the first case, when the scale effect coefficient is equal to 0.2 ($\lambda = 0.2$), observing the impact of β on the position of the CODP. Based on Section 4 and the data of Section 5.1, we observe the change of the CODP position when β takes different values. The results are shown in Figure 10.

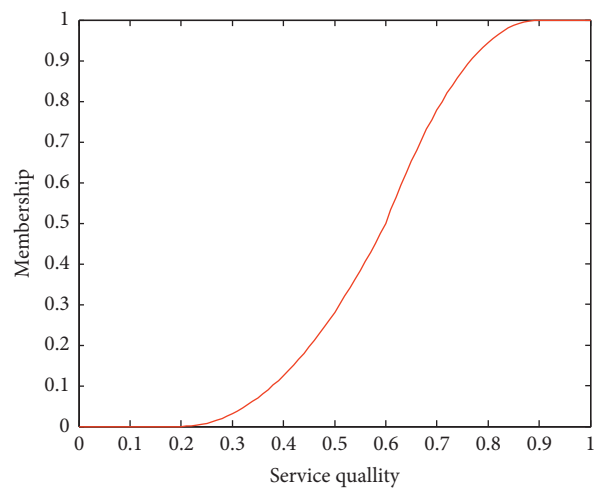

Figure 8: A's membership function.

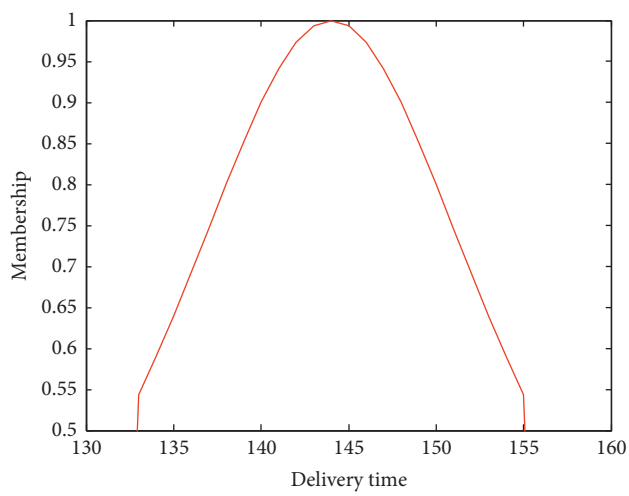

Figure 9: $\widetilde{B}$'s membership function.

Table 9: The membership of $\widetilde{M}_G$, $\widetilde{A}$, $\widetilde{B}$, and $\widetilde{S}$.

k	k_1	k_2	k_3	k_4	k_5	k_6	k_7	k_8
$\widetilde{M}_G$	1	0.867526	0.654851	0.549946	0.374866	0.24991	0.099893	0
$\widetilde{A}$	0.4892	0.5102	0.7046	0.8768	0.9024	0.9267	0.8539	0.8166
$\widetilde{B}$	0	0	0.509345	0.584808	0.6864	0.782136	0.863169	0.945219
$\widetilde{S}$	0.2446	0.2551	0.606972	0.730804	0.7944	0.854418	0.858534	0.880909

Table 10: Absolutely optimal level.

α	S_α	$k(\alpha)$	$M_G(k(\alpha))$
$0.8 < \alpha \leq 1$	k_6, k_7, k_8	k_6	0.25
$0.7 < \alpha \leq 0.8$	k_4, k_5, k_6, k_7, k_8	k_4	055
$0.6 < \alpha \leq 0.7$	$k_3, k_4, k_5, k_6, k_7, k_8$	k_3	061
$0.2 < \alpha \leq 0.6$	$k_1, k_2, k_3, k_4, k_5, k_6, k_7, k_8$	k_1	1

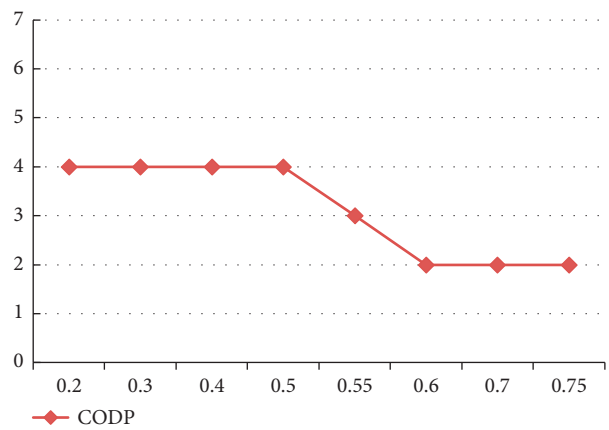

Figure 10: Optimal CODP when different β values are taken.

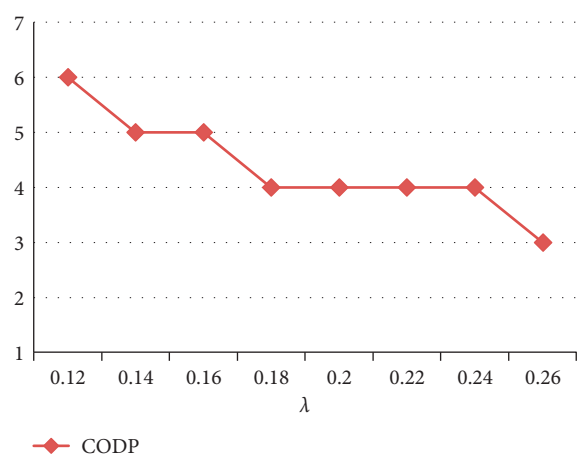

Figure 11: The optimal CODP when λ changes from 0.12 to 0.26.

As shown above, in this case, as the β increases, the CODP moves upstream. This means that the LSI, in the pursuit of higher returns, will tend to ignore the needs of customers, which will enhance the level of LSI profits in the short term, but in the long term, poor quality of service or unsatisfactory delivery time will reduce customer satisfaction and affect the partnerships between the enterprise and the customers.

Considering the second case, namely, when β is constant, we observe the change of the position of the optimal CODP caused by the change of λ. Since the value of β will affect the LSI's decision, we observe the impact of λ on the results when $\beta = 0.3$ (i.e., the LSI focuses more on customer needs) and $\beta = 0.7$ (i.e., LSI pays more attention to current earnings).

When $\beta = 0.3$, the position change of the optimal CODP is recorded in the process of λ rising from 0.12 to 0.26. Using the numerical examples in Section 5.1, calculate the position of the CODP when λ takes different values. The results are shown in Figure 11.

As shown in Figure 11, when $\beta = 0.3$, the position of the optimal CODP will move upstream with the increase of λ. This occurs because the closer the decoupling point is to the downstream, the longer the delivery time, resulting in a decrease in time satisfaction. The bigger the λ, the faster the rate of time satisfaction drops, and thus, the CODP has the power to move upstream.

When $\beta = 0.7$, to repeat the above steps and observe the position change of the CODP, we found that the optimal CODP is always located in the 2nd subprocedure. In this case, the LSI pays more attention to its income level. Since the change of λ will only change the size of earnings and will not change the variation trend of income, the LSI tends to locate the CODP in a higher income position. Figure 12 shows the change of LSI earnings in the process of CODP movement from upstream to downstream when the value of λ is different.

5.2.2. Sensitivity Analysis of λ and B *under the Pricing Strategy of 2.* If we change the pricing function to $P(k) = P_s \cdot [1 + 1/16(1-\lambda) \cdot D(k)]$ to meet the requirements of pricing strategy 2, the profit function is monotonically increasing, analysing the impact of λ and β on the position of the CODP. Similarly, we still divided it into two cases and

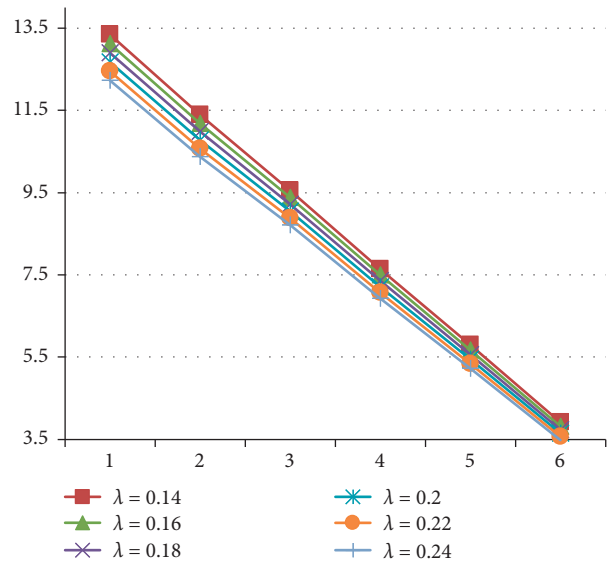

Figure 12: The LSI's profit when selecting different CODPs under the premise that λ takes different values.

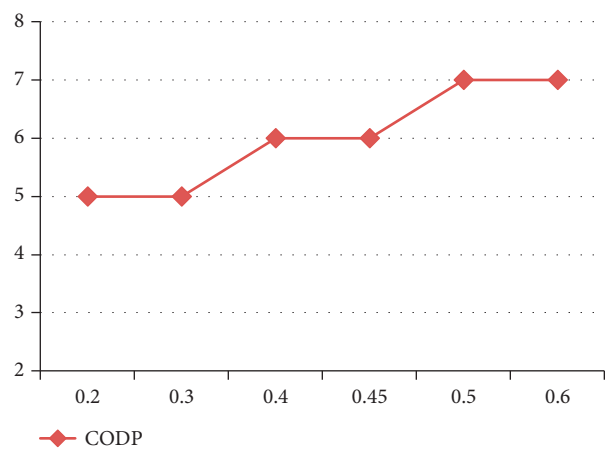

Figure 13: The optimal CODP when different β values are taken under price strategy 2.

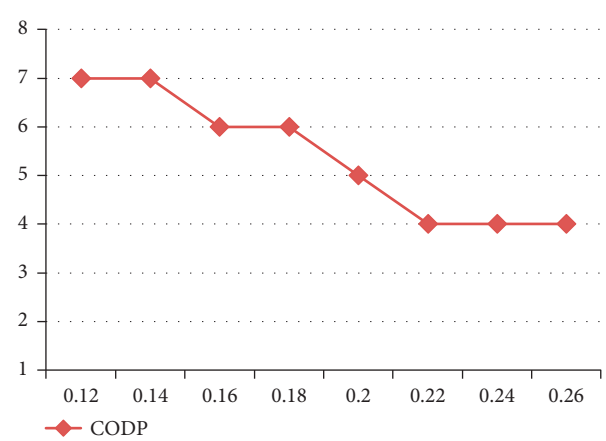

Figure 14: The optimal CODP when λ changes from 0.12 to 0.26.

Table 11: Customer scoring information on the relative importance of the 8 service quality indicators.

		Service quality factors							
		$Q1$	$Q2$	$Q3$	$Q4$	$Q5$	$Q6$	$Q7$	$Q8$
Importance judgment by linguistic rating scale	$h1$	H	VH	MH	H	MH	MH	H	MH
	$h2$	VH	VH	H	MH	H	H	H	MH
	$h3$	H	H	MH	H	MH	H	H	MH
	$h4$	VH	VH	MH	H	MH	VH	H	H
	$h5$	MH	MH	H	H	VH	MH	MH	H
Importance described by fuzzy numbers	$h1$	(7.5, 9, 10)	(9, 10, 10)	(4.5, 6, 7.5)	(7.5, 9, 10)	(4.5, 6, 7.5)	(4.5, 6, 7.5)	(7.5, 9, 10)	(4.5, 6, 7.5)
	$h2$	(9, 10, 10)	(9, 10, 10)	(7.5, 9, 10)	(4.5, 6, 7.5)	(7.5, 9, 10)	(7.5, 9, 10)	(7.5, 9, 10)	(4.5, 6, 7.5)
	$h3$	(7.5, 9, 10)	(7.5, 9, 10)	(4.5, 6, 7.5)	(7.5, 9, 10)	(4.5, 6, 7.5)	(7.5, 9, 10)	(7.5, 9, 10)	(4.5, 6, 7.5)
	$h4$	(9, 10, 10)	(9, 10, 10)	(4.5, 6, 7.5)	(7.5, 9, 10)	(4.5, 6, 7.5)	(9, 10, 10)	(7.5, 9, 10)	(7.5, 9, 10)
	$h5$	(4.5, 6, 7.5)	(4.5, 6, 7.5)	(7.5, 9, 10)	(7.5, 9, 10)	(9, 10, 10)	(4.5, 6, 7.5)	(4.5, 6, 7.5)	(7.5, 9, 10)
Relative importance of service quality factors: W_i		(7.5, 8.8, 9.5)	(7.8, 9, 9.5)	(6, 7.4, 8.5)	(7.2, 8.6, 9.5)	(6, 7.4, 8.5)	(6.6, 8, 9)	(6.9, 8.4, 9.5)	(5.7, 7.2, 8.5)

Table 12: The impact of various logistics service capabilities on different service quality indicators: scoring by the expert judgment method.

	A_1			A_2			A_3			A_4			A_5		
	C_1	C_2	C_3	C_1	C_2	C_3	C_1	C_2	C_3	C_1	C_2	C_3	C_1	C_2	C_3
$Q1$	VH	H	H	M	M	MH	M	ML	M	H	M	MH	ML	M	M
Q_2	VH	H	VH	MH	MH	M	L	VL	VL	ML	VL	L	L	L	ML
Q_3	MH	M	M	H	H	H	MH	H	H	M	M	ML	VH	VH	VH
Q_4	M	M	M	VH	H	VH	H	VH	MH	MH	VH	H	M	ML	ML
Q_5	H	H	MH	H	H	MH	M	M	M	M	M	MH	ML	M	M
Q_6	MH	MH	H	ML	L	L	L	ML	ML	ML	VL	L	ML	ML	L
Q_7	L	L	ML	MH	MH	H	H	MH	MH	MH	H	MH	MH	M	M
Q_8	ML	ML	ML	MH	H	MH	MH	MH	MH	VH	VH	H	VL	VL	L

Table 13: The impact of various logistics service capabilities on different service quality indicators: described by fuzzy numbers.

	A_1	A_2	A_3	A_4	A_5
Q_1	(8.5, 9.7, 10)	(3, 4.5, 6)	(2.5, 4, 5.5)	(5, 6.5, 7.8)	(2.5, 4, 5.5)
Q_2	(8.5, 9.7, 10)	(4, 5.5, 7)	(0, 0.5, 2)	(0.5, 1.5, 3)	(0.5, 1.5, 3)
Q_3	(3.5, 5, 6.5)	(7.5, 9, 10)	(6, 7.5, 8.7)	(2.5, 4, 5.5)	(9, 10, 10)
Q_4	(3, 4.5, 6)	(8.5, 9.7, 10)	(7, 8.3, 9.2)	(6, 7.5, 8.7)	(2, 3.5, 5)
Q_5	(6.5, 8, 9.2)	(6.5, 8, 9.2)	(3, 4.5, 6)	(3.5, 5, 6.5)	(2.5, 4, 5.5)
Q_6	(5.5, 7, 8.3)	(0.5, 2, 3.5)	(1, 2.5, 4)	(0.5, 1.5, 3)	(1, 2.5, 4)
Q_7	(0.5, 2, 3.5)	(3.5, 5, 6.5)	(5.5, 7, 8.3)	(5.5, 7, 8.3)	(3.5, 5, 6.5)
Q_8	(1.5, 3, 4.5)	(5.5, 7, 8.3)	(4.5, 6, 7.5)	(8.5, 9.7, 10)	(0, 0.5, 2)

Table 14: The impact of different service capabilities on overall service quality.

f_1	f_2	f_3	f_4	f_5
(32, 50, 66)	(31, 48, 63)	(24, 40, 58)	(26, 43, 60)	(17, 32, 47)

discussed them separately; the first case is observing the impact of β on the position of the CODP when the scale effect coefficient is constant (set $\lambda = 0.2$).

As shown in Figure 13, when $\lambda = 0.2$, the CODP moves downstream with the increasing of β. A greater β means that the LSI is more concerned about the current level of income, and in this case, the level of earnings will increase as the decoupling points move downstream, so the movement of the CODP will show the trend in the graph above.

Consider the second case, namely, when β is constant, observing the change of the optimal CODP position caused by the change of λ. Similarly, the value of β will influence the LSI's decision. Therefore, we observe, respectively, the impact of λ on the results when $\beta = 0.3$ and $\beta = 0.7$. When $\beta = 0.3$, observing the change of the CODP position with λ rising from 0.12 to 0.26, the results are shown in Figure 14.

As shown in Figure 14, when $\beta = 0.3$, the CODP moved upstream with the increasing of λ. $\beta = 0.3$ means that the LSI

Table 15: LSI logistics service capability scoring information when decoupling points are in different positions: scoring by the expert judgment method.

	A_1			A_2			A_3			A_4			A_5		
	e_1	e_2	e_3	e_1	e_2	e_3	e_1	e_2	e_3	e_1	e_2	e_3	e_1	e_2	e_3
$k = 1$	VH	H	H	M	M	M	M	L	L	VL	VL	L	VH	VH	VH
$k = 2$	H	H	VH	ML	L	ML	ML	ML	ML	ML	VL	L	H	H	VH
$k = 3$	MH	MH	M	M	M	M	M	M	MH	MH	MH	M	MH	H	MH
$k = 4$	ML	ML	ML	H	H	MH	VH	H	H	H	H	H	ML	M	ML
$k = 5$	L	L	VL	VH	H	H	VH	VH	H	VH	H	H	VL	ML	L
$k = 6$	M	M	ML	MH	H	H	MH	MH	MH	MH	VH	H	MH	H	MH
$k = 7$	L	VL	VL	VH	VH	H	VH	VH	H	VH	VH	H	VL	L	L
$k = 8$	VL	VL	VL	VH	VH	VH	VH	VH	VH	VH	VH	VH	VL	VL	VL

Table 16: LSI logistics service capability scoring information when decoupling points are in different positions: described by fuzzy numbers.

	A_1	A_2	A_3	A_4	A_5
$k = 1$	(8.5, 9.7, 10)	(3, 4.5, 6)	(0, 1.5, 3)	(0, 0, 1.5)	(9, 10, 10)
$k = 2$	(8, 9.3, 10)	(1, 2.5, 4)	(1.5, 3, 4.5)	(0.5, 2, 3.5)	(8, 9.3, 10)
$k = 3$	(4, 5.5, 7)	(3, 4, 5.6)	(3.5, 5, 6.5)	(4, 5.5, 7)	(5.5, 7, 8.3)
$k = 4$	(1.5, 3, 4.5)	(6, 7.5, 8.7)	(8, 9.3, 10)	(7.5, 7.5, 7.5)	(2, 3.5, 5)
$k = 5$	(0, 1, 2.5)	(9, 10, 10)	(8.5, 9.7, 10)	(8, 9.3, 10)	(0.5, 1.5, 3)
$k = 6$	(2.5, 4, 5.5)	(6.5, 8, 9.17)	(4.5, 6, 7.5)	(7.5, 8.3, 9.2)	(3.5, 5, 6.5)
$k = 7$	(0, 0.5, 2)	(8.5, 9.7, 10)	(8.5, 9.7, 10)	(8.5, 9.7, 10)	(0, 1, 2.5)
$k = 8$	(0, 0, 1.5)	(9, 10, 10)	(9, 10, 10)	(9, 10, 10)	(0, 0, 1.5)

pays great attention to the customer's quality of service and delivery time ($1 - \beta = 0.7$). The lead time will increase with the rising of λ. To make the delivery time more in line with the customer's requirements, the LSI has to sacrifice short-term earnings to maintain customer relationships so that CODP moves upstream.

When $\beta = 0.7$, the optimal CODP always locates in the 7th subprocedure for any value of λ in interval $[0.12, 026]$. $\beta = 0.7$ means that LSI attaches great importance to the current income, while it ignores the needs of the customer enterprises. Under the price strategy of 2, the earning level of the LSI will gradually increase as the CODP moves from upstream to downstream, and the variation of λ will only affect the value of earnings but will not change the trend.

6. Conclusions

This paper constructs a fuzzy programming model based on the fuzzy set of the high-quality service and the fuzzy set of the satisfactory delivery time by means of combination of qualitative analysis and quantitative analysis. Compared with traditional deterministic programming models, we consider the ambiguity of the requirements for service quality and delivery time and use the fuzzy set theory to describe the fuzziness, which makes the model closer to the real situation. Under this model, decision makers can consider more indicators to measure the logistics service quality, and at the same time, the decision-making process is more flexible, which can better reflect the subjective preferences of decision makers. The CODP positioning method designed in this paper is helpful to the continuous improvement of service quality and sustainable development of the logistics service supply chain.

The research of this paper provides some useful perspectives for enterprise managers who provide logistics services. First, the scale effect coefficient has a significant effect on the position of the optimal CODP. Therefore, enterprise managers should increase the scale effect as much as possible within the scope of logistics service capabilities, such as expanding the scope of services to obtain more logistics orders, improving standardized operation capabilities, strengthening staff training on standardized operation procedures, and scientifically using order delay strategies to gather similar services types of orders.

Second, it is difficult to find a CODP that can maximize the LSI profits and the customer satisfaction at the same time. Therefore, business managers need to make a trade-off during decision-making and decide if they are willing to improve the short-term income level and ignore customer satisfaction or maintain long-term cooperation with customers at the expense of part of the proceeds.

Both the operation time of the mass service and the operation time of the customized service are assumed to be definite in this paper, and in reality, there often exist some fluctuation in the operation time. Therefore, a possible extension of the study includes considering the CODP positioning problem in the case of fuzzy operation time of the FLSPs.

Appendix

According to the scoring information of customers and experts for different indicators (as shown in Tables 11~13), we calculate the impact of different service capabilities on overall service quality based on Section 4.2. procedures (the calculation results are shown in Table 14). According to the scoring

information of experts for LSI's service abilities when selecting different CODP (scoring information are shown in Tables 15 and 16), combining the data of Table 14, we can calculate the value of logistics service quality under different decoupling points, and the results are shown in Table 8.

Data Availability

Data can be available upon request to the corresponding author.

Conflicts of Interest

The authors declare that they have no conflicts of interest.

Acknowledgments

This research was supported by Ministry of Education Humanities and Social Sciences Research Project of China (16YJA630017) and Open Research Fund Program of Key Laboratory of Process Optimization and Intelligent Decision-making (Hefei University of Technology), Ministry of Education.

References

[1] Q. Zhao, H. Ding, and H. Liu, "Logistics service process reengineering for mass customization," in *Proceedings of the IEEE International Conference on Services Systems and Services Management*, pp. 369–374, Chongquing, China, June 2005.

[2] W. Liu, H. Xu, X. Sun, Y. Yang, and Y. Mo, "Order allocation research of logistics service supply chain with mass customization logistics service," *Mathematical Problems in Engineering*, vol. 2013, Article ID 957260, 13 pages, 2013.

[3] C. Wang and F. Dargahi, "Service customization under capacity constraints: an auction-based model," *Journal of Intelligent Manufacturing*, vol. 24, no. 5, pp. 1033–1045, 2012.

[4] F. S. Fogliatto, G. J. C. Da Silveira, and R. Royer, "Flexibility-driven index for measuring mass customization feasibility on industrialized products," *International Journal of Production Research*, vol. 41, no. 8, pp. 1811–1829, 2003.

[5] B. Joseph Pine and A. C. Boynton, *Making Mass Customization Work*, pp. 109–116, Harvard Business Review, Brighton, MA, USA, 1993.

[6] W. Liu, Y. Yang, H. Xu, X. Liu, Y. Wang, and Z. Liang, "A time scheduling model of logistics service supply chain based on the customer order decoupling point: a perspective from the constant service operation time," *The Scientific World Journal*, vol. 2014, Article ID 756178, 22 pages, 2014.

[7] J. Olhager, "The role of the customer order decoupling point in production and supply chain management," *Computers in Industry*, vol. 61, no. 9, pp. 863–868, 2010.

[8] J. Olhager, "Strategic positioning of the order penetration point," *International Journal of Production Economics*, vol. 85, no. 3, pp. 319–329, 2003.

[9] M. Rudberg and J. Wikner, "Mass customization in terms of the customer order decoupling point," *Production Planning & Control*, vol. 15, no. 4, pp. 445–458, 2004.

[10] J. Wikner, "A service decoupling point framework for logistics, manufacturing, and service operations," *International Journal of Services Sciences*, vol. 4, no. 3/4, pp. 330–357, 2012.

[11] W. Liu, R. Wu, Z. Liang, and D. Zhu, "Decision model for the customer order decoupling point considering order insertion scheduling with capacity and time constraints in logistics service supply chain," *Applied Mathematical Modelling*, vol. 54, pp. 112–135, 2018.

[12] W. Liu, X. Shen, and D. Xie, "Decision method for the optimal number of logistics service providers with service quality guarantee and revenue fairness," *Applied Mathematical Modelling*, vol. 48, pp. 53–69, 2017.

[13] W. Liu, Z. Liang, Z. Ye, and L. Liu, "The optimal decision of customer order decoupling point for order insertion scheduling in logistics service supply chain," *International Journal of Production Economics*, vol. 175, pp. 50–60, 2016.

[14] A. K. Rahmat and N. Faisol, "Manufacturers satisfaction on logistics service quality: operational, relational and national culture," *Procedia-Social and Behavioral Sciences*, vol. 224, pp. 339–346, 2016.

[15] S. Limbourg, H. T. Q. Giang, and M. Cools, "Logistics service quality: the case of Da Nang City," *Procedia Engineering*, vol. 142, pp. 124–130, 2016.

[16] I. Meidutė-Kavaliauskienė, A. Aranskis, and M. Litvinenko, "Consumer satisfaction with the quality of logistics services," *Procedia-Social and Behavioral Sciences*, vol. 110, pp. 330–340, 2014.

[17] F. Franceschini and C. Rafele, "Quality evaluation in logistic services," *International Journal of Agile Management Systems*, vol. 2, no. 1, pp. 49–54, 2000.

[18] L. M. R. R. A. Novack and C. John Langley Jr., "An internal assessment of logistics value," *Journal of Business Logistics*, vol. 15, pp. 113–152, 1994.

[19] J. T. Mentzer, "Developing a logistics service quality scale," *Journal of Business Logistics*, vol. 20, no. 1, pp. 1–7, 1999.

[20] X. Y. Sun, P. Ji, L. Y. Sun, and Y. L. Wang, "Positioning multiple decoupling points in a supply network," *International Journal of Production Economics*, vol. 113, no. 2, pp. 943–956, 2008.

[21] Y. Wang and Y. Chen, "Multi-CODP adjustment model and algorithm driven by customer requirements in dynamic environments," *Cluster Computing*, vol. 19, no. 4, pp. 2119–2131, 2016.

[22] J.-h. Ji, L.-l. Qi, and Q.-l. Gu, "Study on CODP position of process industry implemented mass customization," *Systems Engineering-Theory & Practice*, vol. 27, no. 12, pp. 151–157, 2007.

[23] F. S. Fogliatto, G. J. C. da Silveira, and D. Borenstein, "The mass customization decade: an updated review of the literature," *International Journal of Production Economics*, vol. 138, no. 1, pp. 14–25, 2012.

[24] S. K. Moon, J. Shu, T. W. Simpson, and S. R. T. Kumara, "A module-based service model for mass customization: service family design," *IIE Transactions*, vol. 43, no. 3, pp. 153–163, 2010.

[25] Z. Wang, X. Xu, and X. Wang, "Mass customization oriented and cost-effective service network," *Lecture Notes in Business Information Processing*, vol. 144, pp. 172–185, 2013.

[26] L. Peters and H. Saidin, "IT and the mass customization of service: the challenge of implementation," *International Journal of Information Management*, vol. 20, pp. 103–119, 2000.

[27] X. Hu, G. Wang, X. Li, Y. Zhang, S. Feng, and A. Yang, "Joint decision model of supplier selection and order allocation for the mass customization of logistics services," *Transportation Research Part E: Logistics and Transportation Review*, vol. 120, pp. 76–95, 2018.

[28] G. Wang, X. Hu, X. Li, Y. Zhang, S. Feng, and A. Yang, "Multiobjective decisions for provider selection and order allocation considering the position of the CODP in a logistics service supply chain," *Computers & Industrial Engineering*, vol. 140, 2020.

[29] I.-J. Jeong, "A dynamic model for the optimization of decoupling point and production planning in a supply chain," *International Journal of Production Economics*, vol. 131, no. 2, pp. 561–567, 2011.

[30] M. Schoenwitz, A. Potter, J. Gosling, and M. Naim, "Product, process and customer preference alignment in prefabricated house building," *International Journal of Production Economics*, vol. 183, pp. 79–90, 2017.

[31] M. de Keizer, R. Akkerman, M. Grunow, J. M. Bloemhof, R. Haijema, and J. G. A. J. van der Vorst, "Logistics network design for perishable products with heterogeneous quality decay," *European Journal of Operational Research*, vol. 262, no. 2, pp. 535–549, 2017.

[32] H. Shidpour, C. Da Cunha, and A. Bernard, "Analyzing single and multiple customer order decoupling point positioning based on customer value: a multi-objective approach," *Procedia CIRP*, vol. 17, pp. 669–674, 2014.

[33] V. G. Cannas, J. Gosling, M. Pero, and T. Rossic, "Engineering and production decoupling configurations: an empirical study in the machinery industry," *International Journal of Production Economics*, vol. 216, pp. 173–189, 2019.

[34] L. C. Guo, Suhao, J. K. Allen, and F. Mistree, "Designing the customer order decoupling point to facilitate mass customization," in *Proceedings of the ASME International Design Engineering Technical Conferences/Computers and Information in Engineering Conference AMER SOC Mechanical Engineers*, Anaheim, CA, USA, August 2020.

[35] W. Liu, Q. Wang, D. Zhu, and Y. Liu, "A determination method of optimal customization degree of logistics service supply chain with mass customization service," *Discrete Dynamics in Nature and Society*, vol. 2014, Article ID 212574, 14 pages, 2014.

[36] C. Babbar and S. H. Amin, "A multi-objective mathematical model integrating environmental concerns for supplier selection and order allocation based on fuzzy QFD in beverages industry," *Expert Systems with Applications*, vol. 92, pp. 27–38, 2018.

[37] H. Akbaş and B. Bilgen, "An integrated fuzzy QFD and TOPSIS methodology for choosing the ideal gas fuel at WWTPs," *Energy*, vol. 125, pp. 484–497, 2017.

[38] C. K. M. Lee, C. T. Y. Ru, C. L. Yeung, K. L. Choy, and W. H. Ip, "Analyze the healthcare service requirement using fuzzy QFD," *Computers in Industry*, vol. 74, pp. 1–15, 2015.

[39] C.-N. Liao and H.-P. Kao, "An evaluation approach to logistics service using fuzzy theory, quality function development and goal programming," *Computers & Industrial Engineering*, vol. 68, pp. 54–64, 2014.

[40] Y. Lin, S. Pekkarinen, and S. Pekkarinen, "QFD-based modular logistics service design," *Journal of Business & Industrial Marketing*, vol. 26, no. 5, pp. 344–356, 2011.

[41] B. Hu, *Foundations of Fuzzy Theory*, Wuhan University Press, Wuhan, China, 2010.

Hindawi
Discrete Dynamics in Nature and Society
Volume 2020, Article ID 6848420, 16 pages
https://doi.org/10.1155/2020/6848420

Research Article

Modelling and Prediction of Random Delays in NCSs Using Double-Chain HMMs

Yuan Ge,[1] Yan Zhang,[1] Wengen Gao,[1] Fanyong Cheng,[1] Nuo Yu,[1] and Jincenzi Wu[2]

[1]*School of Electrical Engineering, Anhui Polytechnic University, Wuhu 241000, China*
[2]*Tandon School of Engineering, New York University, New York, NY, USA*

Correspondence should be addressed to Yuan Ge; ygetoby@mail.ustc.edu.cn

Received 31 July 2020; Revised 17 September 2020; Accepted 30 September 2020; Published 29 October 2020

Academic Editor: Licheng Wang

This paper is concerned with the modelling and prediction of random delays in networked control systems. The stochastic distribution of the random delay in the current sampling period is assumed to be affected by the network state in the current sampling period as well as the random delay in the previous sampling period. Based on this assumption, the double-chain hidden Markov model (DCHMM) is proposed in this paper to model the delays. There are two Markov chains in this model. One is the hidden Markov chain which consists of the network states and the other is the observable Markov chain which consists of the delays. Moreover, the delays are also affected by the hidden network states, which constructs the DCHMM-based delay model. The initialization and optimization problems of the model parameters are solved by using the segmental K-mean clustering algorithm and the expectation maximization algorithm, respectively. Based on the model, the prediction of the controller-to-actuator (CA) delay in the current sampling period is obtained. The prediction can be used to design a controller to compensate the CA delay in the future research. Some comparative experiments are carried out to demonstrate the effectiveness and superiority of the proposed method.

1. Introduction

In traditional control systems, system nodes (such as sensors, controllers, and actuators) are usually connected by the port to port wiring, which may cause many problems such as the difficult wiring and maintenance and the low flexibility and reliability. Such drawbacks appear in many automation systems due to the increasing complexity of controlled plants. With the advent and development of networks, traditional point-to-point control systems are being reshaped and redefined, which gives birth to networked control systems (NCSs) wherein feedback control loops are closed through communication networks [1]. The utilization of a multipurpose shared network to connect spatially distributed components endows control systems with several advantages such as decreased volume of wiring, low installation and maintenance costs, increased system flexibility, and high reliability [2]. Nowadays, NCSs have been extensively applied in many practical systems such as unmanned marine vehicles [3], intelligent manufacture [4], transportation network [5], and haptics collaboration over the Internet [6].

Compared with traditional control systems, the integration of communication network in the control loops leads to network-induced delays, data dropouts, packet disorder, and congestion. Among them, the network-induced delay is the most significant phenomenon that degrades the system performance or even destabilizes the control systems. See [3] for an example of dealing with random delays in networked unmanned marine vehicles. Therefore, it is very necessary and urgent to investigate the random delays while implementing networked control. This is the initial research motivation of this paper. Over the past decade, considerable attention has been paid to the studying of NCSs with delays, and many significant results have been reported in the literature (see [7, 8] and references therein).

Based on the networked structure for the UMV (Figure 1 in [3]), we can draw a typical structure of NCS as shown in Figure 2. The sensor-to-controller delay (called SC delay) in the k th sampling period (denoted as τ_k^{sc}) is exposed when

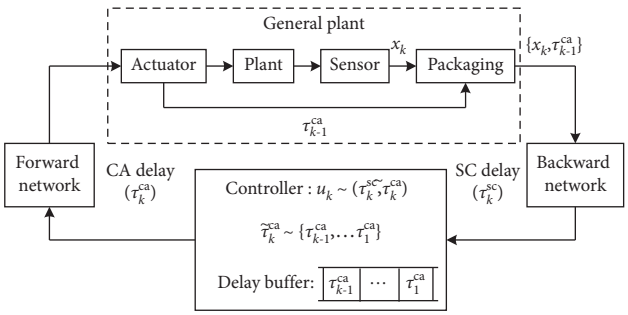

Figure 1: Refined diagram of Figure 2 with some other data.

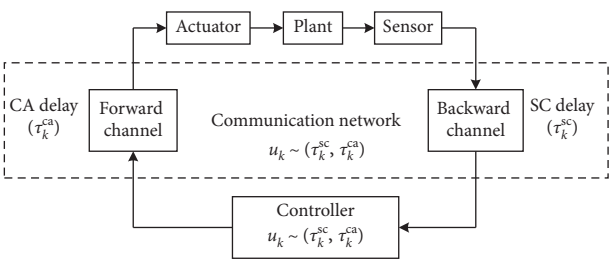

Figure 2: Typical structure of NCS.

the sensor measurement is transmitted from the sensor to the controller. Similarly, the controller-to-actuator delay (called CA delay) in the k th sampling period (denoted as τ_k^{ca}) is exposed when the control law is transmitted from the controller to the actuator. Regardless of the type of network (wired or wireless communication network), the performance of NCSs is always affected by these delays, which can be constant or time-varying according to their distribution characteristics. To compensate the delays, it is often necessary to establish the mathematical model of delays first. The last two decades have witnessed the flourishing evolution of this area in NCSs.

The constant delay occurs in NCSs when a buffer is used on the controller (or actuator) side, and the data in the buffer are read periodically by the controller (or actuator) [9]. For this case, the delay is simply modelled as a constant. As a result, the NCSs can be transformed into deterministic systems, and some conventional deterministic control methodologies have been applied to NCSs in [10, 11]. Nevertheless, the buffer makes the delay artificially increased because the data packet can be used only at some fixed time instant although it has already arrived for a while. The main limitation of the constant delay model leads to much design conservatism, or, even worse, the system stability margin decreases so much that the system becomes unstable.

On the other hand, the controller and actuator in NCSs are usually event-driven, which results in the time-varying delay in NCSs. For this case, two divisions can be found in the literature, i.e., the deterministically varying delay and the stochastically varying delay. In the former division, the variation of delays is not known a priori, but the instantaneous value is available to designers in real time. In the latter division, the variation of the delays is associated with some statistical descriptions: either the case of the current delay being independent of the previous ones or the case of some correlation existing between the current delay and the previous ones.

For the deterministically varying delay, there are three main approaches to analyze the NCSs although the statistics of time-varying delay is not available. The first approach is to transform the network-induced delay into the input delay, and then the recent advances on the delay system approaches can be applied for the analysis and control of NCSs [12, 13]. The second approach is to treat the network-induced delay as a variation parameter of the system, and, more specifically, it is usually called as the exponential uncertainty [14, 15]. Then, the stability and stabilization problems can be solved based on the robust control approach. The third approach is to introduce a new working mode of the actuator, by which the delay can take finite values only, and ultimately the NCS is modelled as a discrete-time switched system with a finite number of subsystems [16, 17]. The main difference between them is that different approaches result in a different system model. The first one models the NCS as a delay system, the second one models the NCS as a parameter-varying system, and the third one models the NCS as a discrete-time switched system.

For the stochastically varying case, the statistics of delays are available for system design, and the stochastic system approach can be applied. To model the random delays, two methods are widely used: one is the independent identically distributed (i.i.d.) model and the other is the Markov chain model. The i.i.d. model is similar to the modelling of stochastic sampling problem, i.e., the delay is partitioned into multiple different time-varying delays and each delay has a certain bound. Then, a delay distribution-based analysis and synthesis approach can be applied for the NCSs with nonuniform distribution characteristics of delays [18, 19]. The same delay distribution-based approach has been extended to fuzzy NCSs in [20, 21]. Different from the i.i.d. model, the Markov chain model is proposed under the assumption that the delay is correlated and the transition of different delays has Markovian property. For the past few years, a lot of effort has been put on the research about Markov chain-based analysis and synthesis methods for random delays in NCSs. These methods can be generally divided into two categories: one considering only SC delays [22] (or CA delays [23]) and the other considering both SC delays and CA delays [24, 25]. In [24, 26], the SC delay and the CA delay were lumped together as a single delay, and then were modelled as a single Markov chain. In [25, 27], the SC delay and the CA delay were modelled as two different Markov chains. Under the Markov chain-based delay model, the NCS is often modelled as a Markovian jump linear system (MJLS), and then many control methodologies (e.g., robust control, predictive control, and fuzzy control) can be used to analyze and synthesize the NCSs with random delays.

The stochastic distribution of current delay is governed by the previous delay in the Markov chain-based delay model. However, some other researchers believe that the stochasticity of current delay should be due in large part to some stochastic network factors (e.g., network load, node competition, and network congestion) which can be described as an abstract random variable named network state. As a result, hidden

Markov models (HMMs) have been successfully used to model random delays of NCSs [28, 29]. In the HMM-based delay model, the stochastic distribution of current delay is only governed by the current network state. This is the main difference between the HMM-based delay model and the Markov chain-based delay model. Along with each packet transmission over the network, the network state will jump from one mode to another following a Markov chain. The network state determines the distribution of random delays. This kind of relationship between the network state and the random delay is referred to as an HMM. According to the delay characteristics, there are mainly three kinds of HMMs to model the random delays of NCSs: discrete-time HMM (DTHMM) [28, 30], continuous-time HMM (CTHMM) [29, 31], and semi-continuous HMM (SCHMM) [32]. Moreover, how to optimally initialize the parameters of HMM-based delay models has been discussed in [33].

Compared with the Markov chain-based delay model which describes the probabilistic relationship among random delays themselves, the HMM-based delay model reveals the essential generation mechanism of random delays and describes the probabilistic relationship between random delays and hidden network states. To a certain extent, the HMM-based delay model is closer to the real distribution of random delays. However, the probabilistic relationship objectively existing among random delays themselves is neglected in the HMM-based delay model. Therefore, to get a more accurate delay model, we prefer to believe that the probabilistic relationship exists not only between random delays and network states, but also between random delays themselves, which is the main motivation of this paper. That is to say, the current delay is governed by the current network state as well as the previous delay. Therefore, the so-called double-chain hidden Markov model (denoted as DCHMM) is introduced in this paper to model the random delays in NCSs. The contribution of this paper lies in the novel modelling method (i.e., DCHMM) that considers the relationship between the random delay and the network state as well as the relationship between the random delay and its previous value. This is the first time in the literature that both the network status and the delay itself are considered simultaneously in the delay modelling. Based on the model, the segmental K-mean clustering algorithm and the expectation maximization algorithm are presented to solve the initialization and optimization problems of the model parameters. Then, the optimized model is used to predict the CA delay and get more accurate delay prediction result than the discrete HMM.

Generally, the CA delay can arbitrarily take values from its acceptable interval, although only a certain discrete value is observed during each sampling period. This is the reason the continuous HMM [29, 31] and semicontinuous HMM [32] have been used to model the CA delays. In these two models, the mixture Gaussian density functions are used to describe the distribution of the CA delays, which improves the modelling accuracy compared with the discrete HMM. However, at the same time, the model parameters to be estimated are augmented and then the computational complexity is increased in these two models. Therefore, for simplicity, the CA delays are limited to a few discrete intervals by using a scalar quantizer, such as the uniform quantizer in [28, 34] and the K-means clustering quantizer in [30], and then the discrete HMM can be used to model the CA delays. Similarly, in this paper, the CA delays will be also quantized into several finite different discrete observations, and more specifically, the observation process will be assumed to possess the Markovian property, which is much different from the discrete HMM in [28, 30] where the observations are independent of each other. Therefore, there are two Markov chains to be considered in this paper, one is the hidden network states and the other is the observable delay observations, which are modelled as the double-chain hidden Markov model (DCHMM). Since the DCHMM concerns the dependency relationship objectively existing among random CA delays, it will present higher precision of modelling and prediction than the discrete HMM, which will be demonstrated through the contrastive experiments in this paper. Nevertheless, the superiority of DCHMM over the continuous or semicontinuous HMM is not so clear unless some continuous stochastic processes other than the Markov chain are used to describe the dependency relationship among random CA delays, which will be investigated in our future work.

The rest of this paper is organized as follows. The problem formulation is given in Section 2. The DCHMM-based delay model and its parameter estimation are presented in Section 3. How to predict the random CA delays based on the DCHMM delay model is proposed in Section 4. The effectiveness and superiority of the proposed methods are illustrated by experimental examples in Section 5. Finally, some concluding remarks are given in Section 6.

2. Problem Formulation

To better present the problem, the block diagram of a typical NCS in Figure 2 is further refined in Figure 1, where some other data (e.g., sensor measurement, control law, and historical CA delays) are annotated. In Figure 1, the sensor is time-driven and samples the plant every h seconds to get the plant state (called sensor measurement and denoted by x_k). Both the controller and the actuator are event-driven, which means that the controller calculates the control law as soon as the sensor measurement arrives at the controller node and the actuator acts as soon as the control law arrives at the actuator node. If the network nodes (i.e., sensor, controller, and actuator) are clock-synchronous (this can be implemented using the method in [35]), the timestamp technology can be used to calculate the SC and CA delays. The sensor measurement is time-stamped before it is transmitted through the backward network, and when it arrives at the controller node, the SC delay can be calculated by comparing the timestamp of the sensor measurement with the local time of the controller node. Similarly, the control law is time-stamped before it is transmitted through the forward network, and when it arrives at the actuator node, the CA delay can be calculated by comparing the timestamp of the control law with the local time of the actuator node.

Both the SC and CA delays may degrade the system performance or even destabilize the control system. Therefore, many kinds of controllers are designed to compensate these delays. When designing the current control law u_k, the current SC delay τ_k^{sc} has occurred and can be measured by using the timestamp

technology (in this paper, the word "current" means the k th sampling period). However, at the same time, the current CA delay τ_k^{ca} has not occurred. In order to compensate the current CA delay τ_k^{ca} by the control law u_k, a feasible way is to predict the current CA delay before designing the control law u_k. Thus, both the predicted CA delay (denoted as $\tilde{\tau}_k^{ca}$) and the measured SC delay τ_k^{sc} are known to the controller and can be compensated only if they are considered into the design of the control law u_k. In this paper, the DCHMM is proposed to model the CA delay and obtain its current predicted value $\tilde{\tau}_k^{ca}$, which aims to improve the prediction accuracy compared with the DTHMM.

There are several parameters (the number of hidden states N, the number of observations M, the probability distribution of the first hidden state π, the transition matrix between hidden states $\mathbf{A}$, and the set of transition matrices between successive outputs given a particular hidden state $\mathbf{B}$) in the DCHMM-based CA delay model (denoted as λ, and $\lambda = (N, M, \pi, \mathbf{A}, \mathbf{B})$). To get the optimal estimation of these parameters, the historical CA delays are needed as the inputs of an iterative optimization process to train these parameters. Therefore, a delay buffer is set at the controller node to collect all the past CA delay data (i.e., $\tau_{k-1}^{ca}, \ldots, \tau_1^{ca}$) as shown in Figure 1. As described above, the adjacent previous CA delay τ_{k-1}^{ca} is calculated at the actuator node and then can be packaged into the current senor measurement x_k to generate a single packet. This packet will be transmitted to the controller through the backward network. Once receiving this packet, the controller will extract the previous CA delay data τ_{k-1}^{ca} from this packet and put it into the delay buffer. In this way, all the past CA delay data are collected in the delay buffer and then can be used to optimally estimate the parameters of the DCHMM-based CA delay model and predict the current CA delay ($\tilde{\tau}_k^{ca}$). Based on the predicted value ($\tilde{\tau}_k^{ca}$) and the real measured value (τ_k^{sc}), some control law can be designed to compensate both the CA delay and the SC delay in the current sampling period. This paper is focused on the modelling and prediction problem, leaving the compensation problem as the future work.

For simplicity, the sum of the SC and CA delay is assumed to be not more than one sampling period (i.e., $\tau_k^{sc} + \tau_k^{ca} \le h$) in this paper, which means that there is no data packet dropout and disorder concerned in this paper.

3. DCHMM-Based Delay Modelling

3.1. Model Derivation. It should be noted that this paper will focus on the discrete-time, discrete-state, and discrete-observation DCHMM, where the state transition probability matrix and the observation transition probability matrix for each state are assumed time homogeneous. Similar to DTHMM, the forward network states are modelled as a time-homogeneous Markov chain with N different states that constitute a discrete finite state set $S = \{1, 2, \ldots, N\}$. Generally, the network state (denoted as s) defines the whole working status of the network and is an abstract variable that comprehensively reflects the stochastic factors (e.g., network load, nodes competition, and network congestion) of the network. The network state in the k th sampling period is represented as s_k. Obviously, $s_k \in S(s)$ holds. Along with each packet transmission in the forward network, the network state may transfer from one mode to another through Markovian property described as the following equation:

$$\begin{aligned} P(s_{k+1} = j | s_k = i, s_{k-1}, \ldots, s_1) \\ = P(s_{k+1} = j | s_k = i) = a_{ij}, \quad (i, j \in S, \forall k \in \mathbb{Z}). \end{aligned} \tag{1}$$

The Markovian property tells us that the conditional probability distribution of the network state in the next sampling period (denoted as s_{k+1}) depends only upon the current network state s_k, not on the past network states $\{s_{k-1}, \ldots, s_1\}$. In equation (1), a_{ij} ($\in [0, 1]$) denotes the one-step transition probability of going from the network state i at time k to the network state j at time $k+1$, satisfying the constraint: $a_{ij} \ge 0$ and $\sum_{j=1}^{N} a_{ij} = 1$. The Markovian property of network states is illustrated in Figure 3(a). All one-step transition probabilities construct a one-step transition matrix $\mathbf{A} = \{a_{ij}\}_{1 \le i,j \le N}$ as shown in Figure 3(b). For the special case of time $k = 1$, a_{ij} is simplified into an initial state probability of the first hidden network state that is defined by π_j as follows:

$$\pi_j = P(s_1 = j). \tag{2}$$

Obviously, $\pi_j \ge 0$ and $\sum_{j=1}^{N} \pi_j = 1$ hold. All possible initial state probabilities construct an initial vector $\pi = \{\pi_j\}_{1 \le j \le N}$.

Now, these parameters (N, π, and $\mathbf{A}$) define a Markov chain of network states. As is known, the DCHMM describes a two-stage stochastic process. The defined Markov chain is exactly the first stage of the DCHMM-based delay model. In the second stage, for every state at time k additionally a CA delay τ_k^{ca} is generated. As mentioned before, the DCHMM proposed in this paper has finite discrete observations and the observations for each state construct a time-homogeneous Markov chain. Similar to the DTHMM [28, 30], the observations are also obtained by quantizing the CA delays, and then they can be used to estimate the parameters of the DCHMM-based delay model. The delay interval ($(0, h]$) is assumed to consist of a complete set such as $(0, h) = (h_0, h_1) \cup (h_1, h_2] \cup \cdots \cup (h_{M-2}, h_{M-1}] \cup (h_{M-1}, h_M]$ (where $h_0 = 0$ and $h_M = h$), and for ($\tau_k \in h_{m-1}, h_m]$ ($m = 1, \ldots, M$), a new observation (o_k) is defined as $o_k = m$ with an observation space $O = \{1, 2, \ldots, M\}$ and $o_k \in O$ holds. After $k-1$ sampling periods, one can get a set of network states: $\bar{s} = \{s_1, s_2, \ldots, s_{k-1}\}$, a set of the CA delays: $\bar{\tau}^{ca} = \{\tau_1^{ca}, \tau_2^{ca}, \ldots, \tau_{k-1}^{ca}\}$ and a corresponding set of observations: $\bar{o} = \{o_1, o_2, \ldots, o_{k-1}\}$ by quantizing the CA delays, which lay a foundation for deriving the DCHMM-based delay model.

Under the previously mentioned time homogeneous assumption, the conditional probability of obtaining the observation o_k for the DCHMM is defined as follows:

$$\begin{aligned} b_{lm}^{(i)} &= P(o_k = m | s_k = i, s_{k-1}, \ldots, s_1, o_{k-1} = l, o_{k-2}, \ldots, o_1) \\ &= P(o_k = m | s_k = i, o_{k-1} = l), \quad (i \in S, l, m \in O, \forall k \in \mathbb{Z}). \end{aligned} \tag{3}$$

In equation (3), $b_{lm}^{(i)}$ ($\in [0, 1]$) denotes the conditional transition probability of going from the observation l at time

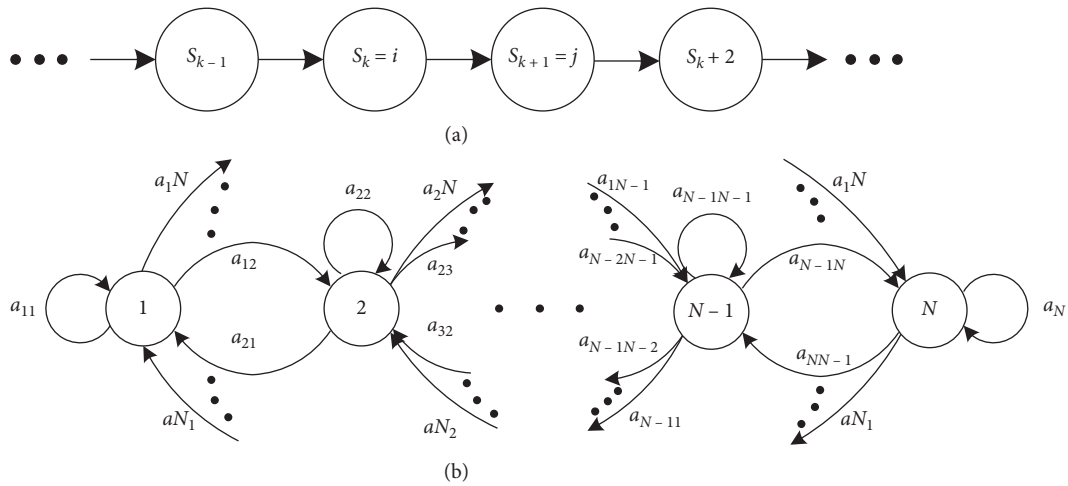

Figure 3: Markov chain for the network states: (a) Markovian property; (b) transition matrix.

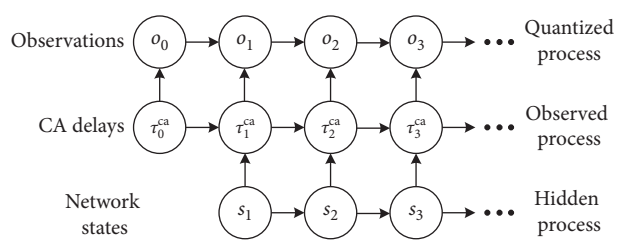

Figure 4: DCHMM-based delay model.

$k-1$ to the observation m at time k for the network state i at time k, satisfying the constraint: $b_{lm}^{(i)} \geq 0$ and $\sum_{m=1}^{M} b_{lm}^{(i)} = 1$. For a given state $i \in S$, let the matrix $\mathbf{B}^{(i)}$ define the conditional observation transition probabilities for the state i, where the (l, m) entry of $\mathbf{B}^{(i)}$ is $b_{lm}^{(i)}$. That is, if the DCHMM is currently in the state i, $\mathbf{B}^{(i)}$ will be the observation transition probability matrix used to determine the observation at the current time point given the observation which was obtained at the previous time point. From this, it can be seen that the observation of the DCHMM-based delay model can be viewed as a time inhomogeneous Markov chain, where the transition probability matrix used for the observations is dependent on the hidden network state of the DCHMM.

Based on the definitions in equations (1), (2), and (3), the DCHMM-based delay model, which is usually denoted as λ, can be completely described as follows:

(1) A finite set of network states $S = \{1, 2, \ldots, N\}$

(2) A matrix $\mathbf{A}$ of state transition probabilities:

$$\mathbf{A} = \left\{a_{ij} | a_{ij} = P\left(s_k = j | s_{k-1} = i\right)\right\}, \quad i, j \in S. \tag{4}$$

(3) A vector π of initial state distribution:

$$\boldsymbol{\pi} = \left\{\pi_j | \pi_j = P\left(s_1 = j\right)\right\}, \quad j \in S. \tag{5}$$

(4) A set of the transition matrix between successive observations given a particular state i $(i \in S)$:

$$\mathbf{B} = \left\{\mathbf{B}^{(i)}\right\} \text{ with } \mathbf{B}^{(i)} = \left[b_{lm}^{(i)}\right], \quad l, m \in O. \tag{6}$$

From the above, $\lambda = (N, M, \pi, \mathbf{A}, \mathbf{B})$. In general, N and M are known in advance, so λ can be rewritten as follows for simplicity:

$$\lambda = (\boldsymbol{\pi}, \mathbf{A}, \mathbf{B}). \tag{7}$$

Equation (7) gives the definition of the DCHMM-based delay model which is represented in Figure 4.

Remark 1. The DCHMM is a generalization of both a visible Markov chain and a hidden Markov chain. When there is only one hidden state $(N = 1)$, the DCHMM reduces to an homogeneous Markov chain with transition matrix $\mathbf{B}^{(1)}$. On the other hand, when there are $N > 1$ hidden states but each matrix $\mathbf{B}^{(i)}$ $(i \in S)$ has identical rows, the model reduces to a DTHMM.

In Figure 4, the observed process is governed by a hidden Markov chain in which successive observations are directly correlated through the Markov property. The DCHMM presented in this paper combines characteristics of both visible and hidden models. It is called "double" since it can be viewed as the superposition of two interlinked Markov chains: the hidden Markov chain governing the relation between states of a nonobservable variable (i.e., network state) and the visible Markov chain governing (together with the hidden state process) the relation between outputs of an

observed variable (i.e., CA delay). That is, the DCHMM has a similar stochastic framework to the HMM, but now it is assumed that, for a given time point k, the current CA delay τ_k^{ca} is not only dependent on the current hidden state s_k but also dependent (through the Markov property) on the previous CA delay τ_{k-1}^{ca}.

In Figure 4, since the value of τ_1^{ca} depends on the past, we consider an initial CA delay value (τ_0^{ca}) at time 0 with no corresponding hidden state, and its corresponding observation is o_0. Based on this consideration, the set of the past CA delays $\overline{\tau}^{\text{ca}}$ is redefined as $\overline{\tau}^{\text{ca}} = \{\tau_0^{\text{ca}}, \tau_1^{\text{ca}}, \tau_2^{\text{ca}}, \ldots, \tau_{k-1}^{\text{ca}}\}$, and the corresponding set of the observations $\overline{o}$ is redefined as $\overline{o} = \{o_0, o_1, o_2, \ldots, o_{k-1}\}$.

Remark 2. The dependence of the current CA delay on both the current network state and the previous CA delay can be explained as follows. The CA delay process can be considered as a Markov chain, where the transition probability matrix is dependent on the current network state occupied. That is, the transition probability matrix of the CA delay process is associated with each state in the network state space, and each time the DCHMM enters a new state, the transition probability matrix of the CA delay process for that network state is used to determine which observation (given the previous CA delay) will be emitted for that time point. The CA delay process can thus be viewed as a time inhomogeneous Markov chain, where the transition probability matrix used for the observation process is driven by the hidden state process of the DCHMM.

One of the benefits to introduce the DCHMM-based delay model is that the advantages of both the Markov chain and the HMM are conserved. That is, the system is driven by an unobserved process, and the successive observations are also directly correlated.

3.2. Model Estimation. In order to get the accurate prediction of the current CA delay ($\tilde{\tau}_k^{\text{ca}}$) by using the DCHMM-based delay model as described in equation (7), three different estimation problems have to be considered as follows:

Q1: the estimation of the likelihood of a sequence of observations $\{o_0, o_1, \ldots, o_k\}$ given a model λ

Q2: the estimation of the parameters π, **A** and **B** given a sequence of observations

Q3: The estimation of the optimal sequence of hidden network states given a model and a sequence of outputs

These three problems are similar to the problems occurring in DTHMM theory and can be solved using similar methods. Q1 is solved using a forward iterative algorithm. Q2 is achieved with an Expectation Maximization (EM) algorithm. Q3 is obtained through the Viterbi algorithm.

Remark 3. In this section, only the resulting formulas for each algorithm are given. The complete derivation is provided in Appendix A. Moreover, as presented here, the three algorithms can lead to numerical problems since they involve the calculation of infinitesimal values. A good solution is to normalize the intermediary results at each step of the calculation. The practical implementation of this method is discussed in Appendix B.

3.2.1. Likelihood of the Observation. The likelihood of the observation $\overline{o}$ ($\overline{o} = \{o_0, o_1, \ldots, o_{k-1}\}$) given the DCHMM-based delay model λ is defined as follows:

$$L = P(o_0, o_1, \ldots, o_{k-1}|\lambda). \tag{8}$$

An iterative procedure similar to the forward procedure developed in [32] for the estimation of the SCHMM is proposed to get the likelihood in equation (8). A forward variable is defined as follows:

$$\alpha_r(j) = P(o_0, \ldots, o_r, s_r = j|\lambda). \tag{9}$$

For $r = 1$, equation (9) becomes

$$\alpha_1(j) = b_{o_0 o_1}^{(j)} \pi_j. \tag{10}$$

In the general case, for $r = 2, \ldots, k-1$,

$$\alpha_r(j) = b_{o_{r-1} o_r}^{(j)} \sum_{i=1}^{N} a_{ij} \alpha_{r-1}(i), \quad i, j \in S. \tag{11}$$

By summing $\alpha_{k-1}(j)$ over j, one can obtain the likelihood of the entire sequence of observation $\overline{o}$:

$$L(o_0, o_1, \ldots, o_{k-1}) = \sum_{j=1}^{N} P(o_0, o_1, \ldots, o_{k-1}, s_{k-1} = j) = \sum_{j=1}^{N} \alpha_{k-1}(j). \tag{12}$$

The iterative computation of $\alpha_r(j)$ is sufficient to obtain the likelihood. Moreover, another iterative algorithm similar to the backward procedure appearing in [32] is defined here. It will be used later for the estimation of the parameters of the DCHMM-based delay model. The backward variable is defined as follows.

$$\beta_r(i) = P(o_{r+1}, \ldots, o_{k-1}|o_r, s_r = i, \lambda). \tag{13}$$

For $r = k-1$, we obtain

$$\beta_{k-1}(i) = 1, \tag{14}$$

and for $r = 1, \ldots, k-2$,

$$\beta_r(i) = \sum_{j=1}^{N} a_{ij} b_{o_r o_{r+1}}^{(j)} \beta_{r+1}(j). \tag{15}$$

With this result, the likelihood in equation (12) can be rewritten as

$$L(o_0, o_1, \ldots, o_{k-1}) = \sum_{i=1}^{N} \alpha_r(i) \beta_r(i), \quad r = 1, \ldots, k-1. \tag{16}$$

Equation (12) corresponds to $r = k-1$.

3.2.2. Estimation of π, $\mathbf{A}$, and $\mathbf{B}$. The complete identification of the DCHMM-based delay model requires the estimation of three sets of probabilities: π, $\mathbf{A}$, and $\mathbf{B}$. We use an expectation maximization (EM) algorithm for the parameter estimation as we have done in [32].

First, we define the joint probability of two successive hidden network states as follows:

$$\varepsilon_r(i,j) = P(s_r = i, s_{r+1} = j | o_0, \ldots, o_{k-1}) = \frac{\alpha_r(i) a_{ij} b^{(j)}_{o_r o_{r+1}} \beta_{r+1}(j)}{L(o_0, \ldots, o_{k-1})}, \quad i, j \in S, r = 1, \ldots, k-2. \tag{17}$$

Then, we define the marginal distribution of the hidden network states as follows:

$$\xi_r(i) = P(s_r = i | o_0, \ldots, o_{k-1}) = \sum_{j=1}^{N} \varepsilon_r(i,j) = \frac{\alpha_r(i)\beta_r(i)}{L(o_0, \ldots, o_{k-1})}, \quad i \in S, r = 1, \ldots, k-2. \tag{18}$$

Using ε_r and ξ_r, we can write the reestimation formula for π, $\mathbf{A}$, and $\mathbf{B}$ as follows:

$$\hat{\pi}_i = P(s_1 = i | o_0, \ldots, o_{k-1}) = \xi_1(i), \tag{19}$$

$$\hat{a}_{ij} = \sum_{r=1}^{k-2} P(s_{r+1} = j | s_r = i, o_0, \ldots, o_{k-1}) = \frac{\sum_{r=1}^{k-2} \varepsilon_r(i,j)}{\sum_{r=1}^{k-2} \xi_r(i)}, \tag{20}$$

$$\begin{aligned} \hat{b}^{(i)}_{lm}(r) &= P(o_r = m | o_0, \ldots, o_{r-1} = l, \ldots, o_{k-1}, s_r = i) \\ &= P(o_r = m | o_{r-1} = l, s_r = i) = \frac{\sum_{r=1}^{k-2} \xi_r(i) \; o_{r-1} = l, o_r = m}{\sum_{r=1}^{k-2} \xi_r(i) \; o_{r-1} = l}. \end{aligned} \tag{21}$$

In practice, the parameter estimation of the DCHMM-based delay model is achieved using iteratively the forward-backward procedure and the reestimation formulas in (19)~(21). Generally, after dozens of iteration, one can obtain the optimum model parameters λ^* ($\lambda^* = (\pi^*, \mathbf{A}^*, \mathbf{B}^*)$, where $\pi^* = \{\pi_i^*\}$, $\mathbf{A}^* = \{a_{ij}^*\}$, and $\mathbf{B}^* = \{b_{lm}^{(i)*}\}$.

3.2.3. Optimal Sequence of Hidden States. Once we have an estimation of the DCHMM-based delay model, we can search the optimal sequence of hidden network states which maximizes the following conditional probability:

$$P(s_1, \ldots, s_{k-1} | o_0, o_1, \ldots, o_{k-1}), \tag{22}$$

or the joint probability

$$P(s_1, \ldots, s_{k-1}, o_0, o_1, \ldots, o_{k-1}). \tag{23}$$

This problem can be solved through an iterative dynamic procedure called the Viterbi algorithm. For $r = 1$ and $j = 1, \ldots, N$, we define

$$\delta_1(j) = P(o_0, o_1, s_1 = j) = \pi_j b^{(j)}_{o_0 o_1}, \tag{24}$$

and for $r = 2, \ldots, k-1$,

$$\begin{aligned} \delta_r(j) &= \max_{i_1, \ldots, i_{r-1}} P(o_0, \ldots, o_r, s_1 = i_1, \ldots, s_{r-1} = i_{r-1}, s_r = j) \\ &= \left[\max_{i_1, \cdots, i_{r-1}} \delta_{r-1}(i_{r-1}) a_{i_{r-1} j} \right] b^{(j)}_{o_{r-1} o_r}. \end{aligned} \tag{25}$$

The optimal network state at time $k-1$ is then predicted as

$$\tilde{s}_{k-1} = \arg \max_{j=1,\cdots,N} \delta_{k-1}(j), \tag{26}$$

and we obtain recursively for $r = k-2, \ldots, 1$:

$$\tilde{s}_r = \arg \max_{j=1,\cdots,N} \delta_{r+1}(j) a_{j \tilde{s}_{r+1}}. \tag{27}$$

Finally, the joint probability of the sequence of hidden network states and the sequence of observed CA delay outputs is equal to

$$P(s_1, \ldots, s_{k-1}, o_0, o_1, \ldots, o_{k-1}) = \max_{j=1,\cdots,N} \delta_{k-1}(j). \tag{28}$$

As a dynamic programming method, every decision in the computation of the $\delta_r(j)$ is only locally optimal in the Viterbi algorithm. The globally optimum of the state sequence $\tilde{s}$ is only known after the evaluation of the $\delta_{k-1}(j)$, i.e., after the CA delay sequence has been considered in its entire length. The state $\tilde{s}_{k-1}$ maximizing $\delta_{k-1}(j)$ denotes the end of the optimal state sequence. The predecessor states can be determined by means of backtracking in (27).

4. Delay Prediction

Based on the optimal prediction of the network state $\tilde{s}_{k-1}$ at time $k-1$ and the optimal estimation of the parameters $\mathbf{A}$ and $\mathbf{B}$, the method to predict the current CA delay ($\tilde{\tau}_k^{\mathrm{ca}}$) is proposed as follows.

Step 1. Predict the optimal network state in the current (i.e., k th) sampling period, which is denoted as $\tilde{s}_k$:

$$\tilde{s}_k = \arg \max_{j \in S} a^*_{\tilde{s}_{k-1} j}. \tag{29}$$

Step 2. Predict the optimal observation of the current CA delay, which is denoted as $\tilde{o}_k$:

$$\tilde{o}_k = \arg\max_{m \in O}\left(b_{o_{k-1}m}^{(\tilde{s}_k)*}\right). \tag{30}$$

Step 3. Predict the optimal CA delay in the current (i.e., k th) sampling period, which is denoted as $\tilde{\tau}_k^{\mathrm{ca}}$:

$$\tilde{\tau}_k^{\mathrm{ca}} = \frac{1}{2}\left(h_{\tilde{o}_k} - h_{\tilde{o}_k - 1}\right). \tag{31}$$

Remark 4. Once we get the optimal network state in the previous sampling period $(\tilde{s}_{k-1})$ by using (26), the probability of different network state j $(j \in S)$ in the current sampling period can be calculated based on the Markovian property of network states in (1), and the state that maximizes the probability is the optimal prediction of the current network state $(\tilde{s}_k)$. Based on the prediction $(\tilde{s}_k)$ and the previous observation of CA delay (o_{k-1}), the probability of different delay observation m $(m \in O)$ in the current sampling period can be calculated according to (3), and the observation that maximizes the probability is the optimal prediction of the current CA delay observation $(\tilde{o}_k)$. For the predicted observation $(\tilde{o}_k)$, how to calculate the prediction of the current CA delay depends on the delay quantization method. As discussed in [30], there are two kinds of delay quantization methods to obtain the observations of historical CA delays, namely, uniform quantization and K-means clustering quantization. For the uniform quantization, the prediction of the current CA delay $(\tilde{\tau}_k^{\mathrm{ca}})$ is set to the midpoint of the subinterval which the current observation $(\tilde{o}_k)$ falls in. Based on the definition of the complete subintervals, the subinterval which the observation $\tilde{o}_k$ falls in is $(h_{\tilde{o}_k - 1}, h_{\tilde{o}_k}]$, and then the prediction of the current CA delay is given in (31). For the K-means clustering quantization, the prediction of the current CA delay $(\tilde{\tau}_k^{\mathrm{ca}})$ is set to the centroid of the cluster which the current observation $(\tilde{o}_k)$ falls in, and the corresponding calculating method is given as following step 3.

Step 4. Predict the optimal CA delay in the current (i.e., k th) sampling period, which is denoted as $\tilde{\tau}_k^{\mathrm{ca}}$:

$$\tilde{\tau}_k^{\mathrm{ca}} = c_{\tilde{o}_k}. \tag{32}$$

In (32), $c_{\tilde{o}_k}$ is the centroid of the cluster which the current observation $(\tilde{o}_k)$ falls in. The detailed K-means clustering quantization method and the definition of the cluster centroid have been given in [30]. Actually, we have proved that the K-means clustering quantization is better than the uniform quantization in improving the prediction accuracy of CA delays. Therefore, we will only use equation (32) to predict the current CA delay in the experiments of this paper.

5. Illustrative Example

Some comparative experiments are carried out in this section to demonstrate the effectiveness and superiority of the methods proposed in this paper. For the sake of comparison, the experimental context is designed as the same as that in [32], and the CA delay values shown in Figure 4 of [32] are used again here to derive the DCHMM-based delay model and validate the prediction of CA delays. For the convenience of reading, Figure 4 of [32] is redrawn as follows. In Figure 5, the first 200 CA delay values (from 1 to 200 on the x-coordinate) are used for the parameter estimation of the DCHMM-based delay model, and the last 200 CA delay values (from 201 to 400 on the x-coordinate) are used to evaluate the predictive effect based on the model. The main difference between the experiments in this paper and that in [32] is that this paper not only considers the relationship between the CA delays and the network states but also considers the relationship between the adjacent CA delays. That is to say, the distribution of the current CA delay in this paper is not only dependent on the current network states but also related to the previous CA delay.

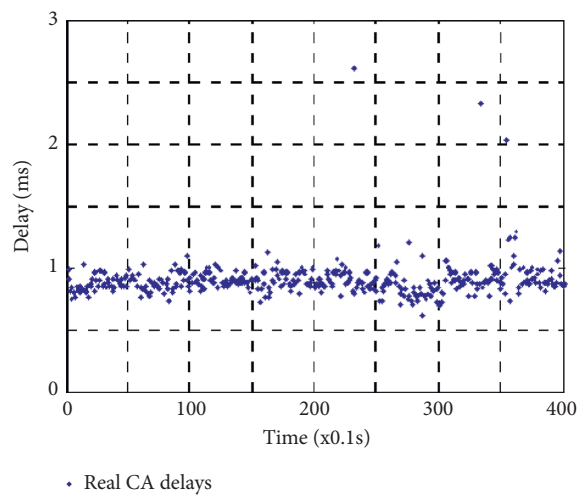

Figure 5: Real CA delay values.

Firstly, we need to initialize the DCHMM-based delay model λ^0 $(\lambda^0 = (N, M, \pi^0, \mathbf{A}^0, \mathbf{B}^0))$. By using the optimal stabilization methods in [33], we can obtain that the optimal initial values of N and M are 4 and 6, respectively, which means that there are four different network states (i.e., $S = \{1, 2, 3, 4\}$), and the delay interval $((0, h])$ can be divided into six complete subinterval (i.e., $M = 6$, and $O = \{1, 2, 3, 4, 5, 6\}$). The vector of initial state distribution (π^0) and the matrix of state transition probabilities $(\mathbf{A}^0)$ can be almost uniformly initialized as follows, since they have little effect on the DCHMM-based delay model:

$$\boldsymbol{\pi}^0 = \begin{bmatrix} 0.25 & 0.25 & 0.25 & 0.25 \end{bmatrix},$$
$$A^0 = \begin{bmatrix} 0.25 & 0.25 & 0.25 & 0.25 \\ 0.25 & 0.25 & 0.25 & 0.25 \\ 0.25 & 0.25 & 0.25 & 0.25 \\ 0.25 & 0.25 & 0.25 & 0.25 \end{bmatrix}. \tag{33}$$

Compared with π^0 and $\mathbf{A}^0$, the initial value of the observation matrix $(\mathbf{B}^0)$ is very crucial to the parameter

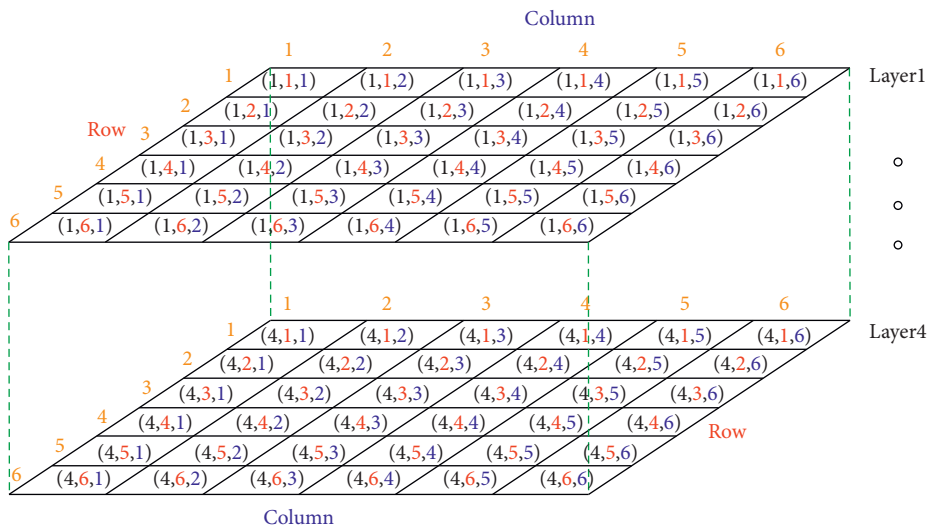

Figure 6: The detailed structure of the observation matrix.

estimation of the DCHMM-based delay model. The uniform initialization method is no longer suitable for obtaining the optimal initial value of the observation matrix ($\mathbf{B}^0$). In this section, the segmental K-means clustering algorithm proposed in [33] is used to optimally initialize the observation matrix ($\mathbf{B}^0$) as follows based on the first 200 CA delay values in Figure 5. With $N = 4$ and $M = 6$, we can rewrite the entry of the observation matrix $\mathbf{B}$ as follows according to equation (3):

$$i \in S = \{1, 2, 3, 4\} \text{ with } i \in S = \{1, 2, 3, 4\}, l, m \in O = \{1, 2, 3, 4, 5, 6\}. \tag{34}$$

Obviously, the matrix $\mathbf{B}$ is a three-dimensional matrix, in which i denotes the layer of the matrix, l denotes the row of each layer, and m denotes the column of each layer. The detailed structure of the matrix $\mathbf{B}$ is given in Figure 6. There are 4 layers in the matrix $\mathbf{B}$, and every layer has 36 elements, which makes the matrix $\mathbf{B}$ have a total of 144 elements. In Figure 6, the black number corresponds to the number of layers, the red number to the number of rows, and the blue number to the number of columns. For simplicity, the matrix elements of the second and third layers are omitted here since they are easy to figure out.

Based on the definition in equation (3), all the elements of the matrix $\mathbf{B}$ satisfy the following constraint relation. Each element is greater than or equal to 0 and less than or equal to 1, and the sum of each row in each layer is equal to 1:

$$0 \le b_{lm}^{(i)} \le 1, \quad \sum_{m=1}^{6} b_{lm}^{(i)} = 1. \tag{35}$$

Based on the first 200 CA delay values in Figure 5, the optimal initial values ($\mathbf{B}^0$) of the observation matrix can be obtained as shown in Figure 7 by using the segmental K-means clustering algorithm proposed in [33].

In general, the network status is good and the large numeric elements have relatively small row and column numbers in Figure 7. In order to illustrate this point, we transform layer 1 in Figure 7 into Figure 8 that is a matrix plot with M rows and M columns. In the same way, the other three layers (layer 2 to 4) in Figure 7 can be transformed into their corresponding matrix plots, and the transformed result is omitted here for simplicity. In the matrix plot of Figure 8, each element is a colored dial. The color value (referring to the right color bar) and the size of the colored sector in one rectangle block (i, j) $(1 \le i, j \le M)$ are determined by the initial value corresponding to the same (i, j) entry of layer 1 in Figure 7. In Figure 8, the region on the left shows the relatively large color values as well as the size of the colored sectors, while the region on the right shows the relatively small color values as well as the size of the colored sectors. Figure 8 illustrates, from another perspective, that the network always shifts to the state with short delay and presents a good status.

Secondly, we can use the EM algorithm to train the DCHMM-based delay model based on the initialized model λ^0 and the first 200 delay values in Figure 5. During this experiment, the maximum iterative number of the training procedure is set to 40 and the threshold ε to terminate the procedure is set to 5×10^{-4}. Under these conditions, it is found that the training procedure can always converge after dozens of iterations. At the end of this procedure, the optimized parameters $(\pi^*, \mathbf{A}^*, \mathbf{B}^*)$ of the DCHMM-based delay model are obtained as follows. Considering that the matrix $\mathbf{B}^*$ contains too many elements (144 in total), which makes it unrepresentable, we present it in the form of a one-dimensional curve as shown in Figure 9 where every 36 coordinates on the horizontal axis corresponds to one layer of $\mathbf{B}^*$:

$$\boldsymbol{\pi}^* = \begin{bmatrix} 0.1377 & 0.3956 & 0.3012 & 0.1655 \end{bmatrix},$$
$$\mathbf{A}^* = \begin{bmatrix} 0.6308 & 0.1317 & 0.1292 & 0.1083 \\ 0.2116 & 0.5719 & 0.1125 & 0.1040 \\ 0.1125 & 0.1726 & 0.5122 & 0.2027 \\ 0.1047 & 0.2108 & 0.2014 & 0.4831 \end{bmatrix}. \tag{36}$$

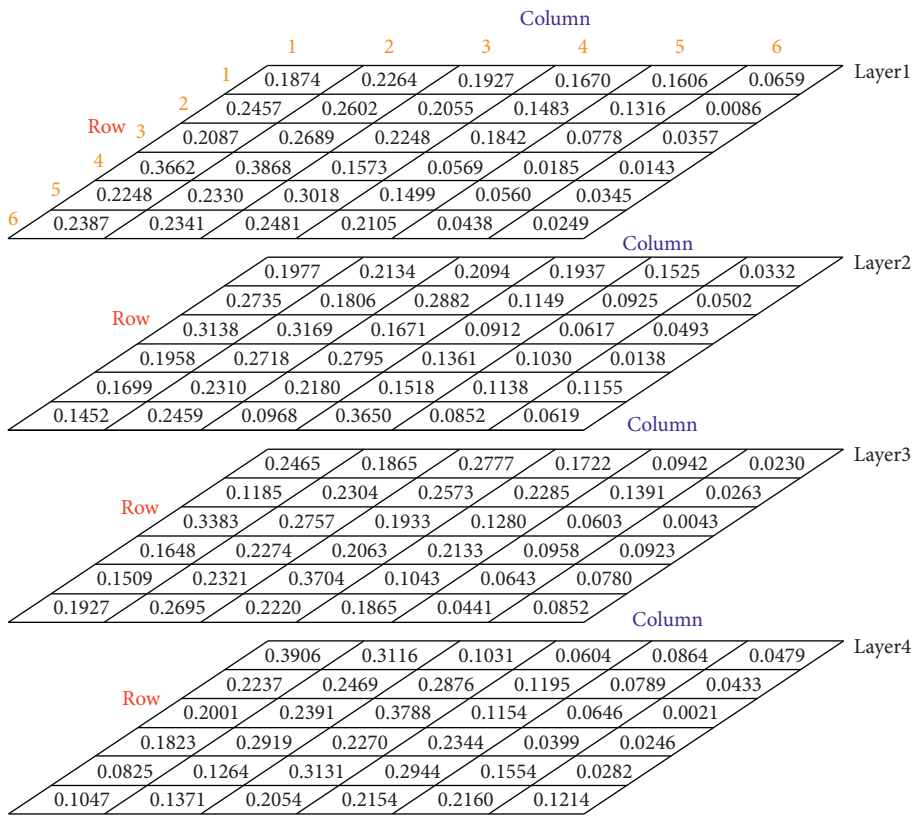

Figure 7: The optimal initial values of the observation matrix.

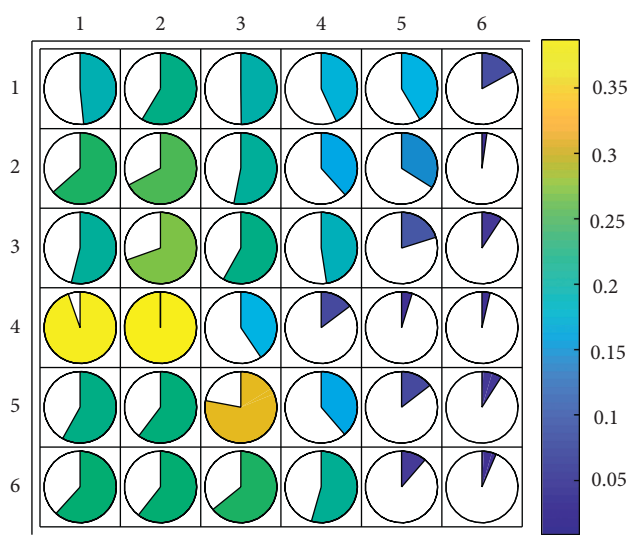

Figure 8: Distribution of the initial values on layer 1 of $\mathbf{B}^0$.

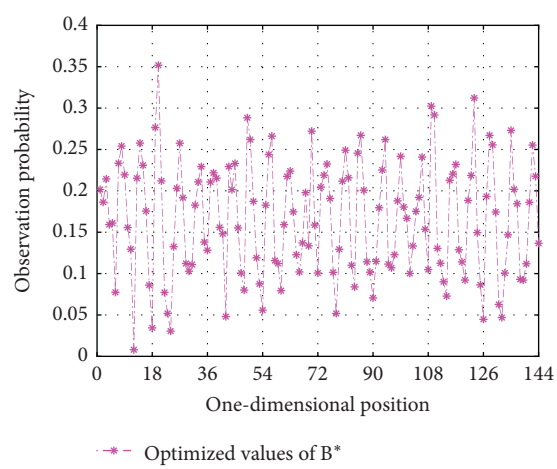

Figure 9: One-dimensional distribution of the optimized values of $\mathbf{B}^*$.

Thirdly, we can use the Viterbi algorithm to get the optimal previous network state and then predict the current CA delay through three steps. The first step uses equation (29) to estimate the optimal current network state. The second step uses equation (30) to estimate the optimal observation of the current CA delay. The third step uses equation (32) to predict the current CA delay. Taking the three steps, the predicted values of CA delays can be obtained. For example, during the 201st period, the predicted value is 0.8591 ms that is close to the real value 0.8432 ms in Figure 5, and the relative error is 1.89%. By recursively executing the three steps in the following periods, we can get other predicted CA delay values from the 202nd to the 400th period as shown in Figure 10.

To judge the predictive precision of the DCHMM-based delay model, the mean-squared error (*MSE*) is defined as follows in this experiment:

$$\mathrm{MSE} = \frac{1}{200} \sum_{r=201}^{400} \left(\tilde{\tau}_r^{\mathrm{ca}} - \tau_r^{\mathrm{ca}}\right)^2. \tag{37}$$

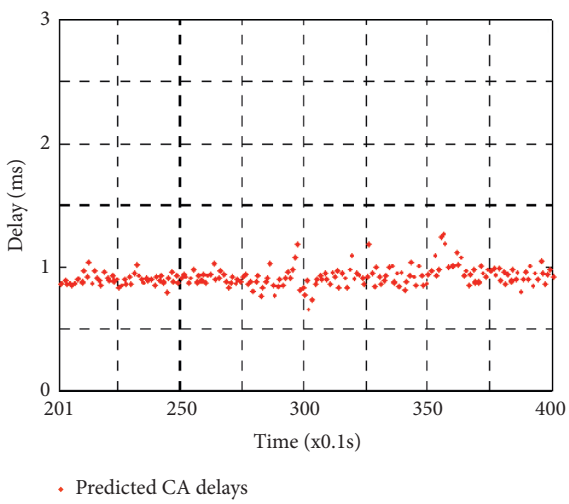

Figure 10: Predicted CA delay values.

According to the predicted values in Figure 10 and the real values in Figure 5, we can calculate that the *MSE* is 0.0032 by using equation (37), which is denoted as $\mathrm{MSE}_{\mathrm{DCHMM}}$ (i.e., $\mathrm{MSE}_{\mathrm{DCHMM}} = 0.0032$). Generally, such prediction accuracy has been very high and is acceptable in NCS.

To illustrate the superiority of the DCHMM-based delay model over the DTHMM-based delay model in the prediction accuracy, we carry out again the experiment under the DTHMM-based delay model in [33]. Without considering the dependence between adjacent CA delays, the observation matrix $\mathbf{B}^0$ degenerates into a two-dimensional matrix, in which the rows represent the network states and the columns represent the intervals of CA delays. Under the same experiment condition, the predicted value is 0.8706 ms during the 201st period for the DTHMM-based delay model, and the relative error is 3.25% (>1.89% for the DCHMM-based delay model). Therefore, the DCHMM-based delay model proposed in this paper gives a better prediction of the CA delay during the 201st period than the DTHMM-based delay model. Moreover, by the end of this experiment, we got that the *MSE* for the DTHMM-based delay model is 0.0043 ($>0.0032 = \mathrm{MSE}_{\mathrm{DCHMM}}$), which is denoted as $\mathrm{MSE}_{\mathrm{DTHMM}}$ (i.e., $\mathrm{MSE}_{\mathrm{DTHMM}} = 0.0043$). Obviously, we have $\mathrm{MSE}_{\mathrm{DTHMM}} > \mathrm{MSE}_{\mathrm{DCHMM}}$, which demonstrates the superiority of the DCHMM-based delay model over the DTHMM-based delay model in the prediction of CA delays.

Besides, we try to compare the DCHMM-based delay model over the SCHMM-based delay model proposed in [32] and get some interesting results. In the experiment of [33], the predicted value is 0.8615 ms during the 201st period for the SCHMM-based delay model, and the relative error is 2.17% (>1.89% for the DCHMM-based delay model). However, we cannot simply assume that the DCHMM-based delay model is superior to the SCHMM-based delay model. Actually, by the end of the experiment, the MSE for the SCHMM-based delay model is 0.0029 ($<0.0032 = \mathrm{MSE}_{\mathrm{DCHMM}}$), which is denoted here as $\mathrm{MSE}_{\mathrm{SCHMM}}$ (i.e., $\mathrm{MSE}_{\mathrm{SCHMM}} = 0.0029$). It is easy to find that $\mathrm{MSE}_{\mathrm{SCHMM}} < \mathrm{MSE}_{\mathrm{DCHMM}} < \mathrm{MSE}_{\mathrm{DTHMM}}$. So, from this point of view, the DCHMM-based delay model is not superior to the SCHMM-based delay model in the prediction of CA delays. This is mainly because that the delays are treated as discrete values and quantized into some limited subintervals in the DCHMM-based delay model. If the delays are treated as continuous values and can take any value in its allowable interval or if the dependency relationship among random CA delays is taken into account in the SCHMM-based delay model, the derived DCHMM-based delay model will give more accurate prediction and show the superiority over the SCHMM-based delay model, which will be demonstrated in our future work.

6. Conclusions

In networked control systems, random delays are the main cause that degrades the system performance and even causes the system instability. A feasible method to compensate the random delays is to take the random delays into the design of the controller. Considering the CA delay has not occurred when the controller is designed, we need to predict the CA delay before designing the controller. To get a high-precision prediction value, it is necessary to establish a high-precision delay model first. Different from the existing modelling methods, this paper considers the dependency between the network states and the CA delays as well as the interdependence between the CA delays. The dependency between the network states and the CA delays is modelled as a hidden Markov model, and the interdependence between the CA delays is modelled as a Markov chain. As a result, the double-chain hidden Markov model (DCHMM) is proposed in this paper to model the random CA delays for the first time in the networked control systems. As the name implies, there are two Markov chains in this model. One is the hidden Markov chain which consists of the network states, and the other is the observable Markov chain which consists of the random CA delays. Moreover, the random CA delays are also affected by the hidden network states, which constructs the DCHMM-based delay model. The DCHMM-based delay model is highly consistent with the distribution of the real network delays. Therefore, the DCHMM, compared with the DTHMM, gets much closer to the real network, which renders the DCHMM-based delay model with higher accuracy than the DTHMM-based delay model. However, it is worth noting that the DCHMM is more complex than the DTHMM in model parameter estimation and will consume more computing time. As a result, the DCHMM has a relatively poor real-time performance when directly applied to actual systems. A feasible solution is to determine the parameter reestimation frequency according to the prediction accuracy. A threshold is defined as in [32], and the event-triggering mechanism proposed in [36, 37] can be

used to trigger the parameter reestimation when the prediction error exceeds the threshold.

The expectation maximization algorithm is presented to obtain the optimal estimation of the model parameters after they are initialized by using the K-mean clustering algorithm. The Viterbi algorithm is presented to obtain the optimal estimation of the network states, and then the prediction of the CA delay in the current sampling period is obtained. Finally, some comparative experiments are carried out to demonstrate the superiority of the DCHMM-based delay model over the DTHMM-based delay model. Nevertheless, the random CA delays considered in this paper are discrete, and the DCHMM-based delay model is derived through quantizing the delays. If the CA delays are treated as continuous values and can take any value in its allowable interval or if the dependency relationship among random CA delays is taken into account in the SCHMM-based delay model, the derived DCHMM-based delay model will give more accurate prediction and show the superiority over the SCHMM-based delay model. In our future research, the predicted CA delay will be used to design the controller in the current sampling period to compensate the imminent real CA delay. Furthermore, we will investigate the adaption of these methods to other systems such as the cyber-physical systems and the multiagent systems.

Appendix

A. Derivation of the Algorithm

In this appendix, we provide the complete derivation of the algorithms of Section 3.

A.1. Likelihood of the Observed CA Delay Sequence. For $r = 1$, equation (9) becomes

$$\alpha_1(j) = P(o_0, o_1, s_1 = j) = P(o_1|o_0, s_1 = j)P(o_0, s_1 = j) = b^{(j)}_{o_0 o_1} P(o_0, s_1 = j). \tag{A.1}$$

Since o_0 and s_1 are independent and the value of o_0 is known, we have

$$\alpha_1(j) = b^{(j)}_{o_0 o_1} P(o_0) P(s_1 = j) = b^{(j)}_{o_0 o_1} P(s_1 = j) = b^{(j)}_{o_0 o_1} \pi_j. \tag{A.2}$$

For $r > 1$, equation (11) becomes

$$\begin{aligned}
\alpha_r(j) &= P(o_0, \ldots, o_r, s_r = j) \\
&= P(o_r|o_0, \ldots, o_{r-1}, s_r = j) P(o_0, \ldots, o_{r-1}, s_r = j) \\
&= P(o_r|o_{r-1}, s_r = j) \sum_{i=1}^{N} P(o_0, \ldots, o_{r-1}, s_{r-1} = i, s_r = j) \\
&= b^{(j)}_{o_{r-1} o_r} \sum_{i=1}^{N} P(s_r = j|o_0, \ldots, o_{r-1}, s_{r-1} = i) P(o_0, \ldots, o_{r-1}, s_{r-1} = i) \\
&= b^{(j)}_{o_{r-1} o_r} \sum_{i=1}^{N} P(s_r = j|s_{r-1} = i) P(o_0, \ldots, o_{r-1}, s_{r-1} = i) \\
&= b^{(j)}_{o_{r-1} o_r} \sum_{i=1}^{N} a_{ij} \alpha_{r-1}(i).
\end{aligned} \tag{A.3}$$

For β_r, $r = 1, \ldots, k-2$, we have

$$\begin{aligned}
\beta_r(i) &= P(o_{r+1},\ldots,o_{k-1}|o_r,s_r=i)\\
&= \frac{P(o_r,o_{r+1},\ldots,o_{k-1},s_r=i)}{P(o_r,s_r=i)}\\
&= \frac{1}{P(o_r,s_r=i)}\sum_{j=1}^{N}P(o_r,o_{r+1},\ldots,o_{k-1},s_r=i,s_{r+1}=j)\\
&= \frac{1}{P(o_r,s_r=i)}\sum_{j=1}^{N}P(o_r,s_r=i)P(s_{r+1}=j||o_r,s_r=i)P(o_{r+1}|o_r,s_r=i,s_{r+1}=j)\cdot P(o_{r+2},\ldots,o_{k-1}|o_r,o_{r+1},s_r=i,s_{r+1}=j)\\
&= \sum_{j=1}^{N}P(s_{r+1}=j|s_r=i)P(o_{r+1}|o_r,s_{r+1}=j)P(o_{r+2},\ldots,o_{k-1}|o_r,o_{r+1},s_r=i,s_{r+1}=j)\\
&= \sum_{j=1}^{N}a_{ij}b^{(j)}_{o_ro_{r+1}}\beta_{r+1}(j).
\end{aligned} \tag{A.4}$$

A.2. Estimation of π, **A**, *and* **B**. Equation (17) for the calculation of $\varepsilon_r(i,j)$ is

$$\begin{aligned}
\varepsilon_r(i,j) &= P(s_r=i,s_{r+1}=j|o_0,\ldots,o_{k-1})\\
&= \frac{1}{P(o_0,\ldots,o_{k-1})}P(o_0,\ldots,o_{k-1},s_r=i,s_{r+1}=j)\\
&= \frac{1}{P(o_0,\ldots,o_{k-1})}P(o_0,\ldots,o_r,s_r=i)P(s_{r+1}=j||o_0,\ldots,o_r,s_r=i)\\
&\quad\cdot P(o_{r+1}|o_0,\ldots,o_r,s_r=i,s_{r+1}=j)P(o_{r+2},\ldots,o_{k-1}|o_0,\ldots,o_{r+1},s_r=i,s_{r+1}=j)\\
&= \frac{1}{P(o_0,\ldots,o_{k-1})}P(o_0,\ldots,o_r,s_r=i)P(s_{r+1}=j|s_r=i)\\
&\quad\cdot P(o_{r+1}|o_r,s_{r+1}=j)P(o_{r+2},\ldots,o_{k-1}|o_{r+1},s_{r+1}=j)\\
&= \frac{\alpha_r(i)a_{ij}b^{(j)}_{o_ro_{r+1}}\beta_{r+1}(j)}{L(o_0,\ldots,o_{k-1})}.
\end{aligned} \tag{A.5}$$

and, for $\xi_r(i)$, we have

$$\begin{aligned}
\xi_r(i) &= P(s_r=i|o_0,\ldots,o_{k-1})\\
&= \frac{P(o_0,\ldots,o_{k-1},s_r=i)}{P(o_0,\ldots,o_{k-1})}\\
&= \frac{P(o_0,\cdots,o_r,s_r=i)P(o_{r+1},\ldots,o_{k-1}|o_0,\ldots,o_r,s_r=i)}{P(o_0,\cdots,o_{k-1})}\\
&= \frac{P(o_0,\ldots,o_r,s_r=i)P(o_{r+1},\ldots,o_{k-1}|o_r,s_r=i)}{P(o_0,\ldots,o_{k-1})}\\
&= \frac{\alpha_r(i)\beta_r(i)}{L(o_0,\ldots,o_{k-1})}.
\end{aligned} \tag{A.6}$$

Then, we can get the reestimation formula:

$$\begin{aligned}
\widehat{a}_{ij} &= \sum_{r=1}^{k-2}P(s_{r+1}=j|s_r=i,o_0,\ldots,o_{k-1})\\
&= \frac{\sum_{r=1}^{k-2}P(s_r=i,s_{r+1}=j,o_0,\ldots,o_{k-1})}{\sum_{r=1}^{k-2}P(s_r=i,o_0,\ldots,o_{k-1})}\\
&= \frac{\sum_{r=1}^{k-2}P(s_r=i,s_{r+1}=j|o_0,\ldots,o_{k-1})P(o_0,\ldots,o_{k-1})}{\sum_{r=1}^{k-2}P(s_r=i|o_0,\ldots,o_{k-1})P(o_0,\ldots,o_{k-1})}\\
&= \frac{\sum_{r=1}^{k-2}P(s_r=i,s_{r+1}=j|o_0,\ldots,o_{k-1})}{\sum_{r=1}^{k-2}P(s_r=i|o_0,\ldots,o_{k-1})}\\
&= \frac{\sum_{r=1}^{k-2}\varepsilon_r(i,j)}{\sum_{r=1}^{k-2}\xi_r(i)},
\end{aligned}$$

$$\begin{aligned}\widehat{b}_{lm}^{(i)}(r) &= P\left(o_r = m | o_0, \ldots, o_{r-2}, o_{r-1} = l, o_{r+1}, \ldots, o_{k-1}, s_r = i\right) \\ &= \frac{P\left(o_0, \ldots, o_{r-2}, o_{r-1} = l, o_r = m, o_{r+1}, \ldots, o_{k-1}, s_r = i\right)}{P\left(o_0, \ldots, o_{r-2}, o_{r-1} = l, o_{r+1}, \ldots, o_{k-1}, s_r = i\right)} \\ &\quad \sum_{r=1}^{k-2} \xi_r(i) \\ &= \frac{o_{r-1} = l, o_r = m}{\sum_{r=1}^{k-2} \xi_r(i)}. \\ &\quad o_{r-1} = l,\end{aligned} \tag{A.7}$$

A.3. Optimal sequence of hidden network states. Equation (24) can be obtained as

$$\begin{aligned}\delta_1(j) &= P\left(o_0, o_1, s_1 = j\right) \\ &= P\left(o_0, s_1 = j\right) P\left(o_1 | o_0, s_1 = j\right) \\ &= P\left(s_1 = j\right) P\left(o_1 | o_0, s_1 = j\right) \\ &= \pi_j b_{o_0 o_1}^{(j)},\end{aligned} \tag{A.8}$$

and, for $r = 2, \ldots, k-1$ and $j = 1, \ldots, N$,

$$\begin{aligned}\delta_r(j) &= \max_{i_1, \cdots, i_{r-1}} P\left(o_0, \ldots, o_r, s_1 = i_1, \ldots, s_{r-1} = i_{r-1}, s_r = j\right) \\ &= \max_{i_1, \cdots, i_{r-1}} P\left(o_0, \ldots, o_{r-1}, s_1 = i_1, \ldots, s_{r-1} = i_{r-1}\right) \\ &\quad \cdot P\left(s_r = j | o_0, \ldots, o_{r-1}, s_1 = i_1, \ldots, s_{r-1} = i_{r-1}\right) \\ &\quad \cdot P\left(o_r | o_0, \ldots, o_{r-1}, s_1 = i_1, \ldots, s_{r-1} = i_{r-1}, s_r = j\right) \\ &= \max_{i_1, \cdots, i_{r-1}} P\left(o_0, \ldots, o_{r-1}, s_1 = i_1, \ldots, s_{r-1} = i_{r-1}\right) \\ &\quad P\left(s_r = j | s_{r-1} = i_{r-1}\right) P\left(o_r | o_{r-1}, s_r = j\right) \\ &= \left[\max_{i_1, \cdots, i_{r-1}} \delta_{r-1}\left(i_{r-1}\right) a_{i_{r-1} j}\right] b_{o_{r-1} o_r}^{(j)}.\end{aligned} \tag{A.9}$$

B. Practical Computation of the Algorithms

Some algorithms in this paper may lead to numerical errors. A good solution is to normalize the intermediary results at each step of the calculation. A computable version of these algorithms is provided in this appendix.

B.1. Computation of the Forward Procedure. The forward variable $\alpha_r(j)$ may easily take values too small to be handled by a computer. To avoid this problem, one solution is to normalize $\alpha_r(j)$ at each step r.

For $r = 1$ and $j = 1, \ldots, N$, we define

$$\widetilde{\alpha}_1(j) = \frac{b_{o_0 o_1}^{(j)} \pi_j}{\overline{\alpha}_1}, \tag{B.1}$$

where $\overline{\alpha}_1 = \sum_{j=1}^{N} b_{o_0 o_1}^{(j)} \pi_j / N$ is the average value of the $\alpha_1(j)$.

Then, for $r = 2, \ldots, k-1$, we have

$$\widetilde{\alpha}_r(j) = \frac{b_{o_{r-1} o_r}^{(j)} \sum_{i=1}^{N} a_{ij} \widetilde{\alpha}_{r-1}(i)}{\overline{\alpha}_r}, \tag{B.2}$$

where $\overline{\alpha}_r = b_{o_{r-1} o_r}^{(j)} \sum_{i=1}^{N} a_{ij} \widetilde{\alpha}_{r-1}(i) / N$ is the average value of the $\alpha_r(j)$.

As a result, the log-likelihood of the sequence of observed CA delays can be obtained as follows:

$$\log\{L(o_0, o_1, \cdots, o_{k-1})\} = \log\left\{\sum_{j=1}^{N} \widetilde{\alpha}_{k-1}(j)\right\} + \sum_{r=1}^{k-1} \log\left(\overline{\alpha}_r\right). \tag{B.3}$$

B.2. Computation of the Backward Procedure. The computation of the backward procedure leads to the same kind of problems as the forward procedure and requires the same type of solution.

For $r = k-1$ and $i = 1, \ldots, N$, we define $\widetilde{\beta}_{k-1}(i) = 1$ and $\overline{\beta}_{k-1}(i) = 1$. Then, for $r = k-2, \ldots, 1$, we have

$$\widetilde{\beta}_r(i) = \frac{\sum_{j=1}^{N} b_{o_r o_{r+1}}^{(j)} \widetilde{\beta}_{r+1}(j) a_{ij}}{\overline{\beta}_r}, \tag{B.4}$$

where $\overline{\beta}_r = \sum_{j=1}^{N} b_{o_r o_{r+1}}^{(j)} \widetilde{\beta}_{r+1}(j) a_{ij} / N$ is the average value of the $\beta_r(i)$.

Therefore, the log-likelihood of the sequence of observed CA delays can be rewritten as follows:

$$\log\{L(o_0, o_1, \ldots, o_{k-1})\} = \log\left\{\sum_{i=1}^{N} \widetilde{\alpha}_r(i) \widetilde{\beta}_r(i)\right\} + \sum_{t=1}^{r} \log\left(\overline{\alpha}_t\right) + \sum_{t=r}^{k-1} \log\left(\overline{\beta}_t\right). \tag{B.5}$$

B.3. Computation of $\varepsilon_r(i, j)$ and $\xi_r(i)$. Based on the scaled version $\widetilde{\alpha}_r$ and $\widetilde{\beta}_r$ of α_r and β_r, the computation of $\varepsilon_r(i, j)$ and $\xi_r(i)$ is achieved as follows.

For $r = 1, \ldots, k-2$,

$$\varepsilon_r(i, j) = \exp\left\{\log\left(\widetilde{\alpha}_r(i)\right) + \sum_{t=1}^{r} \log\left(\overline{\alpha}_t\right) + \log\left(a_{ij}\right) + \log\left(b_{o_r o_{r+1}}^{(j)}\right)\right\} \left\{+\log\left(\widetilde{\beta}_r(i)\right) + \sum_{t=r}^{k-2} \log\left(\overline{\beta}_t\right) - \log\left(L\left(o_0, o_1, \ldots, o_{k-1}\right)\right)\right., \tag{B.6}$$

and, for $r = 1, \ldots, k-1$,

$$\xi_r(i) = \exp\left\{\log(\widetilde{\alpha}_r(i)) + \sum_{t=1}^{r}\log(\overline{\alpha}_t) + \log(\widetilde{\beta}_r(i))\right\{ + \sum_{t=r}^{k-1}\log(\overline{\beta}_t) - \log(L(o_0, o_1, \ldots, o_{k-1})). \tag{B.7}$$

For $r = 1, \ldots .k-2$, the relation (18) holds. The reestimation of π, $\mathbf{A}$, and $\mathbf{B}$ is obtained through formulas (19), (20), and (21):

B.4. Computation of the Optimal Sequence of Hidden Network States. In order to avoid numerical errors, it is necessary to scale the quantity δ used in the Viterbi algorithm.

For $r = 1$ and $j = 1, \ldots, N$, we define

$$\widetilde{\delta}_1(j) = \frac{\pi_j b_{o_0 o_1}^{(j)}}{\overline{\delta}_1}, \tag{B.8}$$

where

$$\overline{\delta}_1 = \frac{\sum_{i=1}^{N}\pi(i) b_{o_0 o_1}^{(j)}}{N}. \tag{B.9}$$

For $r = 2, \ldots, k-1$ and $j = 1, \ldots, N$, we compute iteratively:

$$\widetilde{\delta}_r(j) = \frac{\left[\max_{i_1,\cdots,i_{r-1}}\delta_{r-1}(i_{r-1})a_{i_{r-1}j}\right]b_{o_{r-1}o_r}^{(j)}}{\overline{\delta}_r},$$
$$\overline{\delta}_r = \frac{\sum_{j=1}^{N}\left[\max_{i_1,\cdots,i_{r-1}}\delta_{r-1}(i_{r-1})a_{i_{r-1}j}\right]b_{o_{r-1}o_r}^{(j)}}{N}. \tag{B.10}$$

The optimal hidden state at time $k-1$ is then

$$\widehat{s}_{k-1} = \arg\max_{j=1,\cdots,N}\widetilde{\delta}_{k-1}(j), \tag{B.11}$$

and we obtain recursively for $r = k-2, \ldots, 1$,

$$\widehat{s}_r = \arg\max_{j=1,\cdots,N}\widetilde{\delta}_{r+1}(j)a_{j\widehat{s}_{r+1}}. \tag{B.12}$$

Finally, the joint probability of the sequence of hidden network states and the sequence of observed CA delay outputs is equal to

$$P(s_1, \ldots, s_{k-1}, o_0, o_1, \ldots, o_{k-1}) = \left[\max_{j=1,\cdots,N}\widetilde{\delta}_{k-1}(j)\right]\prod_{r=1}^{k-1}\overline{\delta}_r. \tag{B.13}$$

Data Availability

All data sets used in this study are provided within the article.

Conflicts of Interest

The authors declare that there are no conflicts of interest regarding the publication of this paper.

Acknowledgments

This work was supported partially by the National Natural Science Foundation of China (61572032) and the Discipline (Major) Top-notch Talent Project of Anhui Provincial Universities (gxbjZD20).

References

[1] G. C. Walsh, H. Hong Ye, and L. G. Bushnell, "Stability analysis of networked control systems," *IEEE Transactions on Control Systems Technology*, vol. 10, no. 3, pp. 438–446, 2002.

[2] M. Lješnjanin, D. Nešić, and D. E. Quevedo, "Robust stability of a class of networked control systems," *Automatica*, vol. 73, pp. 117–124, 2016.

[3] Y.-L. Wang and Q.-L. Han, "Network-based modelling and dynamic output feedback control for unmanned marine vehicles in network environments," *Automatica*, vol. 91, pp. 43–53, 2018.

[4] M. E. M. B. Gaid, A. Cela, and Y. Hamam, "Optimal integrated control and scheduling of networked control systems with communication constraints: application to a car suspension system," *IEEE Transactions on Control Systems Technology*, vol. 14, no. 4, pp. 776–787, 2006.

[5] P. Park, H. Khadilkar, H. Balakrishnan, and C. J. Tomlin, "High confidence networked control for next generation air transportation systems," *IEEE Transactions on Automatic Control*, vol. 59, no. 12, pp. 3357–3372, 2014.

[6] A. Maciel, G. Sankaranarayanan, T. Halic, V. S. Arikatla, Z. Lu, and S. De, "Surgical model-view-controller simulation software framework for local and collaborative applications," *International Journal of Computer Assisted Radiology and Surgery*, vol. 6, no. 4, pp. 457–471, 2011.

[7] M. Li and Y. Chen, "Challenging research for networked control systems: a survey," *Transactions of the Institute of Measurement and Control*, vol. 41, no. 9, pp. 2400–2418, 2019.

[8] X. M. Zhang, Q. L. Han, X. H. Ge et al., "Networked control systems: a survey of trends and techniques," *IEEE/CAA Journal of Automatica Sinica*, vol. 7, no. 1, pp. 1–17, 2020.

[9] W. Zhang, M. S. Branicky, and S. M. Phillips, "Stability of networked control systems," *IEEE Control Systems Magazine*, vol. 21, no. 1, pp. 84–99, 2001.

[10] D. K. Kim, J. W. Ko, and P. Park, "Stabilization of the asymmetric network control system using a deterministic switching system approach," in *Proceedings of the Forty First IEEE Conference on Decision and Control*, pp. 1638–1642, Las Vegas, NV, USA, December 2002.

[11] L. A. Montestruque and P. J. Antsaklis, "On the model-based control of networked systems," *Automatica*, vol. 39, no. 10, pp. 1837–1843, 2003.

[12] D. Yue, Q. L. Han, and J. Lam, "Network-based robust H∞ control of systems with uncertainty," *Automatica*, vol. 41, no. 6, pp. 999–1007, 2005.

[13] A. Farnam and R. M. Esfanjani, "Improved stabilization method for networked control systems with variable transmission delays and packet dropout," *ISA Transactions*, vol. 53, no. 6, pp. 1746–1753, 2016.

[14] M. B. G. Cloosterman, N. van de Wouw, W. P. M. H. Heemels, and H. Nijmeijer, "Stability of networked control systems with

uncertain time-varying delays," *IEEE Transactions on Automatic Control*, vol. 54, no. 7, pp. 1575–1580, 2009.

[15] H. Zhang, Z. Zhang, Z. Wang, and Q. Shan, "New results on stability and stabilization of networked control systems with short time-varying delay," *IEEE Transactions on Cybernetics*, vol. 46, no. 12, pp. 2772–2781, 2016.

[16] Y.-L. Wang and G.-H. Yang, "H∞ control of networked control systems with time delay and packet disordering," *IET Control Theory & Applications*, vol. 1, no. 5, pp. 1344–1354, 2007.

[17] H. Song, G.-P. Liu, and L. Yu, "Networked predictive control of uncertain systems with multiple feedback channels," *IEEE Transactions on Industrial Electronics*, vol. 60, no. 11, pp. 5228–5238, 2013.

[18] D. Yue, E. G. Tian, Z. D. Wang et al., "Stabilization of systems with probabilistic interval input delays and its applications to networked control systems," *IEEE Transactions on Systems, Man and Cybernetics - Part A*, vol. 39, no. 4, pp. 939–945, 2009.

[19] C. Peng, D. Yue, E. Tian, and Z. Gu, "A delay distribution based stability analysis and synthesis approach for networked control systems," *Journal of the Franklin Institute*, vol. 346, no. 4, pp. 349–365, 2009.

[20] D. Yue, E. G. Tian, Y. J. Zhang et al., "Delay-distribution-dependent stability and stabilization of T-S fuzzy systems with probabilistic interval delay," *IEEE Transactions on Systems, Man and Cybernetics - Part B*, vol. 39, no. 2, pp. 503–516, 2009.

[21] C. Peng and T. C. Yang, "Communication-delay-distribution-dependent networked control for a class of T-S fuzzy systems," *IEEE Transactions on Fuzzy Systems*, vol. 18, no. 2, pp. 326–335, 2010.

[22] X. He, Z. Wang, and D. H. Zhou, "Robust fault detection for networked systems with communication delay and data missing," *Automatica*, vol. 45, no. 11, pp. 2634–2639, 2009.

[23] W. Wu, "Fault-tolerant control of uncertain non-linear networked control systems with time-varying delay, packet dropout and packet disordering," *IET Control Theory & Applications*, vol. 11, no. 7, pp. 973–984, 2017.

[24] D. Sauter, S. Li, and C. Aubrun, "Robust fault diagnosis of networked control systems," *International Journal of Adaptive Control and Signal Processing*, vol. 23, no. 8, pp. 722–736, 2009.

[25] H. Zhang and J. Wang, "Robust two-mode-dependent controller design for networked control systems with random delays modelled by Markov chains," *International Journal of Control*, vol. 88, no. 12, pp. 2499–2509, 2015.

[26] C. Yang, Z.-H. Guan, and J. Huang, "Design of stochastic switching controller of networked control systems based on greedy algorithm," *IET Control Theory & Applications*, vol. 4, no. 1, pp. 164–172, 2010.

[27] L. Zhang, Y. Shi, T. W. Chen et al., "A new method for stabilization of networked control systems with random delays," *IEEE Transactions on Automatic Control*, vol. 50, no. 8, pp. 1177–1181, 2005.

[28] S. Cong, Y. Ge, Q. Chen, M. Jiang, and W. Shang, "DTHMM based delay modeling and prediction for networked control systems," *Journal of Systems Engineering and Electronics*, vol. 21, no. 6, pp. 1014–1024, 2010.

[29] Y. Liu and D. Sun, "Delay-dependent H∞ stabilisation criterion for continuous-time networked control systems with random delays," *International Journal of Systems Science*, vol. 41, no. 11, pp. 1399–1410, 2010.

[30] Y. Ge, S. Cong, and W. Shang, "K-means based delay quantization and prediction in networked control systems," in *Proceedings of the 31st Chinese Control Conference*, pp. 5921–5926, Hefei, China, July 2012.

[31] D. Huang and S. K. Nguang, "State feedback control of uncertain networked control systems with random time delays," *IEEE Transactions on Automatic Control*, vol. 53, no. 3, pp. 829–834, 2008.

[32] Y. Ge, Q. Chen, M. Jiang, and Y. Huang, "SCHMM-based modeling and prediction of random delays in networked control systems," *Journal of the Franklin Institute*, vol. 351, no. 5, pp. 2430–2453, 2014.

[33] Y. Ge, X. Zhang, Q. Chen, and M. Jiang, "Initialization of the HMM-based delay model in networked control systems," *Information Sciences*, vol. 364-365, pp. 1–15, 2016.

[34] Y. Ge, S. Cong, and W. Shang, "DTHMM based optimal controller design for networked control systems," *Journal of University of Science and Technology of China*, vol. 42, no. 2, pp. 161–169, 2012.

[35] T. Liu, D. J. Hill, and J. Zhao, "Synchronization of dynamical networks by network control," *IEEE Transactions on Automatic Control*, vol. 57, no. 6, pp. 1574–1580, 2012.

[36] Q. Li, B. Shen, Z. D. Wang et al., "Recursive distributed filtering over sensor networks on Gilbert-Elliott channels: a dynamic event-triggered approach," *Automatica*, vol. 113, Article ID 108681, 2020.

[37] Q. Li, Z. Wang, W. Sheng, F. E. Alsaadi, and F. E. Alsaadi, "Dynamic event-triggered mechanism for H∞ non-fragile state estimation of complex networks under randomly occurring sensor saturations," *Information Sciences*, vol. 509, pp. 304–316, 2020.